Development of a Highly Sensitive Protein Diagnostic Device using Isothermal Strand Displacement
Amplification

Dylan Guelig

A thesis submitted in partial fulfillment of the requirements for the degree of

Master of Science in Bioengineering

University of Washington

2018

Committee:

Dr. Paul Yager

Dr. Barry Lutz

Program Authorized to Offer Degree:

Bioengineering

University of Washington

ABSTRACT

Development of a Highly Sensitive Protein Diagnostic Device using Isothermal Strand Displacement

Amplification

Dylan Guelig

Chair of the Supervisory Committee:

Dr. Paul Yager

Department of Bioengineering

The lateral flow test (LFT) is the preferred tool for detection of protein biomarkers in low-resource

settings. While low-cost and rapid, these immunoassay devices often suffer from limited sensitivity in the

single chemical step format. Our group has addressed this deficiency by coupling a lateral flow test to

isothermal strand displacement amplification (iSDA), a nucleic-acid amplification test (NAAT). This

novel method is called LFT-iSDA and uses an oligonucleotide-labelled detection antibody in the

immunoassay as the target template for iSDA. In its current embodiment, LFT-iSDA is ~10,000x more

sensitive than gold nanoparticle-based LFTs, but is highly manual and relies on laboratory infrastructure.

Here we present preliminary development of a diagnostic device integrating the highly sensitive LFT-

iSDA into a cartridge supporting rapid time-to-results and minimal user-steps— a format amenable to

decentralized test settings. We characterized performance limitations of this assay, developed a real-time

fluorescence detection system, and used a two-dimensional paper network (2DPN) to semi-automate this

multi-step chemical process. These results show important progress toward enabling highly sensitive

protein detection in a user-friendly, low-cost device, at the point of care.

Table of Contents

Table of Figures

1 INTRODUCTION

1.1 Significance

The value of diagnostics

Medical diagnostics provide essential data across health care levels to inform clinical decision-making, infection prevention, and epidemiological surveillance, guiding both immediate and long-term efforts to improve health outcomes. [1] Broadly, diagnostics are critical tools in clinical workflows in both high-income and low-income countries, with numerous applications in both communicable and non-communicable diseases (NCDs). However, infectious diseases disproportionately affect low-income countries, as evident in comparing the distribution of disability adjusted life-years (DALYs) between the United States and Sub-Saharan Africa. (Figure 1) While global efforts continue to extend the reach of healthcare into low-resource settings (LRS), infrastructure and economic limitations preclude the use of laboratory-based diagnostics typically used in high-income countries.[2]
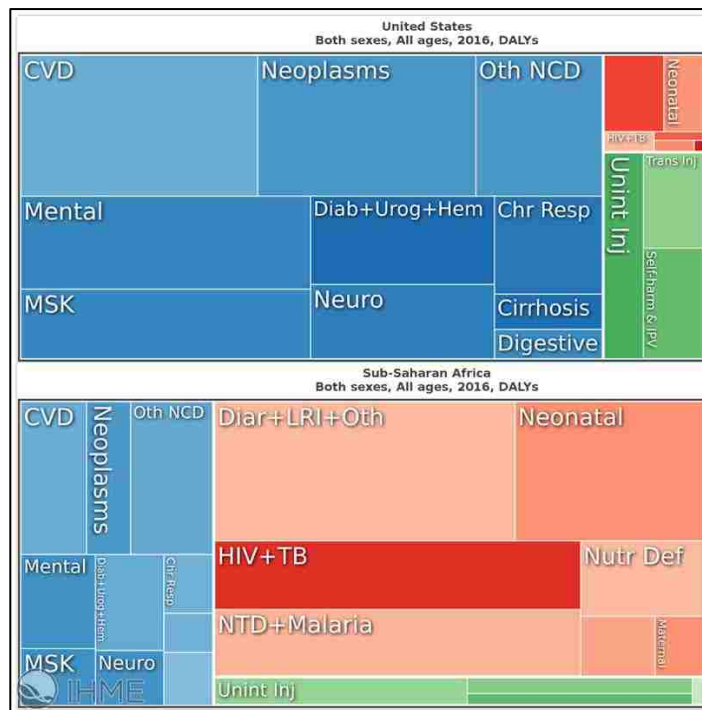
Figure 1: Disease burden in the United States and Sub-Saharan Africa: Disability adjusted life years (DALYs) for entire population. Less than 5% of DALYs in the United States are attributed to WHO

Group 1 diseases: communicable and infectious diseases, maternal, neonatal, and nutritional diseases (red regions in treemap). In contrast, Group 1 diseases comprise 65% of DALYs in Sub Saharan Africa. Blue regions show DALYs from non-communicable disease group; green regions show DALYs from injuries.[3]

Constraints in LRS such as unreliable electricity, limited medical equipment, high ambient temperatures, and limited technical skills in remote areas have been met with point-of-care diagnostic (POC) technologies.[4] This class of diagnostics are low-cost, easy to use, and provide rapid results, enabling faster treatment and better outcomes, marking significant progress in reducing disease burden in LRS. The evidence for the economic value POC diagnostics provide in LRS is well documented, but there is also potential opportunity for decentralized testing in high-income countries(e.g. at home or pharmacy-based testing). [5]

Need for protein testing at the POC

Current POC diagnostics for infectious disease can be broken into two analyte classes: (1) nucleic-acid and (2) protein and small molecule detection. Nucleic acid amplification test (NAAT) platforms have proven essential in clinical diagnostics and are regarded as the gold standard for many disease diagnoses including malaria, HIV-1, tuberculosis (TB), and influenza. [6] Mature NAATs such as polymerase chain reaction (PCR) hold tremendous analytical sensitivity, are capable of amplifying fewer than 10 copies of target nucleic acids, but also have extreme specificity and versatility over a range of nucleic acid targets.[7] Although NAATs are traditionally performed in a centralized laboratory setting, commercial platforms such as the Cepheid Gene Xpert Omni, Alere i, and Roche Cobas LIAT RT-PCR system, continue to expand into LRS, holding great potential for rapid and multiplexed nucleic acid detection at the POC.[8]–[10] Despite these advances in bringing ultrasensitive NAAT technology out of the lab, there are many use cases where sensitive detection of protein or small molecule targets is needed at the POC.

One of the most commonly used methods for detecting proteins at the POC is the lateral flow test (LFT). It is a widespread, user-friendly, low-cost immunoassay technology used to detect protein and small molecule analytes; it is rapid (<30 mins) and simple, yet much less sensitive than NAATs. [11] LFTs provide an important complement to NAATs and serve a critical role in front-line or screening methods for many viruses including HIV, malaria, dengue, hepatitis C, and influenza. [12]
It is well suited for applications where nucleic acid targets are not available/accessible or high sensitivity is not required. Applications such as food-borne toxin testing, biomarker discovery, serology assays to identify malaria transmission trends, or identification of metabolic biomarkers, are examples where LFTs provide a low-cost solution with acceptable specificities and sensitivities. [13]–[15]

Subsequent generations of LFTs have demonstrated improved analytical performance, yet certain applications still lack required sensitivity compared to lab-based tests.[16] The need for improved LFTs was highlighted in recent guidelines for influenza diagnosis from the Centers for Disease Control and Prevention (Atlanta, USA). Current LFTs provide results in a clinically relevant 15 mins, but have limited sensitivity (50-70%) compared to RT-PCR, leading to false negatives and population risk during outbreaks.[17] While the specificity of these tests is sufficient (90% compared to RT-PCR), sensitivity is clearly deficient.

In short, protein detection LFTs play critical roles in POC diagnostics, yet improved sensitivity is needed across many clinical applications ranging from outbreak response, to at-home testing, to surveillance. While NAAT tests continue to push into more decentralized areas, there is a global need for highly sensitive POC immunoassay tests while maintaining the ubiquitous and simple format of LFTs.

1.2 Proposed solution

This project investigates the development of a highly sensitive protein diagnostic device using an LFT format with isothermal strand displacement signal amplification (LFT-iSDA) of a detection antibody-synthetic oligonucleotide conjugate. This project aims to take the recently developed LFT-iSDA

assay closer to the POC by integrating the manual, lab-based analytical method into an easy-to-use, cartridge-based format. In an effort to provide universal signal enhancement to LFTs, the project has used nitrocellulose porous membranes for the immunoassay component. This work used (1) influenza-A nucleoprotein (flu-NP) and (2) Ebola virus soluble glycoprotein (EBOV-sGP) LFT-iSDA assays as model systems. Expanding upon the traditional one-dimensional LFT, the project leverages principles of two-dimensional paper networks (2DPNs) to simplify the multi-step assay, combined with fluorescence detection to reduce overall test time. [18] The LFT-iSDA assay, detection strategy, and device integration are characterized to understand the challenges in transposing the manual, lab-based format toward a semi-automated, point-of-care device.

1.3 Layout of thesis

The introduction highlights the need and challenges in POC diagnostics in LRS and describes the proposed solution of this thesis. Chapter 2 provides the background to POC diagnostics and existing lab-based and POC signal enhancement strategies for immunoassays. Chapter 3 investigates the performance of the LFT-iSDA assay in two model systems and illuminates performance challenges. Chapter 4 describes development of a fluorescence detection method for LFT-iSDA using fluorogenic probes. Chapter 5 details the design of an integrated cartridge and the factors influencing the assay performance in this format. Chapter 6 presents final conclusions and suggestions for future work.

2 BACKGROUND

2.1   Point of care diagnostics design criteria

Since the introduction of the at-home rapid pregnancy test in 1977, POC diagnostics have been designed to address resource constraints in the intended use-case environment.[2] The WHO characteristics for affordable, sensitive, specific, user-friendly, rapid and robust, equipment-free and deliverable to end users (ASSURED) diagnostics provide widely accepted guidelines test developers. [19] It is estimated that tests complying ASSURED guidelines while achieving 76-97% specificity and 85-95% sensitivity could significantly reduce the disease burden in LRS.[20]

In accordance to these recommendations, this project strives for ASSURED compliance, but expands the interpretation of "equipment-free" to "low-cost equipment" or "minimally-instrumented", as advances and cost reductions in mobile computing, portable sensor technology (e.g. smartphone cameras), and hand-held devices merit use of previously centralized methods at the POC. For example, integration of POC test results with cloud-connectivity through minimally instrumented, portable systems, enables new models for efficient data transfer and clinical decision making. [21] In addition to describing a use-case environment, POC can be thought of as much as a strategy enabled through technology. The sensitivity and specificity requirements are disease and use case specific and should meet the clinical demand for minimizing time to test result.[2]

Similarly, the "affordable" characteristic is difficult to quantify, as some POC tests receive philanthropic subsidies (e.g. GeneXpert MTB/RIF Cartridges cost subsidized by ~50%) to promote scale-up and rapid dissemination. [22] The cost analysis must also account for the healthcare worker's salary per test, the consequent counselling salary per test, and ancillary costs such as instrument calibration (if applicable), and supply chain factors. In short, the affordable characteristic should be interpreted as making tests amenable to the POC environment at the lowest cost achievable while retaining sufficient features to reduce the reliance on traditional laboratory infrastructure. The <10 USD consumable precedent set by the GeneXpert cartridges will be used for this project as an "affordable" target. [23]

The remaining "user-friendly", "robust", and "deliverable to end user" characteristics are desirable across all use-care scenarios. Lastly, the rapid characteristic should strive to match predicate POC diagnostics time-to-result of <60 min. [20], [21], [24]

2.2   Lateral flow tests

Over the last half-century, LFTs have been the preferred format to meet POC diagnostics design criteria for protein and small molecule analytes. LTFs are paper microfluidic (the term "paper" is used broadly to encompass porous materials used in the lateral flow industry) analytical devices used to detect analytes in complex mixtures in less than 30 minutes. They can identify a diverse set of biomarkers in biological samples such as urine, whole blood, saliva, or plasma. The commonly used sandwich lateral flow immunoassay employs antibodies to detect protein or small molecule biomarkers. (Figure 2) The operating principle of this assay is as follows: (1) a liquid biological sample containing analyte is added to the sample pad—the starting end of the porous membrane network. (2) The sample flows through the porous membrane network *via* capillary action and passes from the sample pad into the conjugate release pad, where the detection molecule, an antibody-nanoparticle label (commonly colloidal gold or plastic beads) conjugate, specific to the target analyte binds to an epitope on the analyte. (4) The target analyte-detection molecule complex then flows with the sample fluid into the nitrocellulose detection membrane, where it crosses an immobilized capture antibody with affinity to a different epitope on the analyte; this region is called the test line. The analyte-detection molecule complexes bind to the test line; the resulting high concentration of nanoparticles produces a colored line of intensity proportional to the concentration of analyte in the sample. (5) Immediately downstream of the test line is the control line, which binds excess detection molecules serving as a visual indicator process control to ensure liquid flowed through the length of the porous membrane. At the distal end of the strip, a cellulose wicking pad provides a fluidic sink to retain excess reagents and prevent backflow. [5], [11], [25]
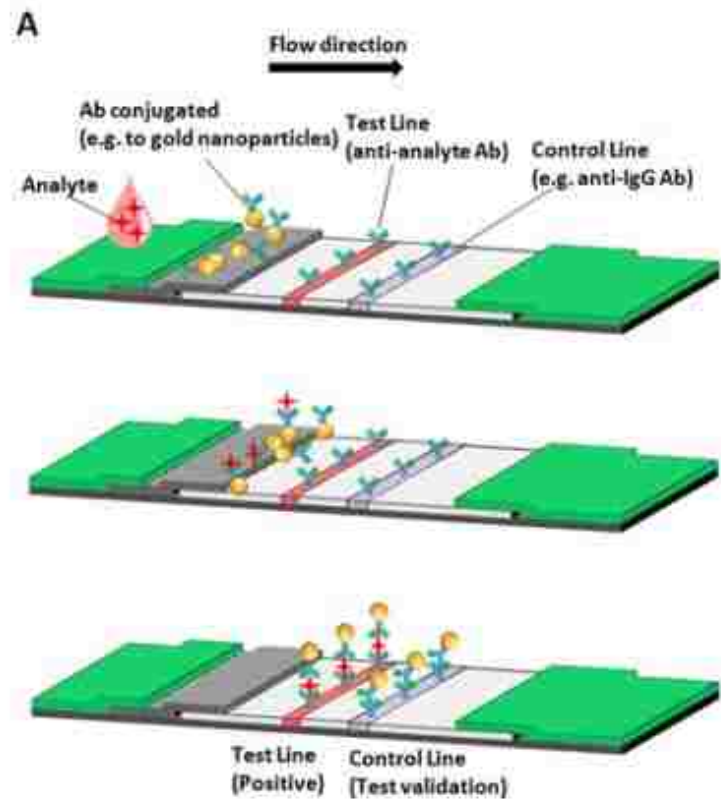
Figure 2: Lateral flow sandwich immunoassay: Sample containing analyte (denoted by red star) is added to the sample pad (left green region), where it flows into the conjugate pad (grey region) to mix with the detection molecule (nanoparticle labelled antibody), which binds to an epitope on the target analyte. This complex then flows into the nitrocellulose detection membrane (white region) where it binds to an immobilized capture antibody with affinity for a different epitope on the target analyte at the test line. Downstream, unbound detection molecule non-specifically binds to the control line indicating a valid test. Concentrations of the colored nanoparticles at the test and control lines create a visual indicator of a dark red line for user interpretation of test results. Schematic from [11].

Fluid flow in porous media

Paper microfluidics (e.g. LFTs) do not require external pumps, commonly used in traditional channel-based microfluidics. Fluid flow in the LFT is pressure-driven by capillary action in the pores of the various materials. Flow, also called "wicking", is driven by the pressure differential between the fluid

source and the leading wetted edge of the fluid in the membrane and the saturation level of the membrane. The smaller the pores in the membrane, the more negative the capillary pressure, thus providing a larger magnitude pressure gradient. This principle explains why fluid readily flows from large pore materials (e.g. glass fiber) to small pore materials (e.g. nitrocellulose) and justifies the use of cellulose as the terminal wicking pad membrane. Understanding the governing equations of flow through porous media is central to optimizing reaction kinetics, time-to-result, and predicting flow between adjacent materials. A more detailed description of flow in porous media is presented in Chapter 5.

The LFT immunoassay is an extremely versatile, low-cost configuration exploiting capillary self-driven flow and obviates the need for external pumping; it is the foundation for many POC protein tests. Despite its widespread adoption, rapid time-to-result, and low cost, the LFT format has limited sensitivity compared to lab-based methods. Principal limitations are due to (1) the lack of signal amplification—analytes bind at a one-to-one ratio with colorimetric nanoparticle labelled detection molecules, and (2) low signal-to-noise ratios due to non-specific interactions between assay components (reagents and porous materials) increasing the background.

2.3   Strategies to improve sensitivities of LFTs

Numerous approaches have been developed to combat the limited sensitivity of LFTs. This section will outline these efforts and comment on performance gains and associated device or assay complexity.

2.3.1   Nanoparticle enhancement

Several groups have demonstrated sensitivity gains in LFTs by enhancing the colorimetric signal of gold nanoparticles using various chemistries. For example, silver enhancement of gold nanoparticles on a sandwich LFT format using silver lactate and hydroquinone mixture with a chloride containing buffer achieved 15x sensitivity gains over a conventional LFT. [26] Another strategy used gold nanoparticle aggregation induced by polyamidoamine dendrimer, showing 20x lower limit of detection

(LOD) than LFT baseline. [27] While these methods improve sensitivity, they come with additional time-dependent user steps and reagent costs. To address the additional complexity of a multi-step assay, our group used a commercial gold enhancement (GE) reagent integrated in to a 2DPN to simplify user steps and showed four-fold improvement over a no-enhancement device. Although the device achieved modest sensitivity gains over the LFT, the device is much more appropriate for POC settings. [28] In short, nanoparticle enhancement strategies achieve sensitivity gains of roughly 1-order of magnitude, have no additional hardware requirements, yet inevitably add steps to the LFT assay operations.

2.3.2 Fluorescent nanoparticles

In a similar strategy to minimally change the conventional format of LFTs, fluorescent reporter labels have proven to be more sensitive than traditional gold nanoparticles. Employing fluorescence over absorbance offers potential for single-molecule detection (with suitable optical sensors), multiplexing using various fluorophore/optical filter combinations to co-locally discern two signals at a test line, and strong signal-to-background ratios. A quantum dot labelled detection molecule for a flu-A nucleoprotein LFT was recently shown to have 7-12x sensitivity gains over gold nanoparticles. The novel approach required only a smartphone camera and lost-cost LED excitation source to detect the fluorescence signal. [29] Similar efforts show ten-fold sensitivity gain using FITC and Ru(bpy) labelling with filter-sets integrated into a smartphone case. [30] Limitations of fluorophore-labelled detection molecules include photobleaching, temperature/pH dependence of the fluorescent signal, and requirement of an external instrument (e.g. smartphone camera or portable reader). In short, use of fluorophore labels in LFTs provide roughly one order of magnitude sensitivity improvement over gold nanoparticles without adding immunoassay complexity, yet require the addition of a low-cost instrument to detect the fluorescence signal.

2.3.3 Enzymatic signal enhancement

While nanoparticle enhancement and fluorescent nanoparticle-based LFTs offer advantages over conventional LFTs, they are still often limited by the one-to-one binding ratio of analyte to detection

molecule. Enzymatic amplification of the analyte capture event has long been used to improve sensitivity of immunoassays. Conventional well-plate enzyme-linked immunosorbent assays (ELISAs) are a powerful and common method for non-POC testing settings with demonstrated automation and high-throughput capabilities; these lab-based methods offer several orders of magnitude better sensitivities over LFTs. Yet, the ELISAs can be time consuming, require skilled technicians, and often instrument intensive, hindering widespread use at the POC. [5]

Recently, groups have combined ELISA-like amplification strategies with 2DPNs into POC devices with sensitivity gains on the order of 10x improvement over LFTs, and capable of matching 96-wp format ELISA sensitivities. [31] The Yager group has extensively demonstrated both multi-step automation and long-term storage of horse-radish peroxidase – diaminobenzidine (HRP-DAB) enzymatic amplification in 2DPN architecture devices.[32] Enzymatic amplification of an flu-A nucleoprotein assay in paper showed 10-fold better sensitivity compared to a high-performing commercial LFT using influenza-A whole virus in buffer.[33] This assay also employed a poly-HRP labeled detection antibody to further increase the amplification rate and consequent signal intensity. (Figure 3)
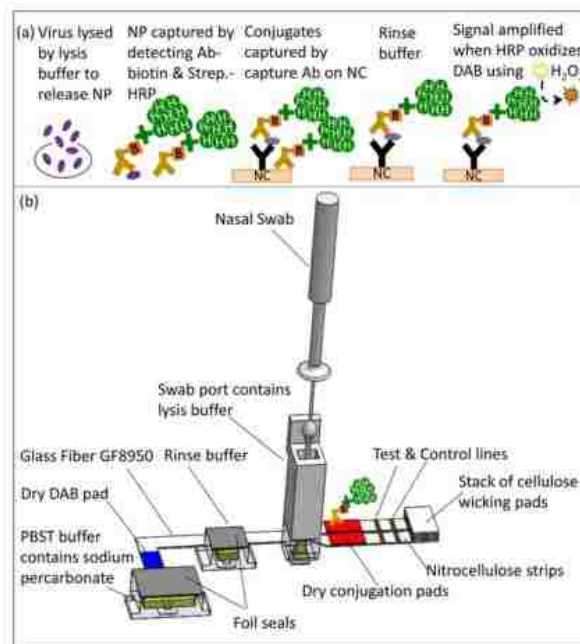
Figure 3: Enzymatic amplification in a flu-A nucleoprotein assay: performed in a fully automated, sample-to-results format. Panel (a) shows the poly-HRP enzyme labelled sandwich immunoassay combined with HRP-DAB chromogenic reaction. Panel (b) shows 3D model of the 2DPN and reagent storage methods. Device showed 10x improvement over commercial LFT. Image adapted from [33].

In summary, enzymatic amplification in the POC format devices offer impressive gains over LFTs, approaching ELISA LODs in a shorter test time with a single-user step. These strategies often employ the versatile 2DPN to automate unit operations and store reagents on-board.

2.3.4   Immuno-NAAT Systems

While the ELISA format is regarded as a gold-standard protein test for many targets, a recent class of protein diagnostics couple NAAT chemistry to amplify a sandwich immunoassay stack; this assay format is termed immuno-NAAT systems. The first embodiment of this method, immuno-polymerase chain reaction (immuno-PCR), described in 1992, used PCR to amplify a synthetic oligonucleotide (oligo) conjugated to a detection antibody.[34] Immuno-PCR exploits exponential signal amplification by targeting a synthetic ssDNA or dsDNA template conjugated to an detection antibody with strong affinity to the target analyte. The oligo template is of an arbitrary sequence, as it is simply an amplifiable reporter label. Many biochemical methods have been developed to conjugate the detection antibody to an oligo template. Biotin/streptavidin linkages are considered the universal method, but covalent attachment of DNA-antibody (e.g. Expedeon Thunder-link kit), or by covalent-linkage of DNA containing liposomes to antibodies can offer advantages. [35], [36]. (Figure 4) The laboratory-based immuno-PCR format follows ELISA protocols: incubation with capture antibodies on a well-plate, addition of successive blocking and washing steps, and lastly with the addition of the detection antibody-DNA molecule followed by PCR master-mix; the plate is then cycled to PCR thermal profiles to yield exponential signal amplification. Reported gains are 10^{3}-10^{4} fold more sensitive than comparable ELISAs, yet the method suffers from (1) high-technical skill level, (2) expensive instrumentation, (3) long

time-to-result, and (4) high degrees of background signal due to non-specific adsorption of the detection molecule giving false-positive amplification in NTC samples. [35], [37]
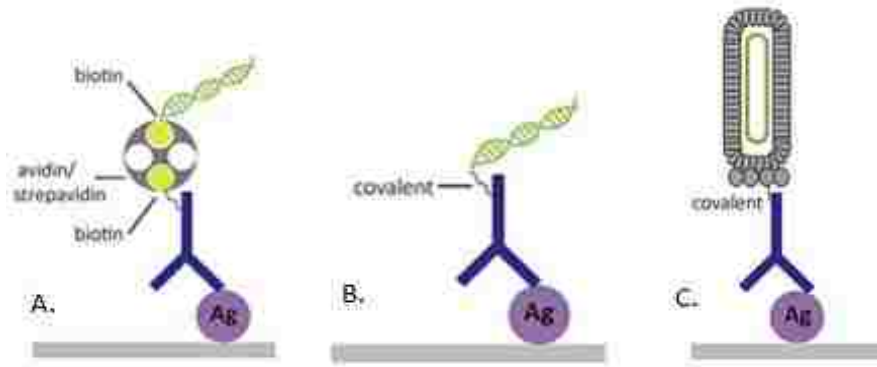
Figure 4: Immuno-NAAT DNA-Antibody conjugation strategies: (A) The universal method of immuno-PCR where a streptavidin/avidin links biotinylated oligo and biotinylated antibody. (B) Covalent attachment of oligo to antibody using various chemistries, (C) attachment of DNA encapsulating liposome or phage. Schematics adapted from *[35]*.

To minimize the instrumentation requirements and bring the immuno-NAAT systems closer to the POC, several groups leveraged the advantages of isothermal nucleic acid amplification tests (iNAATs) with immuno-NAAT principles. iNAATS are auto cycling analogues of PCR, requiring only a single incubation temperature, drastically simplifying devices which can achieve PCR-like sensitivities. Instead of thermal denaturation of dsDNA (as in PCR), iNAATs use a range of additional enzymes to nick, unwind, displace, or invade dsDNA to create ssDNA templates for amplification via primer extension by polymerase. This mechanistic distinction or enzymatic- *vs* thermal-cycling makes quantification of these reactions more challenging than PCR. Various POC tests have integrated iNAAT assays for DNA/RNA detection in low-cost devices; the technology is mature. [24], [38]–[40]

Demonstrations using iNAATs to amplify a protein capture event include immuno-LAMP, where magnetic bead-antibody capture of analyte was combined with detection of a DNA encapsulating liposome linked antibody and amplified using loop-mediated isothermal amplification, immuno-RCA,

where rolling-circle amplification (RCA) was used in a multiplexed microarray format. [41], [42] When coupled with a sandwich immunoassay *via* immuno-PCR style linkages, immuno-iNAATs extend the reach of ultrasensitive by eliminating the need for a thermal-cycler. However, they still require ELISA infrastructure, high skill level, and time-intensive protocols.

Despite the potential of immuno-NAAT systems to combine protein detection with NAAT sensitivity, the technology has not exploded at the same rate as older sibling PCR. A cursory pubmed.gov literature search showed only 221 results for "immuno-PCR" vs. 455,737 results for "PCR"; although immuno-PCR is a newer method, its use is obviously limited. The central challenge of immuno-NAAT systems is optimizing the assay to increase the signal-to-background ratio (SBR); the characteristic high background is caused by non-specific binding (NSB) of antibodies, antigens, or DNA to stationary surfaces within the analytical process (e.g. high-adsorption ELISA plates, microarrays). Stringency and composition of wash are extremely important, as the exponential amplification of non-specifically bound molecules can yield false positive signals from samples containing no analyte. In summary, there is tremendous potential for the immuno-NAAT assay format and efforts to extend the reach to the POC holds immense value to protein diagnostics.

2.3.5   LFT-isothermal strand displacement amplification (LFT-iSDA)

To address this gap between immuno-NAAT assays and the POC use-case, our lab recently developed a method using isothermal strand displacement amplification (iSDA) NAAT chemistry to amplify the signal generated from an analyte captured in a LFT immunoassay; this technique is called LFT-iSDA. [43] This powerful, indirect amplification method improved limits-of-detection 10,000x compared to a gold-nanoparticle LFT. To our knowledge, this is the first demonstration of integrating an immuno-NAAT chemistry with a nitrocellulose-based sandwich immunoassay. While the first embodiment used influenza antibodies against flu-A nucleoprotein (flu-NP), we omitted the "immuno-" distinction in the name as we have also developed non-antibody "protein binder" lateral flow tests

amenable to this method. While conventional NAATs exponentially amplify the target analyte (direct amplification), LFT-iSDA exponentially amplifies a molecule bound to the target analyte (indirect amplification), potentially compromising test specificity.

Our lab has extensive experience with iSDA, a truly isothermal (no-heat denaturation step), extremely fast (<10 min) NAAT capable of detecting <10 copies of DNA target in buffer in tube format, and ~5 x 10^3 copies of DNA target in a porous media format in a fully automated, POC device. [24], [44] iSDA uses a nicking enzyme to cut one strand of a dsDNA template, allowing primers to anneal, and extend by a strand-displacing polymerase (Warmstart Bst 2.0) at 49-50°C, yielding exponential amplification. The assay is robust to background genomic DNA and mucins found in clinical matrices and demonstrates long-term stability after lyophilization. These key assay characteristics of (1) rapid time-to-result, (2) compatibility with a 2DPN, (3) minimal instrumentation requirements, and (4) stability in lyophilized format make iSDA an ideal signal amplification chemistry for a POC-LFT device.

The first embodiment of LFT-iSDA employed the universal immuno-PCR method of biotin-streptavidin mediated ssDNA-antibody conjugation. The workflow starts with running a conventional pre-mixed sandwich immunoassay, followed by addition of a glass fiber pad containing freshly prepared, iSDA master-mix reagents and incubation. Following incubation, amplicons are detected using polyacrylamide gel electrophoresis (PAGE) and/or DNA lateral flow detection (DNA-LFT). (Figure 5) This manual format used a custom laminated Mylar and PDMS double-sided adhesive card to hold porous membranes and seal each LFT prior to incubation. The immunoassay reagents were delivered to the LFTs in vertical flow, "dipstick" format; iSDA reagents were pipetted onto glass pads placed at a second time point directly over the test line. We refer to this workflow as the "manual LFT-iSDA" format: a laboratory-based analytical method using low-cost, widely available LFT materials and commonly available instrumentation.
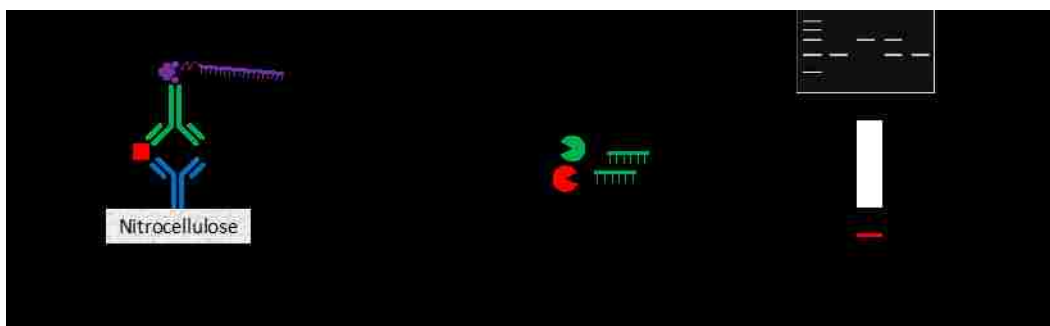
Figure 5: LFT-iSDA Assay stack and workflow: The capture antibody is immobilized at the test line of a nitrocellulose reaction membrane. A premixed solution containing analyte, biotinylated detection antibody, streptavidin, and biotinylated oligo template is then added and binds at the test line. A stringent wash, and iSDA buffer rinse is then flowed through the membrane; iSDA master-mix is consequently added via a glass-fiber pad added directly over the test line. The assembly is sealed and incubated, followed by fluid removal from porous media by centrifugation. Amplicon generation is verified by polyacrylamide gel electrophoresis (PAGE) and/or DNA lateral flow detection (DNA-LFT). Figure adapted from [43].

In short, LFT-iSDA is a novel format approaching NAAT-like sensitivity with the simplicity of LFTs. By harnessing the simplicity of an LFT-immunoassay—over the multistep protocols of ELISAs, the reduced instrumentation requirements of iSDA—over the thermal cycling requirements of PCR, and the shorter time to result over other immuno-NAAT tests (LFT-iSDA takes ~2hrs), we have taken highly sensitive protein detection one step closer to decentralized applications. While we have demonstrated 10,000-fold improvement over a traditional LFT, automation and device integration are required to create utility at the POC.

2.4   Conclusions

The canonical LFT format has demonstrated broad utility in POC testing, addressing many of the design criteria defined in Section 2.1. Despite the critical role protein LFTs play in disease diagnosis, they are still lacking sensitivity required for low-abundance analytes. Strategies to address this shortcoming using

the traditional format include nanoparticle enhancement and fluorophore labelling, adding little to no additional device complexity, and gain roughly 10-20-fold better sensitivities. Methods introducing 2DPN architectures to automate multi-step enzymatic assays can match ELISA performance for certain analytes yet add marginal device and reagent costs. Use of immuno-NAAT platforms achieve up to 10^4-fold improvement over ELISAs but are bound to laboratory infrastructure and skill-level. Gold-standard protein microarray immunoassay analyzers such as the Quanterix Simoa platform achieve $10^3 - 10^4$ fold better sensitivities over ELISAs and are intended for high throughput, lab-based testing. (Table 1) Our group's recent development of LFT-iSDA is an important bridge in taking high sensitivity protein diagnostics closer to achieving all POC diagnostics design criteria. In conclusion, there is an obvious gap between highly sensitive protein diagnostics and POC settings. This project aims to address this gap by developing a highly sensitive protein diagnostic in an integrated device using LFT-iSDA at the POC.

Table 1: Comparison of technologies for protein detection: Sensitivity was reported relative to reported baseline to reduce biases from differing target antigens, differing statistical methods of defining limits-of-detection, and generally to attempt to normalize sensitivity across references. Asterisk (*) denotes technologies not (yet) appropriate at the POC.

Assay format	Typical sensitivity	Performance gains over baseline	Example technology	Advantages	Limitations	References
Gold nanoparticle (Gold-NP) immunoassay	Low	Baseline	Numerous POC infectious disease tests, at-home pregnancy test	Low cost, simple, rapid	Insufficient sensitivity, user steps	[11]
Nanoparticle enhancement	Low-Med	4-15x over gold-NP LFT	Silver-gold nanoparticle enhancement	Moderate gains for minimal added complexity	Additional reagent cost and (potentially) timed step	[26], [27], [45]
Fluorescent Nanoparticles	Low-Med	7-12x over gold-NP LFT	Quantum dot labeled antibody	No addition complexity over LFT	Requires instrument / optics	[29], [46]
Enzymatic amplification	Med	10x over gold-NP; Match ELISA LOD	HRP-DAB amplification	Low-cost, easy to use	2DPN complexity	[31]–[33]

Immuno-NAAT*	High	1000-10,000x over ELISA	Immuno-PCR Immuno-LAMP Immuno-RCA	NAAT-like Sensitivity	High background signal, infrastructure/ time/skill intensive.	[34], [35], [41]
LFT-iSDA*	High	10,000x over gold-NP	LFT-iSDA FluA NP Assay	Low-cost, ultrasensitive format	Not POC test	[43]
Protein array immuno-analyzers*	High	>1200x over ELISA	Quanterix Simoa	High-throughput, biomarker discovery	Expensive instrument, lab-based	[47], [48]

3 LFT-iSDA ASSAY DEVELOPMENT

3.1 Objectives

Expanding the utility of LFT-iSDA requires understanding the assay performance, limitations, and challenges in the most basic system prior to device integration. Here, "device integration" refers to engineering efforts to take laboratory-based, manual protocols toward manufacturable, devices suitable for POC applications. This section investigates the LFT-iSDA, first developed with a flu-NP target, with an alternative analyte, EBOV-sGP, to understand platform capabilities of this technology. Secondly, the fundamental challenge of immuno-NAAT systems—high background signal caused from non-specific binding (NSB) —is examined in the LFT-iSDA configuration. Lastly, strategies to prevent NSB in and consequent false positive test results are presented.

These research efforts are in support of the EbolaBox project (#HDTRA1-16-C-0029), the goal of which was to develop a disposable instrument-free diagnostic platform using highly sensitive protein assays for detection of Ebola virus in POC settings. Investigation of the EBOV-sGP LFT-iSDA assay was central to achieving desired sensitivity of the EbolaBox device.

3.2 Introduction

3.2.1 LFT-iSDA assay stack

The universal immuno-PCR method of a biotin-streptavidin linkages was used for the EBOV-sGP assay to join oligo to antibody. Capture antibodies were gifted from the Baker Lab (University of Washington, Seattle, WA, USA) and detection antibodies were sourced from a commercially available EBOV-sGP ELISA kit; we reasoned that this sandwich immunoassay has been already been optimized to have minimal cross-reactivity between antibodies. The oligo template is a synthetic ssDNA strand of a *mecA* target sequence (a gene conferring methicillin resistance in *Staphylococcus aureus* (MRSA), as our group has extensive experience and reagents for this NAAT target. The oligo template contains an

internal PEG spacer and biotin at the 5' end. Streptavidin bridges the two biotinylated species to form the conjugated detection molecule (detection antibody + streptavidin + ssDNA). (Figure 6)

	Component	Reagent		
A	*Capture Antibody*	BDBV– Ab (Baker Lab)		
B	*Analyte*	Recombinant-EBOV sGP (IBT)		
C	*Detection Antibody*	ELISA kit – Biotinylated Ab (IBT)		
D	*Oligo template*	Biotin-PEG Spacer-ssDNA		
E	*Linker*	Streptavidin		
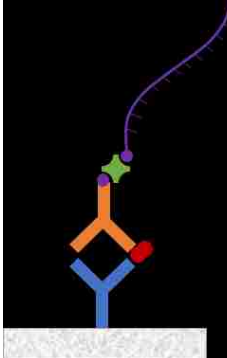
Figure 6: EBOV-sGP LFT-iSDA Assay stack: Schematic shows capture antibody test line immobilized on nitrocellulose membrane (grey rectangle); all other assay components cross the test line under flow. The detection molecule (C,D,E) and analyte are pre-mixed. Assay components are color coded.

All detection molecule reagents are at equimolar amounts (1:1:1 ratio) to maximize the number of appropriately formed conjugates (further described in section 3.5). The extant flu-NP assay guided development and optimization of the EBOV-sGP assay parameters (e.g. detection Ab concentration, buffer composition). The key differences between assays was a (1) use of new nitrocellulose material, and (2) a different antibody pair. The flu-NP assay was optimized in HF120 (Millipore, Burlington, MA, USA), a common nitrocellulose favored by assay developers that was discontinued mid-way through the EBOV-sGP development. Consequently, we developed the assay in CN-95 (Sartorius, Göttingen, Germany), a recommended alternative.

3.3   Materials and methods

The EBOV-sGP LFT-iSDA assay was developed using modifications to the previously described manual assay test card. [43] This format dips vertically oriented LFTs into the pre-filled wells of fluid

and is manually moved to successive reagent wells. The manual test card holds 12 LFTs in parallel, maximizing experimental throughput and allowing simultaneous sequential delivery of reagents.

3.3.1 LFT fabrication

The LFT immunoassay component was made from a 3 mm x 18 mm wide UniSart CN-95 membrane, comprised of cast nitrocellulose on a 100 µm clear polyester backing(Sartorius, Göttingen, Germany) joined to a cellulose wicking pad (C083, Millipore) by a Mylar adhesive backing sheet (T-5501-10/1, Fralock, Valencia, CA, USA) (Figure 7**: LFT test card schematic**)
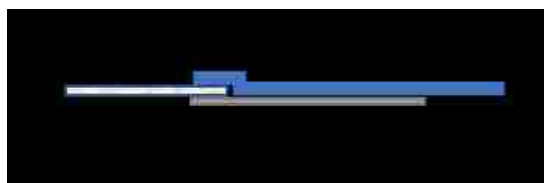
Figure 7: LFT test card schematic: Fluids flow through system from left to right. Nitrocellulose (CN-95) and cellulose wicking pad (C083) joined with Mylar backing. Not to scale.

The capture antibody, human anti-BDBV (Bundibugyo Ebola virus) monoclonal antibody (mAb) for sGP, (1 mg/ml, gift from Baker Lab) was striped to form a test line at 7 mm from the leading edge of the nitrocellulose membrane using a reagent dispenser (Biojet HR Solenoid Dispense, BioDot, Irvine, CA, USA). The striped card was dried for 2 hrs at 37°C, cut into 3mm x 18mm wide strips and stored in sealed pouches in a desiccated chamber at room temperature. Striped membranes were manually adhered to a laser-cut Mylar backing (VLS 3.60 CO_2 laser cutter, Universal Laser Systems, Scottsdale, AZ) and overlapped with laser-cut C083 wicks immediately prior to running experiment.

3.3.2 iSDA reaction

The iSDA reaction master-mix solution was prepared fresh immediately before use. The *mecA* gene target (for *S. aureus* differentiation) was selected for the iSDA reaction owing to its rapid time-to-results (<10 min), robust SBRs, and extensive characterization over a five-year period in our lab. It is

important to note that the iSDA target is entirely arbitrary; a synthetic target system could improve assay

performance, yet we chose this target due to availability of reagents and known performance. The

mechanism of iSDA is previously described. [24], [44] The master-mix was prepared in a reaction buffer

(pH 7.6) consisting of 42.5 mM potassium phosphate, dibasic (P8584, Sigma, St. Louis, MO, USA), 7.5

mM potassium phosphate, monobasic (8709, Sigma); this buffer is referred to as $KiPO_4$ buffer. The

master-mix also contains 3.75 mM magnesium sulfate (New England Biolabs, Ipswich, MA, USA), 250

µM of each dNTP (New England Biolabs), 0.2 U/µL Bst 2.0 WarmStart DNA Polymerase (NEB), 1.6%

v/v nicking endonuclease Nt.BbvCI (mutant strain, NEB), and four target-specific primers: 500 nM

forward, 250 nM reverse, 50 nM of forward and reverse bumpers (Integrated DNA Technologies,

Coralville, IA, USA). No sequence-specific detection probes were used in PAGE detection experiments.

iSDA mecA DNA sequences are found in Appendix A. The master-mix was added to a 4 x 10 mm glass

fiber pad (8950, Ahlstrom, Helsinki, Finland) as the nitrocellulose has insufficient volumetric capacity to

hold the required master-mix volume. The glass pads were laser cut (Universal Laser Systems) and

blocked with 1% (w/v) bovine serum albumin (BSA), 0.1% Tween20 solution *via* 1 hr incubation

followed by overnight drying at 37℃.

Real-time fluorescence experiments were conducted in a CFX96 Touch thermal cycler (Bio-Rad,

Hercules, CA, USA) using minor-groove binder hybridization probes (MGB-probes, Pleiades Probe,

ELITech Group, Bothell, WA, USA)) in 20 µL reaction volumes incubated between 49-50℃.

3.3.3   LFT-iSDA protocol

<u>Pre-mixed sample preparation</u>

The analyte and detection molecule were combined in a "pre-mixed sample," as the LFT lacks a

conjugate release pad. This format is commonly employed in early stage LFT assay development.

Recombinant EBOV-sGP (#0565-001, IBT Bioservices, Rockville, MD) was combined with biotinylated

detection antibody (10.19.2016-B, IBT Bioservices), streptavidin (S4762, Sigma), and incubated for 20

minutes at room temperature. Lastly, a biotinylated ssDNA *mecA* template (oEH1139 sequence,

21

Integrated DNA Technologies) was added and the solution was vortexed. The pre-mixed sample was prepared in PBS buffer with 1% (w/v) BSA (A-3249, Sigma) Concentrations of the detection molecule were varied between tests, while the molar ratios were always 1:1:1 (equimolar).

Buffer compositions

The wash (conventionally called running buffer) consisted of 1% (w/v) BSA in PBST (P3563, Sigma), with 0.8% Triton X-100 to increase stringency. The rinse buffer consisted of 1% (w/v) BSA and 0.05% Tween 20 (P9416, Sigma) in $KiPO_4$ buffer, displacing the PBS buffer with an iSDA compatible solution, as residual cations from PBS could potentially iSDA hybridization and consequent performance.

Detailed protocol

The assay protocol is broken into immunoassay and iSDA unit operations and carried out in a 96-well plate (96wp) with 12 LFT tests per test card.

Immunoassay operations were as follows: 20 µL of pre-mixed sample was added to the first row of wells in the 96wp, the test card is dipped into this well. After the entire sample volume flowed from well to nitrocellulose membrane, the card is moved to 20 µL well of PBS wash buffer, followed by 40 µL of $KiPO_4$ rinse buffer. The wicking pad was then removed to stop the flow, thus ending the immunoassay capture operation. The total time for the immunoassay is approximately 40 minutes. The nitrocellulose strip was then added to 10 µL excess $KiPO_4$ buffer to retain saturation levels prior to adding iSDA master-mix. The test card was removed from the 96wp and glass fiber pads were added directly over top of the nitrocellulose test line. A custom laser cut acrylic jig ensured alignment. Freshly prepared iSDA master-mix (10 µL) was then added to the glass fiber pad. Additional laser cut Mylar layers and PDMS seals were added to the test card to physically isolate the membranes from one another and hermetically seal the system. The sealed card is then added to a laboratory fixture "clam-shell" isothermal heater set to 50^oC for 60 minutes. (Figure 8)
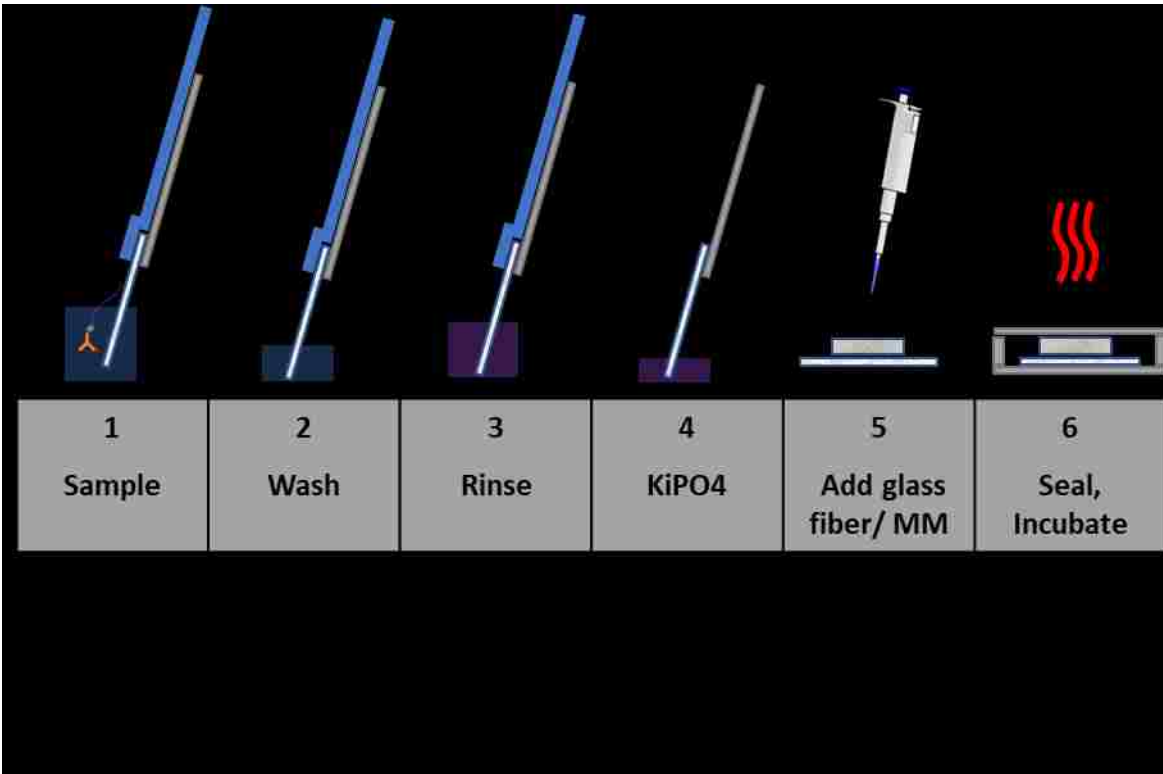
Figure 8: LFT-iSDA test card protocol: Unit operations are carried out in dipstick format in a 96-well plate with each reagent occupying its own well. The immunoassay consists of (1) pre-mixed sample added to LFT, (2) phosphate-buffered saline (PBS)-wash added to LFT, (3) KiPO$_4$-rinse added to LFT, (4) wicking pad removed and excess KiPO$_4$-rinse added to membrane to maintain saturation. A glass fiber pad (5) is placed over top of nitrocellulose membrane and filled with master-mix. Finally, the card is (6) sealed and incubated for 60 min at 50°C. Reagent volumes are shown in bottom row of table. C083 shown in blue, Mylar backing card shown in grey.

After incubation, test cards were cut into individual LFT segments, and fluid was removed from membranes *via* centrifugation. The iSDA amplicon containing extracted fluid was loaded into a 15% TBE-Urea denaturing polyacrylamide gel (Novex EC68855BOX, Invitrogen, Carlsbad, CA, USA), subject to electrophoresis (160V, 40 min), and stained with SYBR Gold nucleic acid intercalating dye (Invitrogen) and imaged with a gel reader (Gel Doc, Bio-Rad). The reagent volumes were established in

23

the LFT-iSDA Flu-NP assay. Deviations from these volumes are noted for certain experiments. Lastly, a visual protocol shows photographs of the manual protocol. (Figure 9)
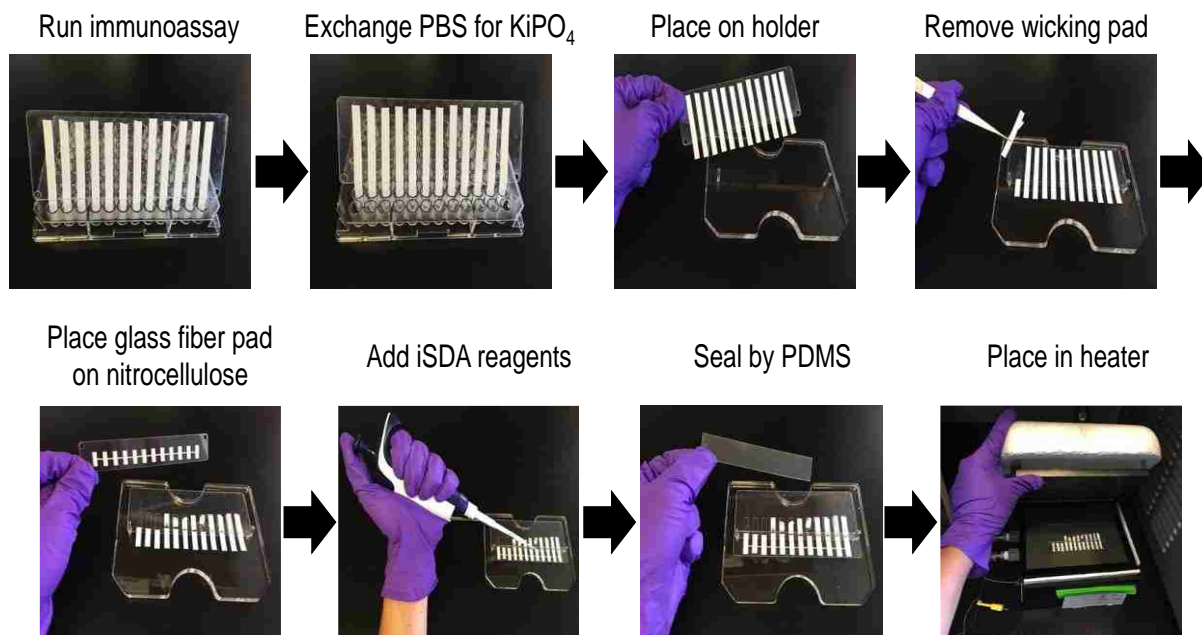
Figure 9: Visual protocol for LFT-iSDA test card format: The same protocol described above represented by photographs. Clam-shell heater shown in lower right image. Images adapted from [43].

3.3.4   Membrane blocking

Blocking buffers are often used in protein detection systems to mitigate NSB of reagents and analytes to surfaces by "blocking" the adsorption sites with generic, non-target proteins. Non-specific interactions between immunoassay components can lead to false positives (e.g. antibody cross-reactivity). "Real-time" or "live" blocking agents are added to a buffer as the LFT is under dynamic flow conditions; the blocking is in situ. "Pre-blocking" entails soaking the porous membranes in a blocking solution followed by drying at an elevated temperature to promote adsorption of proteins to the porous material. For the following blocking experiments, nitrocellulose membranes were incubated with blocking solution for 2 hrs on a shaker table, blotted with Kimwipes (Kimberly Clark, Irving, TX, USA) and dried overnight in a desiccator at room temperature. Three common ELISA blocking buffers were selected for nitrocellulose blocking: BSA(A-3249, Sigma) SEA BLOCK, (37527, Thermo Fisher-Scientific,

Waltham, MA, USA) a proprietary solution of fish serum to minimize cross reactivity with mammalian antibodies, and StartingBlock, (37538, Thermo Fisher-Scientific), a proprietary protein blend optimized for ELISA and Western blots.

3.4 Results

3.4.1 Detection molecule titration

The first objective of LFT-iSDA EBOV-sGP assay development was to determine the optimal detection molecule concentration. Excessively high concentrations can lead to NSB and consequent false positive results. Excessively low concentrations compromise overall test sensitivity, leading to false negative results at low analyte concentrations. A false positive screening test consisted of adding a negative sample containing no analyte, and only the detection molecule to the LFT-iSDA workflow. NSB of the detection molecule anywhere in at or near the test line can yield false positives, due to the extreme sensitivity of iSDA. The detection molecule was titrated from 10^9 cps / sample to 10^6 cps / sample in 10-fold increments and amplified by LFT-iSDA. The highest concentration not yielding false positives was 10^7 copies of detection molecule / sample, as detectable by PAGE. (Figure 10)
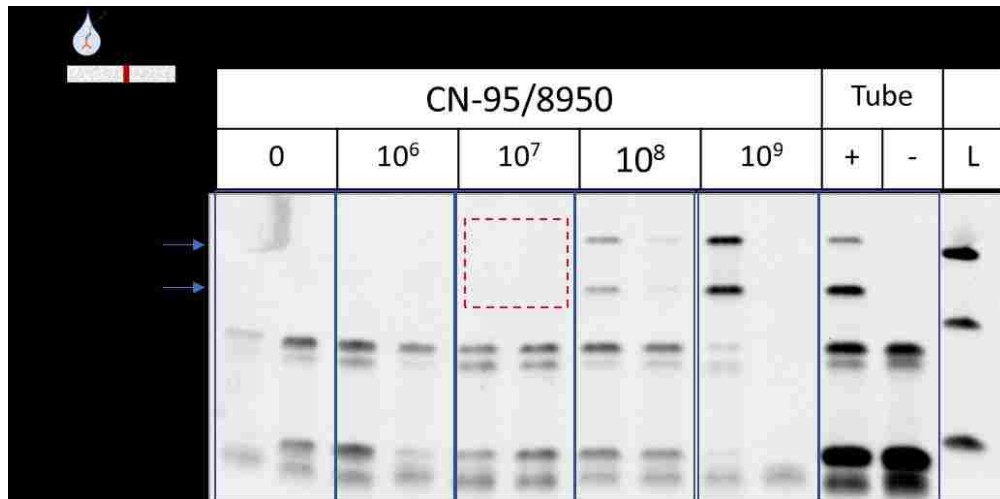
Figure 10: Detection molecule titration to 10^7 input copies/ test: Titration of detection molecule in false positive screening test. Target amplicon length is indicated by blue arrows. Tube controls and ladder are shown at right. Red box indicates the highest concentration where true negative result was obtained.

Replicates were performed at each concentration. For 10^9 cps/test, 1/2 replicates did not amplify, as indicated by absence of iSDA background reaction. Tube controls indicate functional master-mix.

After determining the optimal detection molecule concentration to prevent false positives, a test was performed to verify that the assay could generate positive results. Positive samples containing 10^{10} cps of EBOV-sGP were added to native CN-95 and 1% BSA pre-blocked nitrocellulose test conditions. Figure 11 shows false negative test results from LFT-iSDA run with 10^7 detection molecules. This result suggests that 10^7 copies/test lacks sensitivity—the concentration is too low. Consequently, 10^8 detection molecules are required to sufficiently generate a positive signal.
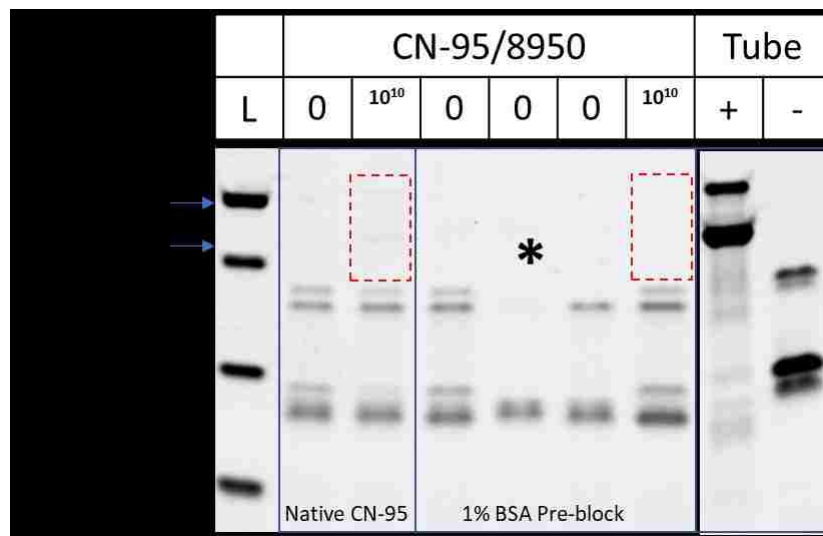
Figure 11: False negative results at 10^7 copies of detection molecule premixed with 10^{10} copies EBOV-sGP: Gel shows absence of target amplicons from sGP positive tests in both a native and 1% BSA blocked membrane. Expected bands represented by red boxes. Asterisk indicates failed iSDA reaction in 0 sGP replicate. Target amplicon length is indicated by blue arrows; tube controls indicate functional master-mix.

3.4.2   Strategies to prevent non-specific binding

Figure 10 shows that 10^8 detection molecules per test generated false positives yet may be required to prevent false negatives as indicated by Figure 11. The assay development goal thus shifted toward preventing false positives at 10^8 detection molecules / test. One approach to suppressing the detection molecule NSB to acceptable levels is pre-blocking the nitrocellulose membrane. Membranes were pre-blocked with three common protein blocking agents and subject to a false positive screening test. (Figure 12)
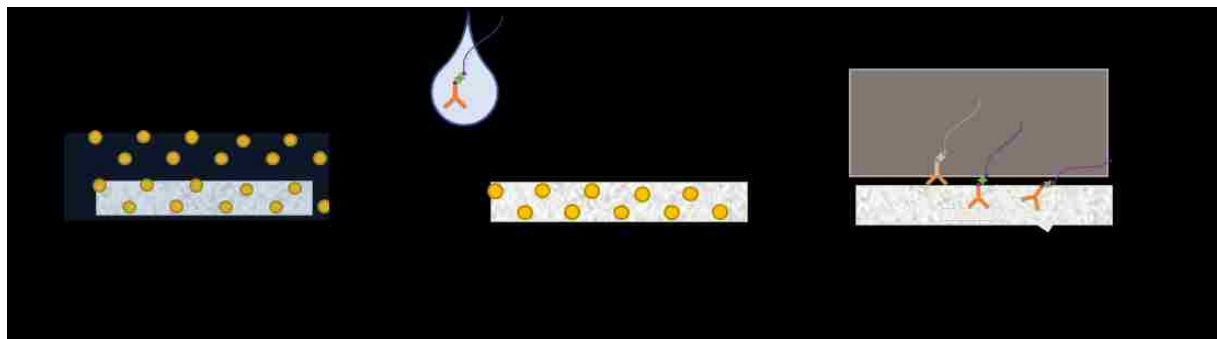
Figure 12: Pre-blocking of nitrocellulose workflow: (1) Membranes are pre-blocked, dried, desiccated, and (2) subject to LFT-iSDA false positive screening test. Yellow circles represent blocking agents, visualization of NSB shown by detection molecules adsorbed to near test line (3).

Table 2 shows results of false positive screening test at various concentrations of pre-blocking buffer. All blocking buffers showed no reduction of the false positive signal by gel detection. Gel image raw data are available in Appendix A (Section 7.3)

Table 2: Membrane pre-blocking to mitigate NSB at 10^8 detection molecules / test: None of the blocking buffers were effective at preventing false positives. Asterisks indicate tests where iSDA did not amplify target due to unidentifiable background competition; we theorized that the StartingBlock buffer contained genomic DNA which competed with the target for reaction resources.

Fraction of false positives by gel detection (# false positives / # total tests)				
Concentration	**0**	**0.1 X**	**0.5 X**	**1 X**
StartingBlock	3/3	3/3	1/1*	2/2*
SEA BLOCK	3/3	3/3	3/3	3/3
Concentration	**0%**	**1%**	**5%**	**10%**
BSA	2/2	3/3	3/3	3/3

3.4.3   Source of non-specific binding

After protein-based blocking buffers proved ineffective against NSB / false positives, we reasoned that identification of the source of NSB was critical to direct blocking strategies. LFT-iSDA false positive screening shows results from incremental truncation of the detection molecule from the complete combination of biotinylated ssDNA-streptavidin-biotinylated detection antibody to reduction of biotinylated ssDNA-streptavidin only. (Figure 13) Variations also included a complete detection molecule with the complementary strand to the biotinylated ssDNA , forming a dsDNA template. This tested a hypothesis that ssDNA adsorbs to nitrocellulose via hydrophobic interactions between the exposed nucleotide bases and the membrane; by annealing the complement to the ssDNA, we theorized that the hydrophobic interactions would be shielded in dsDNA, as the hydrophilic sugar-phosphate backbone is outward facing and less "sticky". Similarly, a dsDNA-streptavidin molecule was tested. Additionally, a condition of pre-wetting the nitrocellulose membrane with PBS buffer prior to adding the complete detection molecule tested the hypothesis that the leading edge of sample wetting out a dry nitrocellulose membrane would have greater NSB than a pre-wetted membrane.
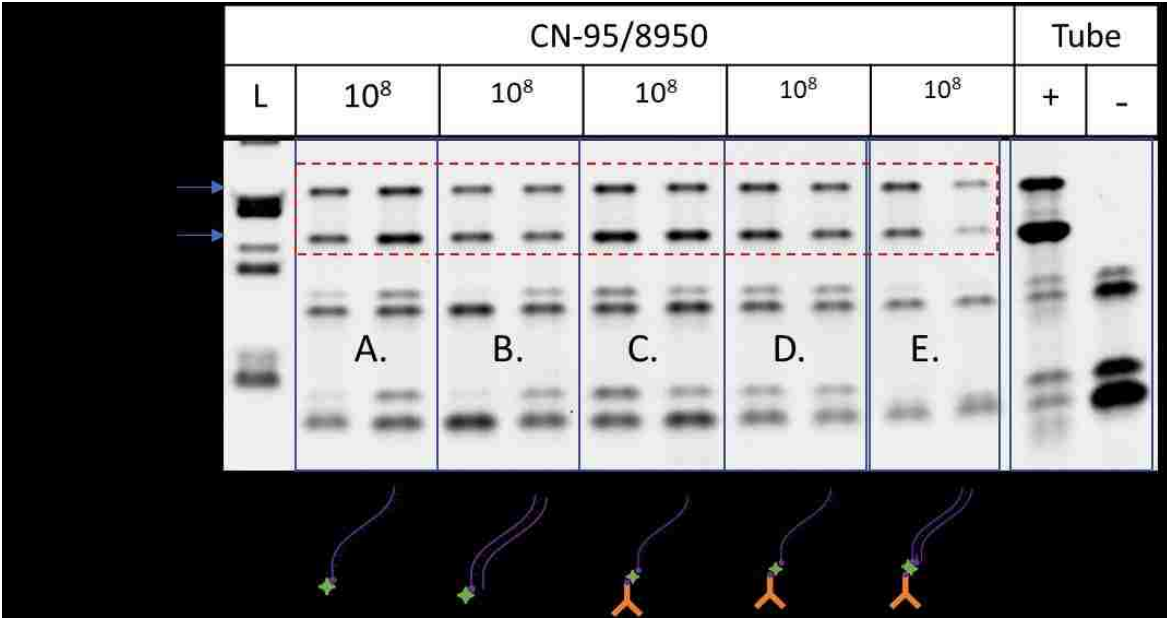
Figure 13 Truncation of detection molecule to isolate dominant source of NSB in false positive test: Gel image shows results from false positive screening test with detection molecule variants. The variations include: (A) streptavidin-biotinylated ssDNA, (B) streptavidin-biotinylated dsDNA, (C) complete detection molecule (detection Ab-streptavidin-biotinylated ssDNA), (D) a pre-wetted membrane with the complete detection molecule, and (E) complete detection molecule with dsDNA. All variants show false positives indicating NSB of the molecule to nitrocellulose. Target amplicon length is indicated by blue arrows; tube controls indicate functional master-mix. N=2 performed for each test condition.

To even further simplify the detection molecule, the biotinylated ssDNA and ssDNA-only templates were also tested. At 10^8 copies / test, both variants yielded false positives. At 10^7 copies / test, both variants showed true negative results; this outcome is consistent with detection molecule titration experiment. (Figure 14)
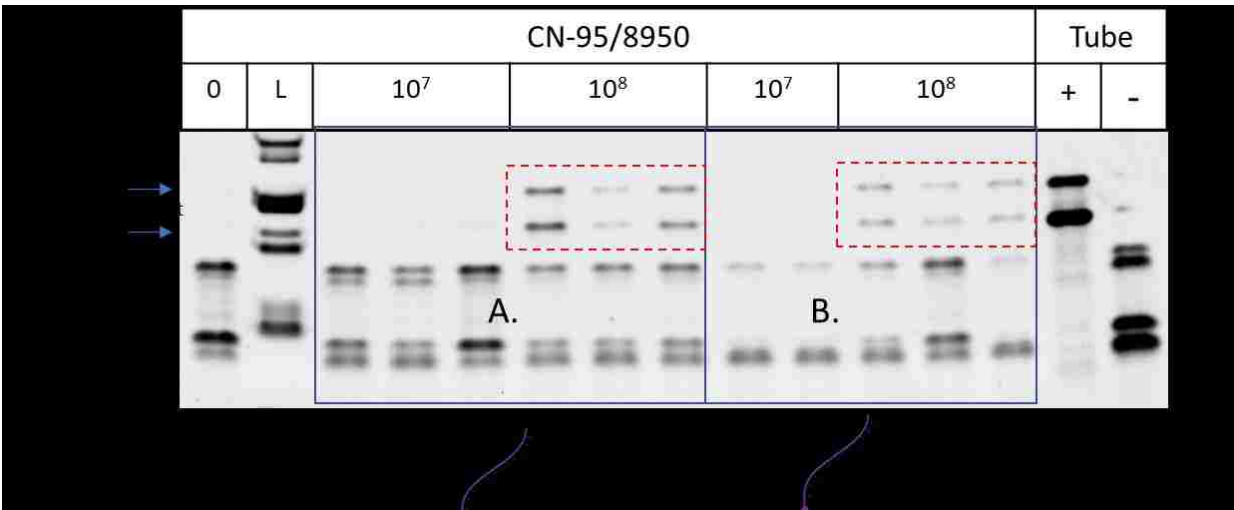
Figure 14 Further truncation of detection molecule to isolate NSB: Gel image shows tube controls in right-most lanes and ladder in left lane. The iSDA reaction was had a shorter incubation time of 30 minutes. Both the ssDNA (A) and biotinylated-ssDNA tests show false positives at 10^8 copies (n=3) and true negatives at 10^7 copies / test (n=2). Target amplicon length is indicated by blue arrows; tube controls indicate functional master-mix.

Results indicate that the dominant source of NSB between detection molecule and nitrocellulose is the ssDNA *mecA* template, as this component is common to all test conditions yielding false positives. While other components undoubtedly contribute to some NSB, ssDNA appears to dominate the interaction.

In parallel to the EBOV-sGP assay development, Flu-NP LFT-iSDA demonstrated that sheared salmon sperm DNA (D9156, Sigma) can be used as a real-time blocking agent to mitigate false positives at 10^8 copies / test. The mechanism of action is likely a combination of ssDNA blocking and iSDA inhibition. [43]

3.4.4 Detune signal amplification sensitivity

An alternative strategy to reducing false positives was to reduce the sensitivity of the iSDA reaction. This approach sacrifices overall LFT-iSDA sensitivity at the expense of increasing the acceptable level of NSB.

A known method of introducing a competitor IAC template which amplifies using the same primers as the target but with a unique probe sequence and fluorophore label was used to reduce iSDA sensitivity. IAC amplicons compete for dNTPs, primers, and enzymes in the multiplexed reaction. Figure 15 shows increasing input IAC concentrations decreased the *mecA* target lowest detectable concentration from $< 10^2$ cps / reaction (0 IAC) to $<10^4$ cps / reaction (10^6 IAC). The experiment demonstrates that IAC competition is a viable strategy to decrease iSDA efficiency and sensitivity, thus lifting the acceptable level of NSB in the LFT operations. However, the method was not applied to LFT-iSDA format.
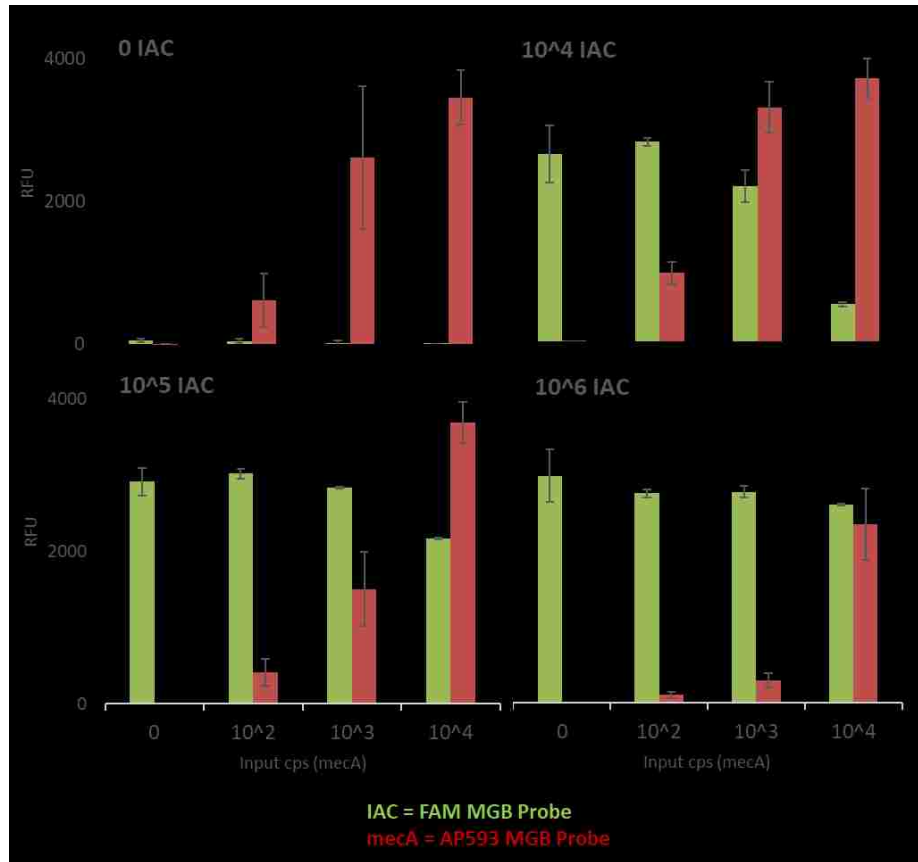
Figure 15: Competitive IAC to reduce sensitivity of iSDA: A multiplexed iSDA reaction of target *mecA* sequence and internal amplification control (IAC) sequence shows reduced target sensitivity with increasing concentrations of IAC template. FAM-labelled (IAC) and AP593-labelled (mecA) fluorescent probes were used to detect amplicon generation. Y-axis shows endpoint RFU measurements taken at t=30 minutes, X-axis shows input *mecA* template copies / reaction. Upper left corners of each panel show input IAC copies / reaction. Error bars show standard deviation (n=3).

3.5   Discussion

3.5.1   Detection molecule may be affinity limited

Titration of the EBOV-sGP detection molecule to 10^7 copies / test was necessary to prevent false positive results (Figure 10), yet failed to generate true positives in the presence of the analyte (Figure 11). This suggests that the detection antibody affinity may limit LFT-iSDA feasibility. The flu-NP assay high affinity antibodies (Capture-Ab equilibrium dissociation constant (K_d) = 4.0 x 10^{-13} M, Detection-Ab K_d =

3.58 x 10^{-10} M), as measured by our group on an Octet system (ForteBio, Menlo Park, CA), demonstrated sufficient binding in the LFT-iSDA format; the assay LOD was ~10^5 copies of flu-NP/ test. Given this baseline, we hypothesized that relatively high-performing antibodies may be essential to compensate for the low concentration of detection molecules in the system. Unfortunately, we could not obtain the K_d of the EBOV-sGP detection antibody from the manufacturer to evaluate this hypothesis. Using a basic binding reaction model of the sandwich immunoassay stack, the relationship between K_d and theoretical assay performance was analyzed. (Figure 16)
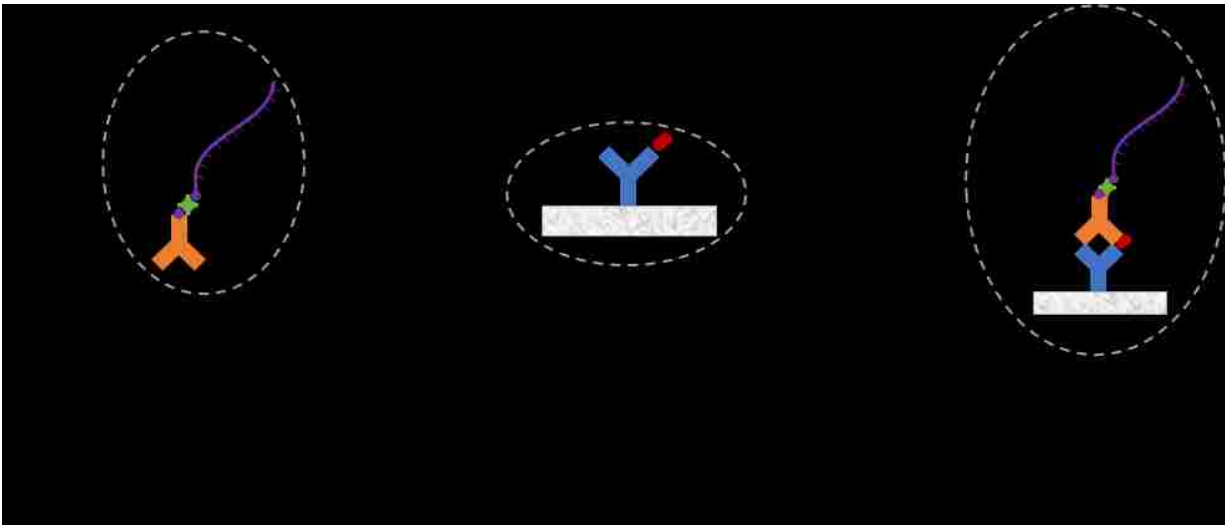
Figure 16: Simplified binding model investigating performance dependency on K_d : [A] is the concentration of detection molecules flowed through the system, [B] is the concentration of analyte bound to the capture antibody, and [AB] is the concentration of sandwich immunocomplexes capable of initiating iSDA. Equation shows the reaction as function of K_d of detection antibody to analyte.

The model assumes the detection molecule biotin-streptavidin bonds do not dissociate (i.e. the ssDNA is covalently attached to the antibody), and that all analytes bind to the capture antibody with no dissociation (i.e. 100% capture efficiency). Strongly limiting assumptions are that (1) the system is not under flow, (2) that species exist in a static 100 µL environment, (3) the reaction reaches dynamic

chemical equilibrium. The minimum [AB] required to generate an iSDA positive test was approximated

as 10^4 copies of the immunocomplex per reaction. Detailed assumptions outlined in Table 3. At

equilibrium, Equation 1 shows the relationship between model parameters.

Equation 1: Simplified binding model equilibrium dissociation constant

$$K_d = \frac{[A][B]}{[AB]}$$

Table 3: Binding Model Parameters

	Parameter	Assumptions
K_d	Equilibrium dissociation constant of detection antibody to analyte	Biotin/Streptavidin $k_{off} \sim 0$ / detection molecule is covalently attached.
A	Detection molecule	Reaction volume is 100 µL. No flow condition.
B	Analyte—Capture Ab complex	[B] is analyte concentration (i.e. all analyte is bound). $k_{off} \sim 0$
AB	Sandwich immunocomplex (full stack)	10^4 cps required to initiate iSDA + amplification in nitrocellulose/glass fiber system

Using the above assumptions and Table 3, Figure 17 shows theoretical LOD plotted against

detection antibody affinity. The baseline Flu-NP antibody (K_d = 3.58 x 10^{-10} M) roughly correlates to the

measured LOD of 5.4 x 10^4 copies/test at 10^8 copies detection molecule. Lines showing detection

antibody / test illustrate the sensitivity loss resulting from lower concentrations of detection molecule.

The blue oval overlays predicted assay performance for low affinity antibodies (>100 nM) across

different detection-Ab concentrations. Although we do not have K_d values for the sGP antibodies, they

could conceivably fall within the low affinity, poor sensitivity regime. This hypothesis may explain false

negative results in Figure 11. The model is limited by its coarse assumptions but suggests that the LFT-

iSDA promise for high sensitivity may hinge on a requirement of high affinity antibodies. This

preliminary analysis could be expanded upon by modeling binding under flow conditions in porous media

and realistic, non-zero k_{on} and k_{off} rates of binding events.
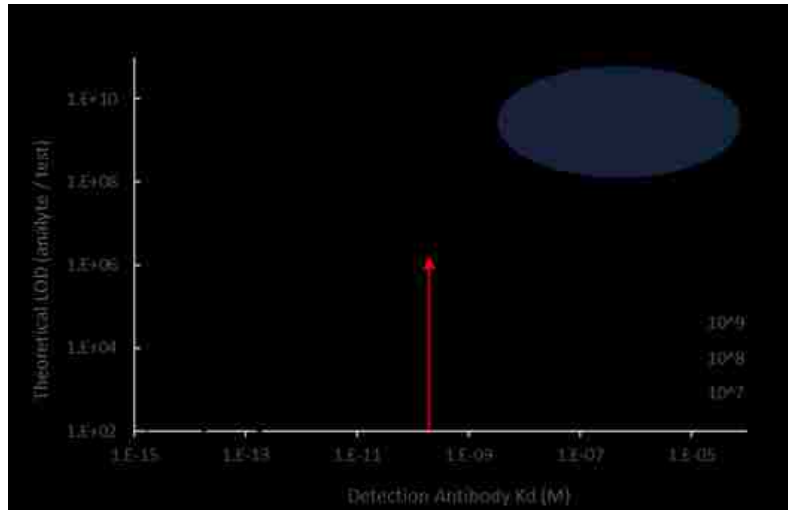
Figure 17: LFT-iSDA theoretical performance as a function of detection antibody affinity:
Theoretical LOD (analyte copies / test) is plotted (log-log plot) as a function of detection-Ab K_d for varying input detection-Ab per test (black lines). Red arrow shows predicted performance of the Flu-NP assay given its known K_d. The blue oval highlights a regime where low affinity antibodies may contribute to poor overall test sensitivity.

3.5.2   Blocking strategies must target the dominant source of NSB

Pre-blocking strategies proved to be ineffective against NSB false positives (Table 2). These agents are traditionally used to block protein-protein interactions in ELISA and protein-nitrocellulose interactions in Western blots and LFTs. The negative results of these experiments may be expected after identifying the dominant source of NSB in the system was the biotinylated ssDNA template. (Figure 13) Thus, future blocking strategies must aim to reduce ssDNA NSB to nitrocellulose, as used in Southern blot experiments to reduce hybridization background levels. The salmon sperm DNA blocking strategy came from this realization. To further support the hypothesis that NSB is dominated by ssDNA and nitrocellulose, and not attributable to cross-reactivity between capture and detection antibodies, Figure 10 was also performed without an immobilized capture antibody (test line). The test showed similar results,

suggesting minimal differences with and without test line. (Data in Appendix A: sGP Detection molecule titration in membranes without test line).

3.5.3   Estimation of NSB in nitrocellulose membrane.

We empirically determined both the maximum concentration of detection antibody which prevented false positives (between 10^7 and 10^8 copies / test) and the lowest detectable concentration of biotinylated ssDNA amplifiable by LFT-iSDA in a static system (no flow); these values can be used to quantitatively approximate NSB in the system.

Figure 18 shows gel result from a modified LFT-iSDA protocol where mock sample (no detection molecule, 70 µL), wash (20 µL), and rinse buffers (40 µL) were flowed through the nitrocellulose, followed by removal of the wicking pad, and addition of varying concentrations of biotinylated ssDNA. At this state the nitrocellulose is close to full saturation, after which a glass fiber pad filled with master-mix is added on top. The flow of buffers through the system mimics the rinsing of the nitrocellulose to approximate the state prior to iSDA master-mix addition. This modified protocol allowed control of the input copies of ssDNA to estimate the sensitivity of iSDA in the stack of nitrocellulose and glass fiber pads. The test showed positive amplification down to $10^3 - 10^4$ copies of biotinylated ssDNA, roughly two orders less sensitive than in glass fiber only (in buffer solution, previously demonstrated by our group). We hypothesize that this lower sensitivity may come from the spatial separation of DNA template and master-mix; minimal bulk flow between membranes requires diffusion of either template to master-mix or vice versa. Additionally, due to the known property of proteins adsorbing to nitrocellulose, we reason that a fraction of enzymes may adsorb to its surface and become knocked out of the reaction, thus reducing iSDA efficiency compared to a glass fiber membrane only format. [49]
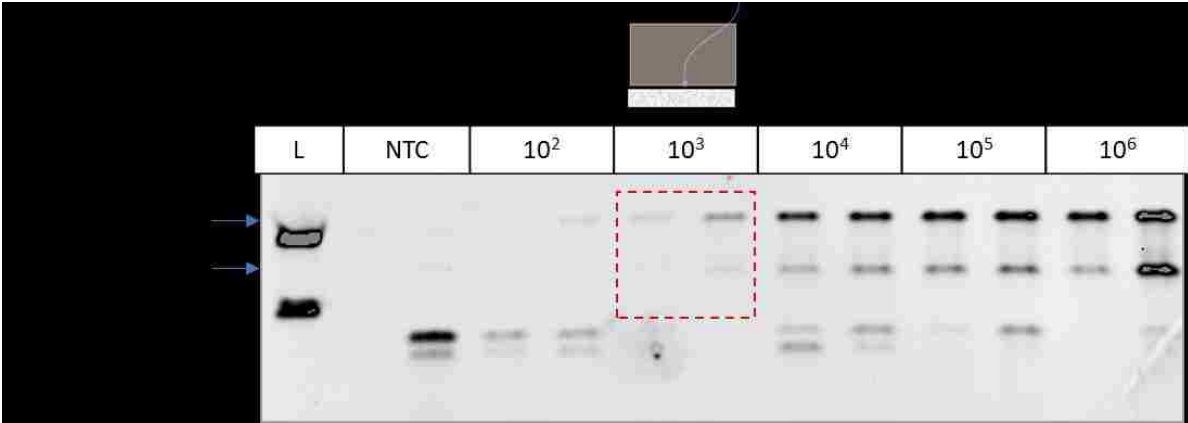
Figure 18: Lowest detectable concentration (LDC) by iSDA of static system: Gel image shows results from a modified LFT-iSDA protocol to study sensitivity in a static system. Known amounts of biotinylated ssDNA added to washed and rinsed nitrocellulose membranes (with no wicking pad), then amplified by iSDA. Red box outlines lowest detected concentration of 10^3 copies / test. Target amplicon length is indicated by blue arrows.

Using these data, the percentage of detection molecules subject to NSB can be estimated by Equation 2.

Equation 2: Estimation of NSB in nitrocellulose membrane

$$\frac{LDC\ iSDA\ in\ static\ system}{Detection\ molecule\ concentration\ yielding\ false\ positives} = \frac{\sim 10^3}{\sim 10^7} copies\ per\ test \cong 0.01\%\ NSB$$

This approximation reveals the high stringency washing of unbound detection molecule required to prevent false positives in LFT-iSDA format. To address this assay requirement, the combined approach of large wash and rinse volumes (20, 40 µL respectively), 0.8% Triton X-100 detergent in the wash buffer, and low concentration of detection molecule have proven successful in the flu-NP assay. A key limitation of this analysis is that the static system LDC had a uniformly distributed template across the nitrocellulose, whereas an actual LFT-iSDA test has a discrete, high concentration test line of bound template. Local concentrations, as well as absolute copy number may affect how iSDA initiates from a porous membrane system.

3.5.4　DNA adsorption to nitrocellulose

Figure 13 isolates the ssDNA as the dominant source of detection molecule NSB to nitrocellulose. Nitrocellulose is a hydrophobic substrate; this property is likely (electrostatic contributions are also possible) the source of its ability to immobilize proteins in LFTs. [50] It has been demonstrated that ssDNA adsorbs stronger than dsDNA to hydrophobic surfaces. Short ssDNA (146bp) was shown to adsorb to hydrophobized silica beads at 0.57 mg/m^2 compared to the dsDNA sequence (complement strand added) binding at 0.08 mg/m^2. In this same experiment, ellipsometry measurements revealed a ssDNA layer was 18 Å thick, whereas a dsDNA layer was 145 Å thick. The 7-fold larger amount of ssDNA adsorption indicates stronger interaction, while the layer thickness suggests ssDNA strands are parallel to the surface. [51] These results can be explained by the greater flexibility and hydrophobicity of ssDNA compared to dsDNA. As dsDNA is held together by a balance of hydrophobic and stacking attractions between nucleotide bases and electrostatic repulsion, it has fewer hydrophobic nucleotide bases exposed than ssDNA. Conceivably the ssDNA strands lie flat on the hydrophobic surface. Figure 19 presents a graphical representation of the proposed NSB between the ssDNA domain of the detection molecule, and the hydrophobic nitrocellulose pore wall.
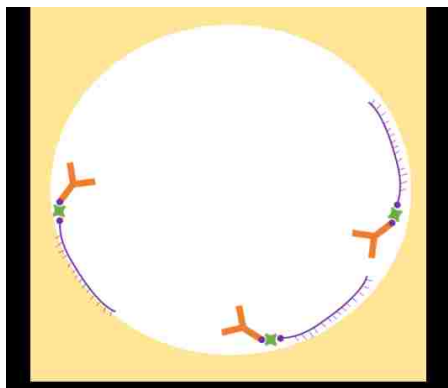
Figure 19: Proposed mechanism of detection molecule adsorption to nitrocellulose: Detection molecules adsorb to nitrocellulose pore surface by the ssDNA domain. The exposed hydrophobic nucleotides lie flat on the pore surface. Nitrocellulose pore walls is tan, ssDNA is purple. Schematic not

to scale. Nitrocellulose pores in CN-95 are nominally 10 µm (true distribution is heterogeneous), while detection molecules are ~100 nm long.

However, a potential weakness of this hypothesis is that NSB bound ssDNA still initiates iSDA, indicating the nucleotide sequence is accessible to primer annealing and enzyme activity. We hypothesize that at elevated temperatures of 50℃ during iSDA incubation, the ssDNA may release from the nitrocellulose, thus freed to participate in the reaction. Further investigation is required.

3.5.5   Detection molecule conjugation

The detection molecule concentration is a critical parameter to LFT-iSDA performance, yet biotin-streptavidin linkages can cause a large distribution of variant complexes in multi-state equilibrium. Some of these complexes can both form the target immunocomplex and amplify by iSDA, while others form the immunocomplex and are un-amplifiable by iSDA, while others do not form the immunocomplex, both depleting reagents and potentially causing false positives. (Figure 20) We reasoned that 1:1:1 stoichiometric ratios would yield the highest fraction of target species in the reaction yet did not validate this assumption. Inarguably, a truly homogenous detection molecule reagent achieved by direct conjugation of ssDNA to antibody or combinatoric optimization of biotin/streptavidin molar ratios would be favorable for future work. (Figure 20)
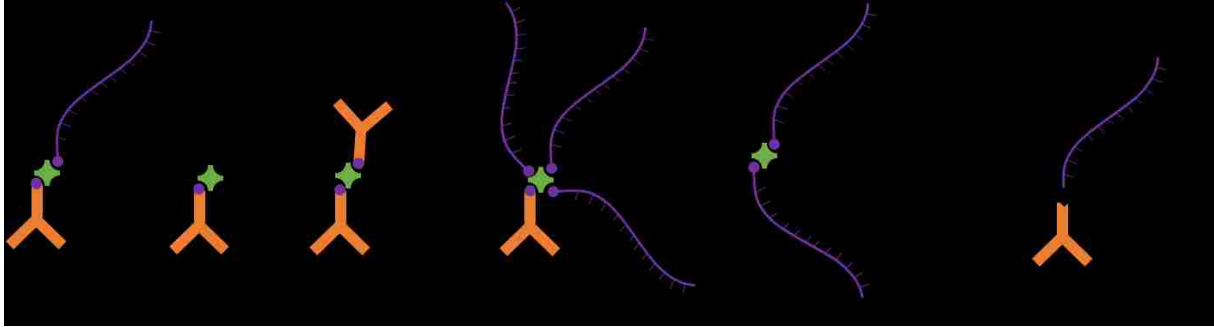
Figure 20 Distribution of possible detection molecule complexes at equilibrium of SA-Biotin linkage: Examples of possible complexes present in the pre-mixed detection molecule. Complex (A) is the preferred and assumed dominant species. Complexes (B) and (C) can form the target immunocomplex (sandwich of capture-Ab:antigen:detection-Ab) but will yield false negative test results as they lack the ssDNA template. Complex (D) and (E) deplete ssDNA from the pre-mixed solution; (D) can form the target immunocomplex and yield positive iSDA results, while (E) cannot form target immunocomplex. (F) represents a direct Ab-ssDNA conjugation which would ensure a single detection molecule species. Six of the 14 multi-molecule combinations possible are capable of both detecting and amplifying.

3.6   Conclusions

Attempting to demonstrate the LFT-iSDA with an EBOV-sGP analyte revealed important principles of the assay performance, and generated hypotheses explaining limitations of this platform. We propose that the detection antibody affinity may limit the feasibility of this assay, where high affinity reagents may be required to compensate for low concentrations of the detection molecule. Protein-based blocking agents were shown to have little to no effect on preventing false positives in the system. We isolated ssDNA as the dominant source of NSB between detection molecule and nitrocellulose; results from literature support this hypothesis. The degree of NSB was estimated at ~0.01% of the detection molecule; future use of qPCR assays could improve this approximation. IAC competition was shown to effectively reduce iSDA sensitivity, enabling a higher NSB ceiling to prevent false positives, although not pursed in LFT-iSDA. The EBOV-sGP assay was not pursued beyond these experiments, although these results shed insight into the fundamental challenges and considerations in the LFT-iSDA format.

4 FLUORESCENCE DETECTION

4.1 Objectives

PAGE and secondary gold-nanoparticle lateral flow detection of amplicons generated from LFT-iSDA is a time-consuming and laboratory-constrained detection modality. Both methods require removal of fluid from the porous media by centrifugation and extensive downstream processing before obtaining an endpoint result. This chapter investigates the use of fluorogenic hybridization probes to provide rapid and real-time detection of amplicons in LFT-iSDA systems. The objective is to identify a fluorescent probe system suitable for the materials, assay, and envisioned optical system to detect LFT-iSDA within the time and sensitivity requirements outlined in Point of care diagnostics design criteria in section 2.1.

4.2 Introduction

Fluorescence is the phenomenon in which an electron in an atom or molecule is excited by an incident photon from its ground state to a higher energy level. The excited molecule then loses vibrational energy and consequently drops back to a lower energy level, resulting in emission of another photon at a lower energy than the excitation photon. In spectral terms, excitation of a shorter wavelength photon results in emission of a longer wavelength photon (e.g. 495 nm excitation (blue) -> 520 nm emission(green) for FAM; the Stokes shift describes this wavelength difference. Fluorophores are molecules exhibiting fluorescence and are conjugated to detection systems in bioassays for innumerable applications. Fluorophores with different spectral properties enable multiplexed reactions with differentiation by optical filtering of excitation and emission wavelengths.

Fluorescence detection of NAATs utilize fluorescent molecules that only emit light in the presence of a positive amplification event. When held in close proximity, quenching molecules prevent the emission of light from the fluorophores, and when used in tandem, increase SBR in detection events. Methods are either endpoint measurements—occurring after completion of the amplification, or real-time measurements—where signal is measured during amplification *in situ*. Detection can either be non-

specific—where production of any dsDNA is probed (i.e. intercalating dye), or sequence-specific—only

target DNA produces fluorescence signal (e.g. hybridization probe). Table 4 highlights several common

methods for fluorescence detection of nucleic acid systems. Assuming a clear optical path, fluorescence

allows direct observation of amplification products, providing spatial and temporal information of

multiple species without secondary operations.

Table 4: Fluorescence detection methods

Method	Mechanism	Design Considerations	References
Minor-groove binder (MGB) probe	Sequence specific hybridization with additional MGB binding to dsDNA complex. MGB provides quenching in addition to fluorophore and quencher interaction.	High SBR, demonstrated with iSDA, temperature independent background	[52]
Molecular beacon (MB)	DNA hairpins made of self-complementary "stem" and target complementary "loop" regions. quencher and fluorophore are conjugated to opposing stem ends and quenched in closed conformation, signal produced when loop hybridizes to target, overcoming stem conformation	Potentially low SBR due to fraction of probes in open conformation at amplification temperatures (stem melting). Slower hybridization rates than MGB-probes.	[53], [54]
Intercalating dye	Small molecule fluorophores bind to dsDNA non-specifically. Low signal in presence of ssDNA.	Can inhibit real-time reaction, nonspecific to dsDNA makes multiplexing impractical.	[55], [56]
Hydrolysis probes	Hybridize to complementary target, exonuclease pol liberates quencher from close proximity to fluorophore, producing signal.	Requires 5'->3' exonuclease activity lacking in Bst 2.0 polymerase used in iSDA.	[57]

4.3   Materials and methods

4.3.1   Lateral flow challenge on nitrocellulose

Nitrocellulose membranes (CN-95, Sartorius) were laser cut to 5 mm x 30 mm strips and joined

to cellulose wick (C083, Ahlstrom) with PDMS tape with a 3mm membrane overlap. The strips were

placed on the inverted epifluorescence microscope stage (Axiovert 25/ 1X objective, Carl Zeiss AG,

Oberkochen, Germany). Membranes were pre-wetted with DI water to near saturation and 1 µL of MGB-

AP593 *mecA* probe (4 µM) and Texas Red (4 µM in PBS) fluorophore were pipetted in the centers of

adjacent nitrocellulose strips. After 1 min, DI-water wash buffer was added in 10 x 50 µL increments to the leading edge of the strips under lateral flow. Fluorescence images were taken at 10 second intervals at 1500 ms exposure, 20x gain, 70 offset with 1x objective using FITC/TXRED-A-000 dual pass filters (Semrock, Rochester, NY) with color CCD (Retiga EXi, Q imaging, Surrey, BC, Canada).

4.3.2   Porous membrane overlap iSDA testing

LFTs were made as follows: nitrocellulose membranes (CN-95, Sartorius or FF80, GE, Boston, MA) were laser cut into a comb pattern with 5 mm wide widths, overlapped with cellulose wicks (C083, Ahlstrom) and adhered to a 10 mil Mylar backing (Fralock)by double sided PDMS tape (ARclad® IS-7876,182 Adhesives Research, Glen Rock, PA, USA) into a test card assembly with 12 parallel LFTs. The following buffers were flowed through the LFT in 96wp dipstick format: (1) 70 µL mock-sample buffer (i.e. no analyte) consisting of 1% BSA (w/v) in PBS, (2) 20 µL wash consisting of 1% (w/v) BSA in PBST (P3563, Sigma) 0.8% Triton X-100, (2) 40 µL rinse buffer consisted of 1% (w/v) BSA and 0.05% Tween 20 (P9416, Sigma) in $KiPO_4$ buffer. This sequence of buffers mimics the LFT-iSDA assay parameters previously establish to approximate the washing that the nitrocellulose would experience prior to iSDA. The test card was then removed from the 96wp, wicks removed, and laser cut glass fiber pads (5x12 mm pre-blocked with 1% BSA(w/v), 0.1% Tween20) were overlapped 5 mm. Fifteen (15) µL of iSDA master-mix and probe was then added to the glass fiber. Positive tests contained 10^8 copies of template with iSDA master-mix, negative samples contained the iSDA master-mix with no template or enzymes. The test card was then sealed with PDMS tape and incubated at 50°C for 60 min in "clam-shell" isothermal heater. Endpoint measurements were then taken on inverted fluorescence microscope (at 1500 ms exposure, 20x gain, 70 offset with 1x objective and previously noted CCD/filters). Figure 21 shows a graphical representation of the workflow. This test was conducted over multiple nitrocellulose and probe types.
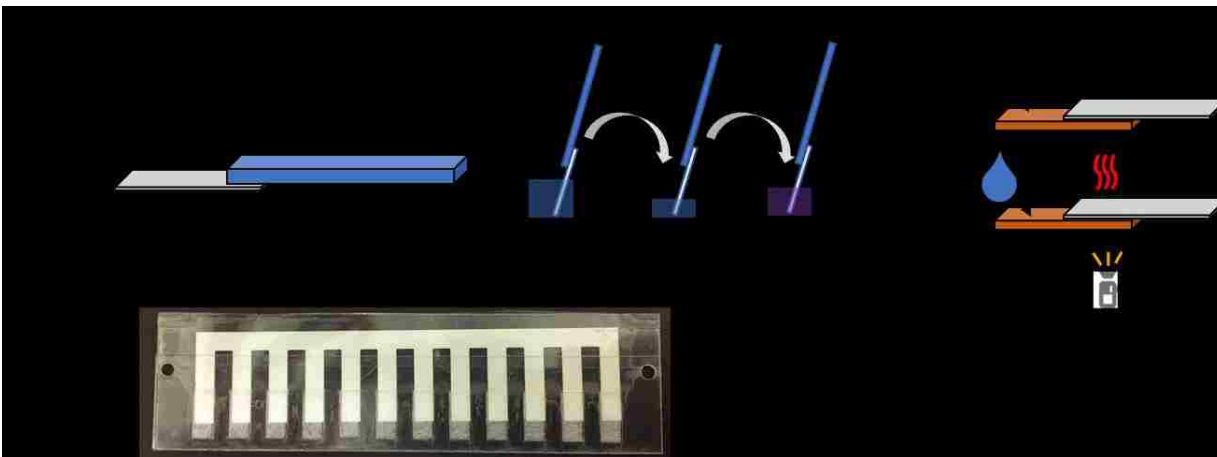
Figure 21: Membrane overlap testing method summary: (A) Nitrocellulose strips were overlapped with cellulose wicks and assembled into a test card. (B) Test cards were then dipped sequentially into 96wp rows containing (1) 70 µL mock sample (no analyte), (2) 20 µL PBS-0.8% Triton wash buffer, (3) 40 µL KiPO$_4$ buffer to simulate the immunoassay operation rinsing of nitrocellulose. (C) The wicking pad was removed; a glass fiber pad was added to the system. (D) 15 µL of iSDA positive (10^8 input template) or iSDA negative (no enzymes, no template) was added to the glass fiber end. Endpoint fluorescence measurements were taken on inverted fluorescence microscope.

4.3.3   Molecular beacon probe screening on real-time thermal cycler

Experiments characterizing molecular beacons used the previously detailed protocol (3.3.2 iSDA reaction) with the addition of molecular beacon and MGB-probes.

4.3.4   Side-pad lyophilization

Glass fiber membrane pads were laser cut into 3.67 x 11 mm rectangles and pre-blocked by soaking in 1% BSA(w/v) and 0.1% Tween-20 for 1 hour, blotted dry, and dried in an incubator at 45°C overnight. A probe solution of 5 mM KiPO$_4$ buffer, 10% Trehalose, 2.5% dextran, and 0.6 µM AP-593 MGB-probe was prepared. Glass fiber pads were arranged in a polystyrene 6wp and 6 µL of the probe solution was to one end of each pad. The pads were then flash frozen in liquid nitrogen and dried overnight in a lyophilizer (FreeZone 4.5, Labconco, Kansas City, MO).

4.3.5   Side-pad LFT-iSDA tests

LFT-iSDA Flu-NP tests were run with MGB-probe side-pads to generate real-time fluorescence curves using the inverted fluorescence microscope. Sample, wash, rinse volumes and composition are unchanged from 3.3.3 LFT-iSDA protocol; recombinant flu-NP (Brisbane/10/2007 [H3N2], International Reagent Resource, Center for Disease Control and Prevention, Atlanta, GA, USA) was substituted for EBOV-sGP analyte. iSDA master-mix concentrations are also unchanged from previous methods, yet the volume was increased to 13 µL to accommodate geometry change of the side-pad. The wider side-pad modified the test card to include only 6 LFTs per test—the test card was changed accordingly.

Real-time measurements required an optical path to the membranes, so a microscope stage mounted, custom laboratory clamshell heater was constructed. (Figure 22) The bottom heated surface (100x150 mm) was made from 1.1 mm thick indium tin oxide (ITO) glass(17 Ohm/sq, Huanyu Instrument, Amazon, Seattle, WA, USA), an optically clear, electrically conductive material. The top heater used an aluminum plate to distribute heat produced by thin-film resistive heaters. The heaters were fixed in laser-cut PMMA housings and fastened with double-sided adhesives. Separate temperature controllers (Watlow, St. Louis, MO, USA) were used to control set-points of heaters independently. Fluorescence images were taken at 1 minute intervals at 1500 ms exposure, 20x gain, 70 offset with 1x objective and previously noted CCD/filters. During amplification, the stage was translated manually to index points between strips to construct discrete, real-time curves, as the objective field of view only covered 1 strip per image. Heater set-points were empirically tuned to provide $50^{\mathrm{o}}C + /- 1^{\mathrm{o}}C$ over the area of the test card. The wider than ideal temperature envelope was due to large thermal gradient across the ITO-glass heater. RFU measurements are 0-255 values in the R-channel of the color CCD image. ImageJ was used to measure mean pixel intensity over a 5x5 mm region of interest (ROI) centered on either overlap or side-pad region.
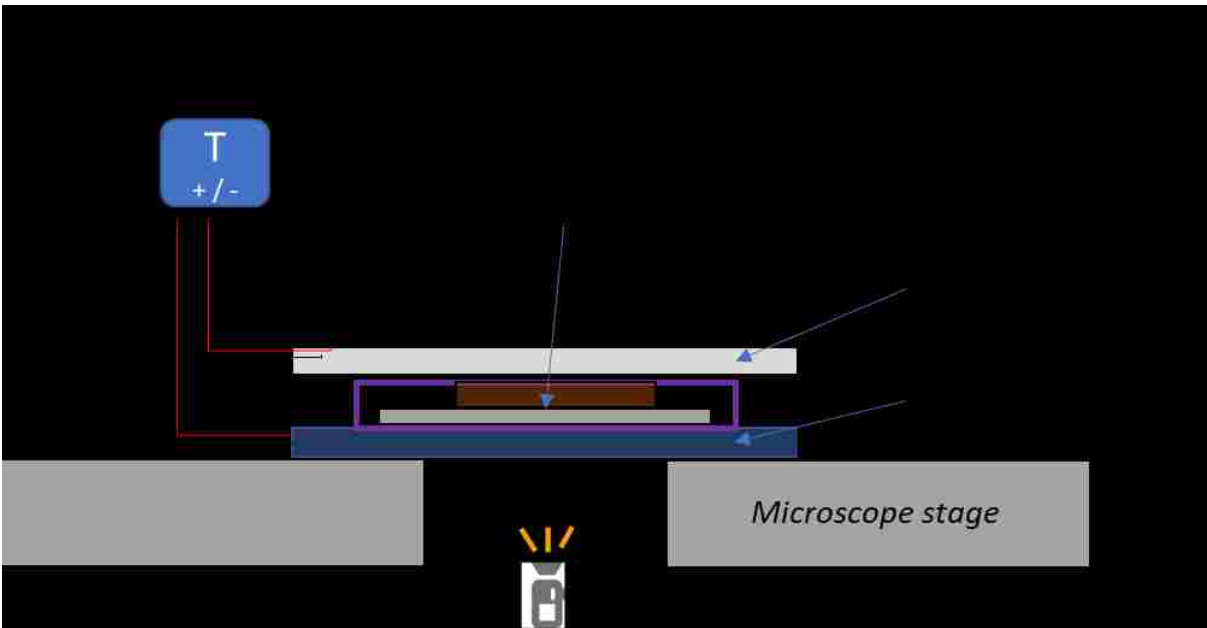
Figure 22: Laboratory clam-shell heater for real-time fluorescence detection: Test card is outlined in purple box. Black housing perimeter is laser cut PMMA and bonded to heated surfaces. The ITO-coated glass provides resistive electrical heating and optical transparency to allow imaging from below using the inverted microscope. The aluminum plate provides a top isothermal boundary, eliminating the need for insulation. Temperature was controlled independently for each heater. (ITO: 47°C set point, Aluminum: 52°C)

4.4   Results

4.4.1   Material Selection

The common porous membranes used in LFTs: nitrocellulose, glass fiber, and cellulose offer advantages of self-driven flow, low manufacturing costs, and support of many biochemical processes, yet exhibit high autofluorescence background levels relative to reporter signals. This background autofluorescence can limit assay sensitivity and must be considered when selecting both substrate and fluorophore combinations to optimize LODs. As this project aimed to develop a universal signal amplification strategy for LFTs, we constrained our immunoassay substrate material to nitrocellulose. Additionally, iSDA has been demonstrated to function at the interface of nitrocellulose and performs

optimally when a glass fiber pad containing master-mix is added to a template-containing nitrocellulose membrane. Recent characterization of these membranes reports much higher autofluorescence in nitrocellulose compared to glass fiber. [58] This is in large part due to the greater porosity and air voids of glass fiber compared to the cast matrix on polyester backing of nitrocellulose. This work also shows autofluorescence in nitrocellulose is more intense in the blue-green spectral region (350-500 nm emission wavelengths) than in yellow-red (500-650 nm). Given this property, we decided to use red fluorophore (e.g. Texas Red, AP-593) labelled hybridization probes for the target amplification to maximize sensitivity in the presence of nitrocellulose, and green-fluorophore (e.g. FAM) labelled probes for the internal control, where decreased sensitivity can be compensated for by IAC template concentrations. In short, background autofluorescence hinders sensitivity in nitrocellulose, but can be addressed through deliberate fluorophore selection.

4.4.2   Probe Selection

Table 4 introduced common methods for fluorescence detection of NAATs. For this assay, intercalating dyes are unsuitable because they inhibit the reaction if used in real-time and lack the ability to multiplex for target and IAC reactions. As iSDA uses Bst 2.0 polymerase, which lacks 5'->3' exonuclease activity, hydrolysis probes are also not feasible in this system. Molecular beacons have straightforward design and have been used in other isothermal NAATs, but their relatively low SBR may compromise sensitivity given the large background autofluorescence of our system.

Our group has prior experience with the MGB-probes (Pleiades Probe, ELITech Group, Bothell, WA, USA) in real-time iSDA tube-based and glass fiber-based reactions. The probes exhibit high SBR and signal temperature stability. In response to the autofluorescence of nitrocellulose and the *mecA* target as the ssDNA detection molecule for LFT-iSDA, we decided to use an existing *mecA* MGB-AP593 probe designed for iSDA. (AP593 is a homologue to Texas Red with peak excitation at 593 nm, emission at 613 nm). IAC hybridization probes were not used in this work but must be included in future development.

 MGB-probes unquench in nitrocellulose

Preliminary real-time fluorescence experiments with the *mecA* MGB-AP593 probe revealed abnormal false positive results when used in a system with glass fiber pads on top of nitrocellulose. (Figure 23)
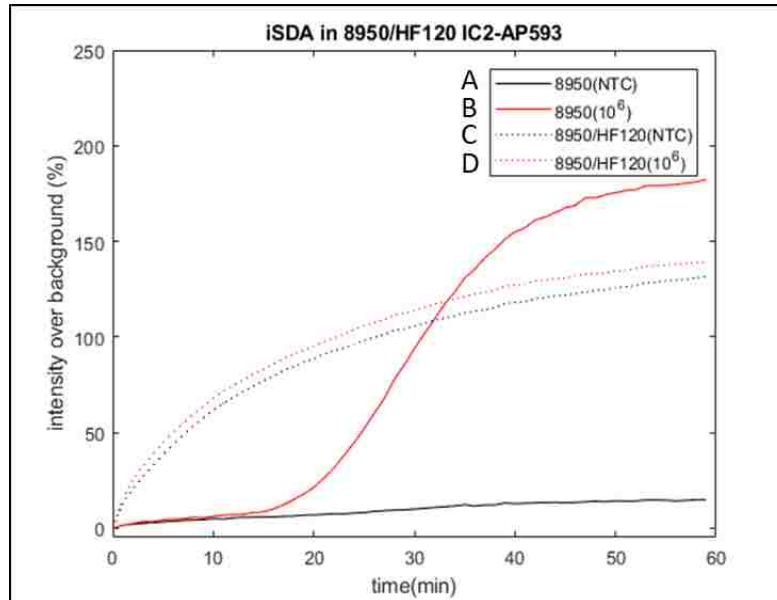
Figure 23: Real-time fluorescence signals from porous membranes: Solid lines (A) and (B) show reactions carried out in glass fiber membranes (8950). Positive sample, 10^6 input copies template (B) shows expected sigmoidal response with "lift-off" at 15 mins; NTC (A) remains flat over 60 min, as expected. Dashed lines (C) and (D) are the same test conditions in a membrane stack of glass fiber directly on top of nitrocellulose (HF120) and show non-exponential response curves in both positive (D) and NTC (C). Intensity over background (%) is shown on the y-axis is plotted against time. These reactions targeted the IC2 *mecA* internal control.

These data (C and D) indicate that the MGB-probes, when in contact with nitrocellulose, are not producing signal in proportion to amplicon generation, as the mechanism of iSDA cannot produce amplicons at rates suggested by these shape factors. Given both NTC and positive samples behaved similarly, we hypothesized that the MGB-probes may be unquenching non-specifically in the presence of nitrocellulose.

48

When subject to the lateral flow challenge, MGB-probes showed strong adsorption to nitrocellulose and unquenching with similar intensity to a fluorophore control. (Figure 24) In this experiment, the expected result for a properly functioning MGB-probe would be the absence of a fluorescent spot (i.e. a dark frame of nitrocellulose), indicating the probe remained in a quenched conformation. The combined results of both unquenching and adsorption indicate that probes are both knocked out of solution, becoming non-functional reporters of amplicon generation. The fluorophore control produces a fluorescence signal, as expected, and washed downstream, indicating no adsorption to the nitrocellulose.
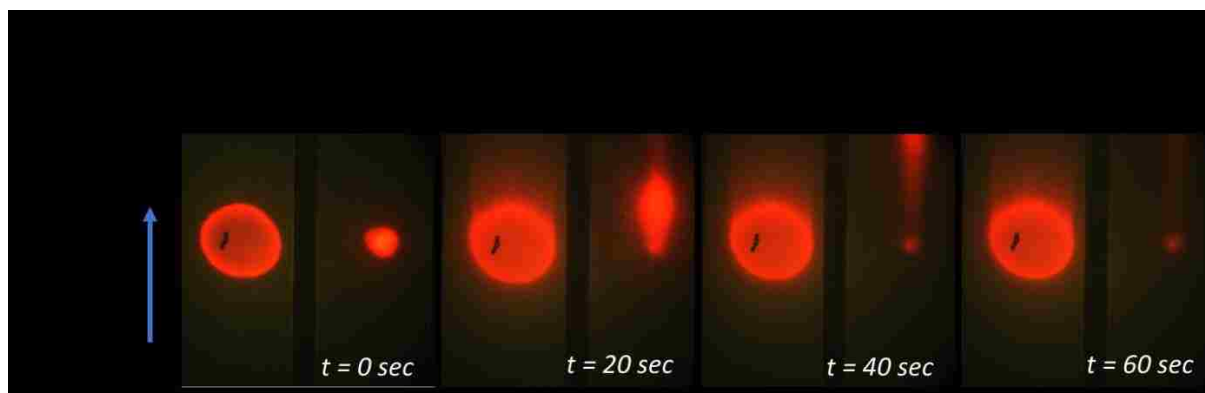
Figure 24: Lateral flow challenge of MGB-Probe and Texas Red: Fluorescence images of adjacent 5 mm wide LFTs constructed of CN-95 show 1 µL of 4 µM solution of (A) AP593 MGB-*mecA* probe and (B) Texas Red fluorophore in PBS buffer spotted onto pre-wet strips. The strips are then subject to 500 µL of rinsing with DI water. Time lapse images show the Texas Red signal wash downstream, while the MGB-AP593 probe exhibits unquenching and strong adsorption to the nitrocellulose. The black line in the center of the MGB-AP593 spot is a scratch from tweezers while handling the membrane.

4.4.3   Membrane overlap iSDA

The unquenching and adsorption of the MGB-AP593 probe to nitrocellulose forced us to investigate alternative fluorophore chemistry (MGB-FAM) and probe mechanisms (Molecular beacon-FAM). The molecular beacon (MB-FAM) was designed to have hybridization kinetic rates similar to

MGB-probes so that total test time would not be increased for real-time detection. This molecular beacon had a 5bp, 80% GC-content stem with a predicted $T_{melt} = 52.4$ ^{o}C. MB stems retain the quenched, "closed" conformation, and their energetic barrier must be overcome by the loop-complement hybridization to liberate the quencher from the fluorophore to produce a signal; this thermodynamic barrier can produce slower time-to-results in MB-probed reactions. [53] Conversely, the suggested quenching mechanism in MGB-probes is through a combination of the quencher 3' label and MGB moiety; no self-complementarity is required for this effect. [52]

Using the membrane overlap test card, nitrocellulose membranes were washed and rinsed to simulate the immunoassay and iSDA master-mix with probes were added to the glass fiber portion to observe the unquenching effect in the overlapping and glass fiber only regions. Figure 25 shows the ROIs measured in the membrane stack.
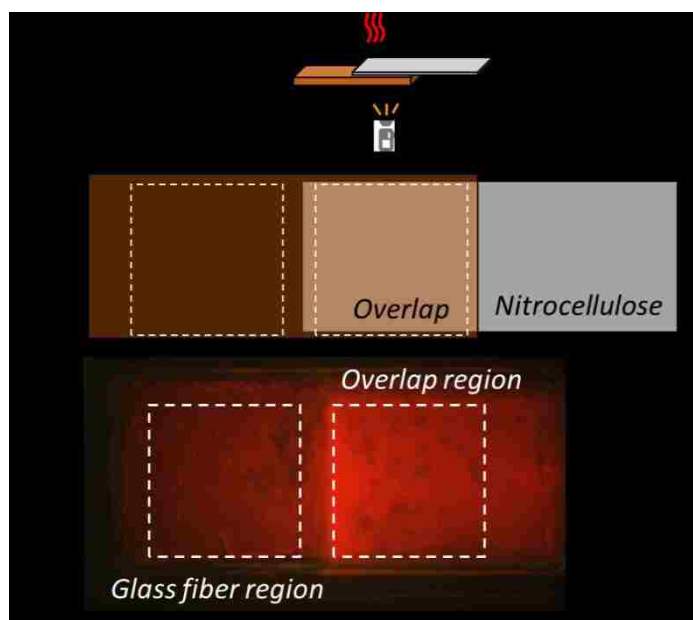
Figure 25: Regions of interest in glass fiber / nitrocellulose membrane overlap experiments: Panel (A) shows 3D schematic from Figure 21; the membranes are place upside down on inverted microscope and image is shot through the glass fiber. Nitrocellulose is grey, glass fiber is brown. (B) Shows the glass

fiber region and overlap region outlined by dashed white box. (C) Shows a representative fluorescence image of the system after 60 min of incubation. At the center of the frame, the line of overlap can be seen.

MGB-AP593, MGB-FAM, and MB-FAM (sequence in Appendix A: 7.1 DNA Sequences) were tested and fluorescence signal measured in both glass fiber and overlap regions. (Figure 26) All probes are complementary to *mecA* gene target. In the overlap region, all probes showed low SBR in both CN-95 and FF80 membranes. MGB-AP593 showed the highest RFU signal in both positive and negative tests, indicating a high quantum yield and large degree of unquenching. The no probe control shows comparable, low signals in positive and negatives, as expected. In the glass fiber only region, the MB-FAM probe shows modest SBR, while the MGB-FAM shows slightly higher, but low SBR. The MGB-AP593 showed a high SBR and low background (negative) signal. No probe controls respond as expected. Table 5 summarizes the SBRs for probe and material types.
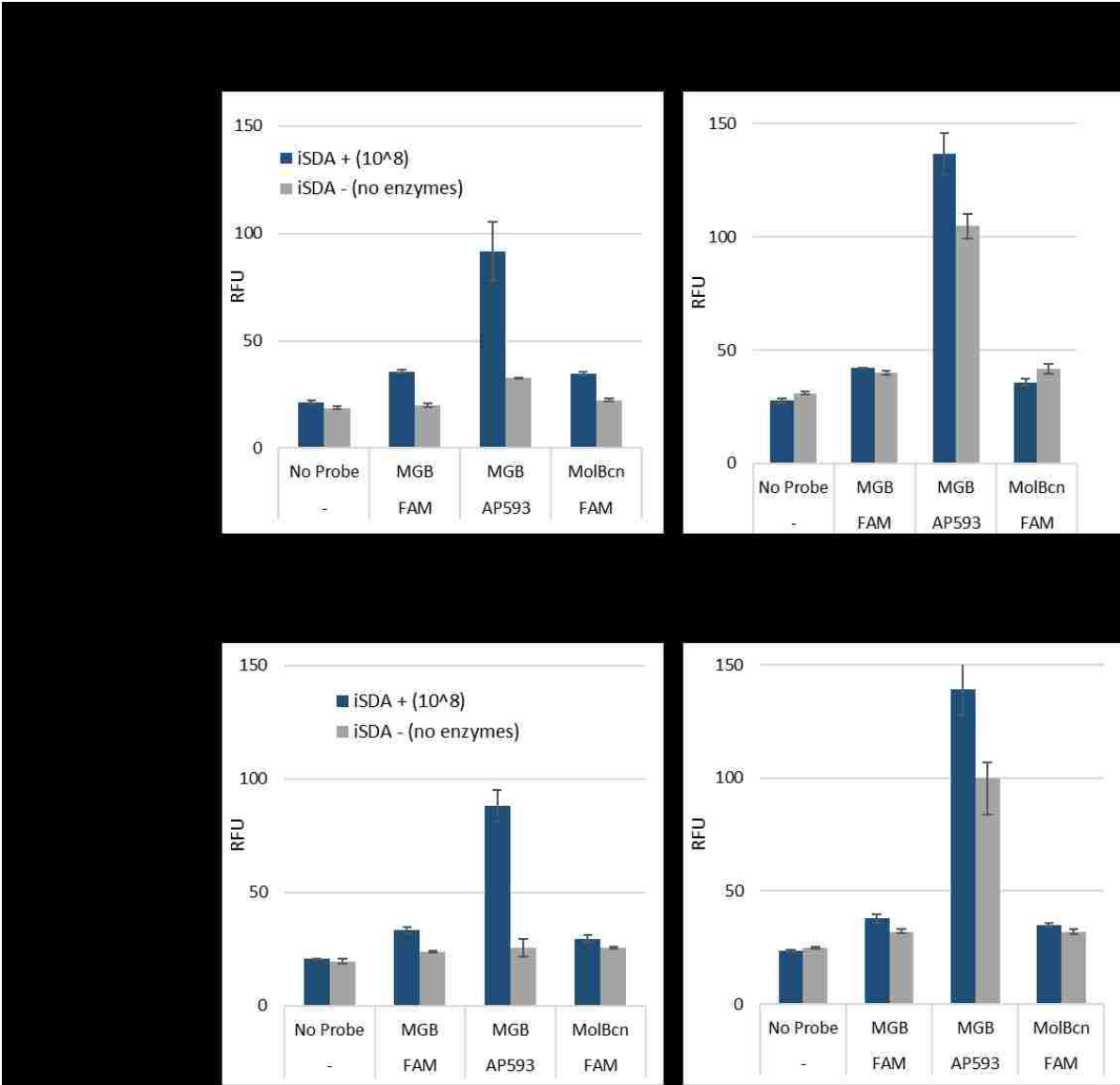
Figure 26: iSDA Signal-to-background ratios (SBR) in overlap and glass fiber regions: Panel (A) shows results for CN-95 membrane, (B) shows FF-80. 8950 glass fiber was overlapped in both tests. RFU (y-axis) is plotted against different probe types: MGB-FAM, MGB-AP593, Molecular Beacon-FAM. All probes targeted the same *mecA* sequence. No probe control indicates background fluorescence of the system in column 1. Dark blue bars are "signal", where 10^8 input copies of template were mixed with iSDA master-mix. Grey bars are "background", where no template or enzymes were added to the master-

mix. The background is a combination of the autofluorescence of the substrate, and the unquenching

effect of the hybridization probe. Error bars show standard deviation (n=3).

Table 5: Summary table of SBR for various probes in CN-95 and FF-80 nitrocellulose with 8950

glass fiber: Ratios calculated from Figure 26, averages of n=3 shown. Bold values indicate highest SBR

and candidate combinations for fluorescence system. Formula to calculate ratio is shown at right.

Signal-to-background ratios			$SBR = \dfrac{Intensity_{iSDA}\ +}{Intensity_{iSDA}\ -}$		
CN-95	**Glass fiber region**	**Overlap region**	**FF80**	**Glass fiber region**	**Overlap region**
MGB-FAM	2.03	1.05	MGB-FAM	1.90	1.19
MGB-AP593	**4.69**	1.30	MGB-AP593	**4.50**	1.39
MolBcn-FAM	1.55	0.86	MolBcn-FAM	1.33	1.10

The CN-95 and FF80 membranes showed qualitatively similar results amongst all probes,

suggesting that the unquenching interaction is not unique to a specific nitrocellulose product number.

Secondly, the input template copy number was very high, to generate the maximum fluorescence signal,

which makes these SBR values an upper-bound, best-case scenario. The MGB-AP593 probe shows

SBR>4.5 in the glass fiber only region, whereas MGB-FAM probes are ~2.0, and MB-FAM SBR ~1.4.

These data led us to select MGB-AP593 in a glass fiber only region the ideal fluorescent probe for the

system.

4.4.4   Side-pad design

To implement the MGB-AP593 probe into the LFT-iSDA assay, a design requires (1) spatial

separation of probes from the nitrocellulose, and (2) a glass fiber only region where fluorescence can be

measured. The side-pad design addresses these requirements by lyophilizing the MGB-AP593 probes into

a distal end of an orthogonally placed glass fiber pad over the nitrocellulose test line. Simply, the side-pad

is a rotated glass fiber rectangle supporting iSDA with probes dried in the non-overlap region. In this

configuration, iSDA master-mix is added to the side-pad directly above the test line in the nitrocellulose. Figure 27 introduces the side-pad design and representative fluorescence data.
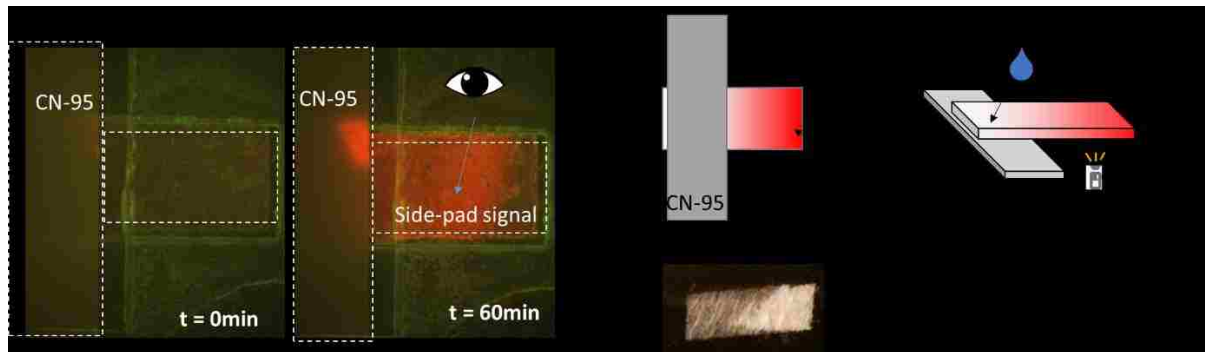
Figure 27: Side-pad design and performance: Panel (A) shows t=0 and t=60 min fluorescence signal in the side-pad region of a positive LFT-iSDA reaction. The profile of the CN-95 nitrocellulose is outlined on the left edge of images from inverted microscope. AP593-MGB Probes produce strong SBR red signal. Test card mylar and adhesive autofluorescence shows green background in perimeter around glass fiber region. (B) shows a schematic of the membranes and a photo of the dry lyophilized probe pad (glass fiber, 8950) prior to being used in device. The right-side white opaque region contains the probes and crystalized sugars. (C) shows a 3D schematic of the system with the inverted microscope underneath the side-pad region and fresh-master mix added to the center of the overlap region. Unquenching and adsorption of the probe to CN-95 is visible in (A) t=60 min.

Using the stage-mounted heating apparatus, real-time fluorescence curves were generated to demonstrate side-pad efficacy. (Figure 28) Despite producing a false positive, the signal shows acceptable lift-off times <20 min, sigmoid shape-functions indicating iSDA amplicon generation, and a flat no template control, indicating the test did not have contamination.
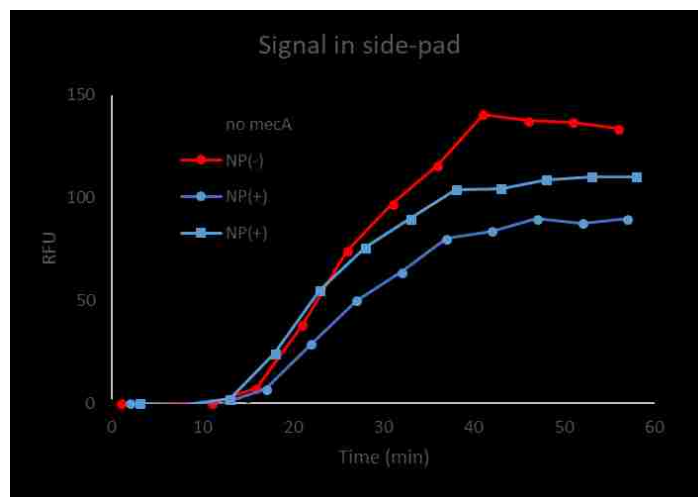
Figure 28: Fluorescence signal measured in side-pad of LFT-iSDA test: Plot shows proof-of-concept real-time results from side-pad LFT-iSDA experiment. RFUs (Y-axis) plotted against time in minutes. "NP (+)" tests contained 10^8 flu-NP analyte in the sample buffer. "NP (-)" contained 0 flu-NP analyte in the sample buffer. This NP(-) line (red) shows false positive amplification lifting-off at the same time as NP(+) results. Black line shows "no mecA" control, a test containing 0 NP and 0 mecA in the detection molecule.

4.5   Discussion

4.5.1   Probe and material selection

After reviewing the landscape of fluorescence options to detection signal in the LFT-iSDA system, MGB-probes seemed an obvious choice. However, preliminary experiments showed rapid unquenching (Figure 23) and adsorption to the nitrocellulose substrate (Figure 24). Alternative substrates (e.g. glass fiber) could eliminate this problem, yet we constrained ourselves to nitrocellulose to make the detection universal to the common LFT architecture. We hypothesized that the unquenching mechanism may be driven by hydrophobic interactions between the nitrocellulose and MGB moiety, where the MGB adsorbs to the substrate, causing the probe to assume an "open" state, producing a fluorescence signal. Following results of Chapter 3, the ssDNA sequence may also contribute to adsorption of probe to nitrocellulose. The proposed mechanism of MGB-probe quenching is that hydrophobic interactions

between MGB and quencher force proximity between the fluorophore and quencher, so it is reasonable

that the MGB (or quencher) may also interact with the hydrophobic nitrocellulose. [52] (Figure 29)
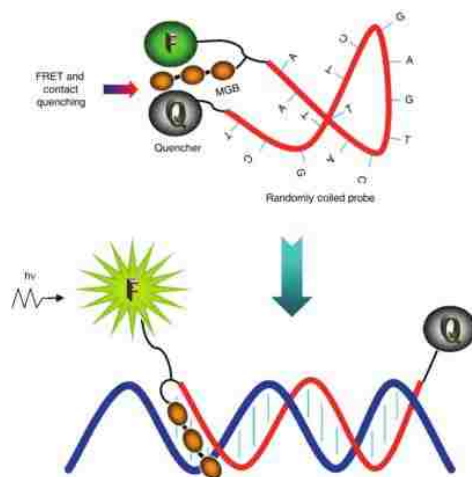
Figure 29: Proposed mechanism of action of MGB-probes: Target complement exists in a random coil

in solution and quencher and fluorophore are held in close proximity by hydrophobic interaction between

quencher and MGB. Quenching mechanism attributed to both FRET and contact quenching. Upon

hybridization with the target, the MGB binds the minor-groove of the dsDNA and liberates fluorophore;

the quencher is forced out of proximity by probe length. Adapted from [52].

Lateral flow challenge results indicate strong adsorption that is not readily washed away under

flow. The probe's DNA sequence may also play a role in the strength of unquenching, as the

hydrophobicity of a ssDNA template will vary with nucleotide sequence. Preliminary data shows that the

mecA MGB-AP593 shows much stronger unquenching that the *IC2* MGB-AP593, suggesting that probe

sequence dominates unquenching. (Appendix A:7.4) However, the same experiment shows *mecA* MGB-

FAM and *IC2* MGB-FAM probes have nearly identical degrees of unquenching, countering the MGB-

AP593 sequence-dependency hypothesis. These experiments report only absolute RFU of an iSDA (-)

result, and should include iSDA(+) results to assess the SBR in the envisioned system. The degree of

MGB-probe unquenching may be a combination of sequence and fluorophore selection and requires

deeper investigation to measure SBR for all candidates.

While the MB-probe (5bp stem, 18bp loop) did not exhibit unquenching in the presence of nitrocellulose, the SBR was insufficient for the background of the LFT-iSDA assay. Several factors constrained this probe design and may have contributed to its low SBR. First, we prioritized fast hybridization rates of probe to target to minimize time-to-result for real-time experiments and to match MGB-probe speed. This was achieved by using a short stem with a low $T_m = 52.4^o$ relative to the assay temperature, contributing to high background level from a large fraction of melted probes (open conformation) at incubation temperatures. Secondly, we used the same target region of the mecA gene as used by the MGB-probes to provide direct comparison of hybridization rates. This AT-rich region of the mecA gene limited the ability to increase the probe:target T_{melt} parameter by increasing the loop complementary region length. Lastly, SBR was limited using FAM fluorophores, which have lower SBR than Texas Red labelled probes; FAM probes were ~1/4 the cost of Texas Red probes. The investment in red probes was not deemed necessary at this stage. Relaxing the design constraints could address these factors to design a MB-probe with acceptable SBR for this assay.

4.5.2   Side-pad design

The side-pad proved to be a viable design for the system fluorescence requirements. Simply, it spatially separates the master-mix from the probes and isolates the probes to a region less affected by the nitrocellulose. The dynamics of this system are complex, involving rehydration, diffusion, and reaction-diffusion, as well as bulk-flow dependencies on membrane saturation levels. The observed slower response times of LFT-iSDA (15-20 min lift-off compared to <15 min lift-off of glass fiber only reactions) can be explained qualitatively by the following key factors: (1) upon rehydration, probes diffuse from the high concentration lyophilized region across the entire glass fiber pad, yet are in low concentration immediately above the test-line, where amplicon generation originates. (2) the master-mix volume fills the side-pad to near full saturation, resulting in minimal convective flow of the master-mix into the nitrocellulose. This ensures that the master-mix does not flow in regions outside of the test-line

and requires the nitrocellulose to also be near full saturation, to prevent draining of the side-pad by the nitrocellulose. Thus, for successful iSDA initiation, the template needs to diffuse to the master-mix or the master-mix needs to diffuse into the nitrocellulose—either of these scenarios results in a slower time to lift-off. Countering the factors slowing down the assay, reaction-diffusion of iSDA causes amplicons to spatially propagate from the test-line region across the side-pad. Theoretically, reaction-diffusion should provide faster amplicon propagation than diffusion alone, thus shortening the time-to-result. Accounting for these dynamics, the side-pad geometry, concentrations, and rehydration method could be optimized to reduce the time-to-result for LFT-iSDA.

An important instrumental limitation in the real-time experiments must be noted: the ITO-coated glass heater (Figure 22) has a low thermal mass and electrical resistance resulting in imperfect isothermal control. Additionally, the uninsulated heater has thermal gradients in XY axes resulting in a $50^{\circ} \pm 1^{\circ}C$ temperature envelope. This translates into the strips having varying incubation temperatures which effect DNA yield / iSDA efficiency between strips. We decided to use this apparatus to maximize experimental throughput at the expense of temperature control precision. Future fixtures should address this deficit.

4.6   Conclusions

The manual LF-iSDA consists of 40 min for immunoassay, 30 min for iSDA, 30 min for incubation of amplicons with probes, and 20 min for DNA-LFT to detect amplicons—a 2-hour time-to-result. The use of fluorescence hybridization probes afforded by the side-pad design enable results in ~1 hr (40 min immunoassay, 20 min time-to-result for iSDA), effectively halving the test time, and achieving the initial target of matching predicate POC diagnostic devices. While we did not replicate the LOD achieved in PAGE detection, and still faced immunoassay-attributed false positive results, solutions developed in this chapter can now be used for both real-time and endpoint fluorescence detection. Future work requires development of an IAC, probed by a different wavelength fluorophore (e.g. FAM IAC, AP593-target). Use of MGB-probes in the side-pad to maximize fluorescence sensitivity (SBR) comes at the expense of a

more complex 2DPN which is not manufacturable by traditional LFT methods. (e.g. stripe and guillotine cut) In short, this design is amenable to integration into a cartridge format for use with a low-cost instrument offering shorter test times and fewer user-steps.

5 CARTRIDGE INTEGRATION

5.1 Objectives

LFT-iSDA is a powerful analytical tool based on the ubiquitous LFT. However, in its current demonstration, the highly manual process is not appropriate in decentralized settings. This chapter aims to integrate the LFT-iSDA assay into a cartridge format with minimal user steps, low-cost instrumentation, and rapid time-to-result, toward a goal of replicating the performance of the flu-NP assay. This model system was selected as it is the most mature and high performing LFT-iSDA assay. This development aims to transpose the 96wp-based assay to a 2DPN-based device.

5.2 Introduction

Cartridge-based tests are simple diagnostics consumables made from a range of injection molded plastics, porous media, and fluid control elements. Simply, the cartridge is a device architecture supporting the bioassay. Cartridge-based LFTs diagnosing infectious disease or pregnancy have remained relatively unchanged since their inception, credence to the cost-effective, intuitive design. Within the last decade, a host of multi-step assays integrated in to Clinical Laboratory Improvement Amendments (CLIA) -waived tests have reached POC settings through careful cartridge designs with minimal potential for error, use of unprocessed specimens, and low required skill level for nonlaboratory users. [59]

Complementary to the development of a cartridge supporting real-time fluorescence detection (Chapter 4) is the need for a low-cost instrument to enable easily interpretable results at the POC. Devices combining optical detection with low-cost computing capabilities (e.g. smartphone) can provide quantification, early and on-site detection, and wireless data transmission. These benefits make the technology pairing well suited for at-home monitoring or tests in LRS. [60] However, use of smartphones and tablets in POC testing, poses problems as an integrated diagnostic technology must adapt to different brands and manufacturers. Factors such as alignment, focal plane, and field of view for optical measurements must be tightly controlled in these applications. Despite these drawbacks and potential

barriers to commercialization, smartphones offer powerful, low-cost sensing and computing abilities appropriate for decentralized test scenarios. These devices are valuable to early-stage researchers and can be treated as placeholder technology—precedence that low-cost sensors can be mass-produced in integrated systems.

5.2.1   Integrated LFT-iSDA concept:

A concept of the LFT-iSDA cartridge in an integrated system is shown in Figure 30. In this system, the cartridge uses the hand-held, LFT form-factor requiring a single user step of adding the sample and inserting into the instrument. The proposed low-cost instrument would contain an LED array for fluorescence excitation, a bandpass emission filter appropriate for the fluorescence channels of the test, a rechargeable battery to supply the electrical power for the isothermal heating, and a control board to provide simple logic for timed steps. The smartphone camera would be used as the detection sensor and would mechanically "key" into the top surface of the instrument. Ideally, the instrument would have an integrated detection system (e.g. photodiode sensor, display screen), but a smartphone could provide acceptable optical performance, signal processing, and allow immediate data transmission via cellular network. Development of this complementary technology is currently underway in our lab in support of the EbolaBox project.
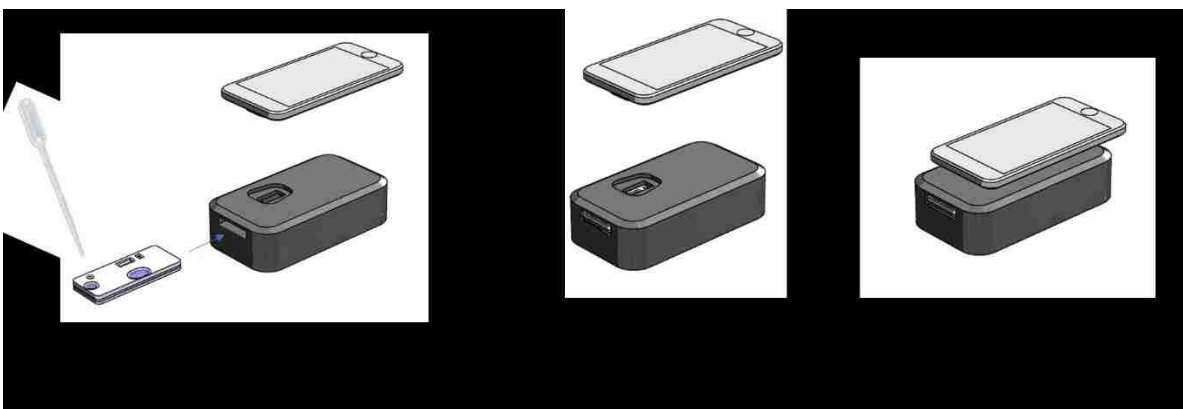

Figure 30: Concept drawing if LFT-iSDA POC system: (A) User adds sample (e.g. diluted nasal swab) to cartridge. (B) cartridge is sealed and inserted into a low-cost instrument. Rechargeable, battery-powered instrument provides isothermal conditions and controls fluid flow in the cartridge. (C) Smart-

phone camera or internal optical system detects and processes real-time fluorescence signal for easy user interpretation on screen display.

5.2.2 LFT-iSDA device unit operations:

The multi-step protocol of LFT-iSDA can be organized into unit operations to inform design requirements prior to integration, as shown in Table 6.

Table 6: Assay unit operations, requirements and methods.

	OPERATION	*REQUIREMENT*	*METHOD*
1	Sample introduction	sample pre-mixed with detection molecule	Diluted nasal matrix pipetted into cartridge (for flu assays)
2	Immunoassay wash	PBS-0.8% Triton wash flowed through nitrocellulose	On-board reagent storage and timed release
3	Immunoassay rinse	iSDA compatible $KiPO_4$ buffer flowed through nitrocellulose	On-board reagent storage and timed release
4	Stop flow	Stop convective flow in nitrocellulose	Fill the wicking pad to full saturation, or remove wicking pad
5	Master-mix addition	Deliver iSDA mater-mix to immunoassay sandwich test line	Rehydrate lyophilized master-mix in glass fiber membrane
6	Incubation	Provide 50°C for 30 min	External electrical heat and control
7	Real-time detection	Detect fluorescence signal in multiple wavelengths	External optical detection from instrument and/or smartphone

Unit operations 1-3 are common to existing LFT manual workflows and can be semi- to fully-automated using a variety of simple mechanisms to provide fluid control and sequential delivery of reagents. [24], [61], [62] Unit operation 4: Stop flow can be achieved by either physical disconnection of the wicking pad from the 2DPN or by filling the wicking pad to full saturation. In either method, the pressure gradient along the membrane network drops to zero with a removed or saturated wicking pad, thus stopping slow in the upstream nitrocellulose region. Ideally, unit operation 5 entails rehydrating a lyophilized pad of master-mix and subsequent delivery to the immunoassay test line (freshly-prepared master-mix was used in this preliminary work). Finally, unit operations 6 and 7 occur simultaneously in a low-cost instrument where isothermal conditions enable the iSDA reaction, and an optically clear line of sight from the signal ROI to optical sensor—in this concept a smartphone. The isothermal heating

requirement translates into a design requirement of high heat transfer rates into the cartridge to minimize temperature ramp time, and low cartridge thermal mass to minimize the total electrical energy requirement per test.

Returning to the immuno-NAAT distinction of this assay, unit operations 1-3 provide the immunoassay capture, operations 5-7 provide NAAT signal amplification, and operation 4 provides a critical linkage between the two methods.

5.2.3   Flow in 2DPNs and design configurations

One-dimensional (1D) capillary flow LFT immunoassays have demonstrated commercial viability, robust manufacturing methods, and numerous applications, yet lack the ability to perform multi-step assays required to gain sensitivity. The 2DPN, introduced nearly one decade ago, expands on the basic 1D-LFT architecture, allowing multiple reagents to be delivered with spatial and temporal manipulation. [63] This class of devices uses common LFT materials in multi-layered networks with active and passive valving of precise fluid volumes(10-100 µL scale) to yield chemical signal amplification of the capture event. [18], [28], [64] Chapter 2 details some of these amplification strategies employing 2DPNs.

Mechanistic understanding of fluid flow in porous media is critical for design of 2DPNs. Beginning with the addition of a sample to the system, the wet out of a dry porous membrane is governed by the Lucas-Washburn equation (Equation 3).

Equation 3 Lucas-Washburn equation: describes wet-out of fluid in dry porous media

$$L^2 = \frac{\gamma d_p \cos(\theta)\, t}{4\mu}$$

(L) describes the length of the wetted fluid column as a function of fluid surface tension(γ), pore diameter (d_p), contact angle (θ), and fluid viscosity (μ). This equation predicts flow in a single material before reaching a junction with another material. Upon reaching a material junction, the flow enters a second regime, where flowrate through the wet-out material into the downstream material is needed.

One commonly held approximation for flow in fully-saturated porous media draws from the Darcy Equation (Darcy's Law), describing flow in hydrogeological models in ground water. Application of this relationship assumes an infinite fluid source and infinite wicking pad sink. (Equation 4)

Equation 4: Darcy's Law: flow in fully saturated porous media

$$Q = \frac{\kappa A \Delta P}{\mu L}$$

Darcy's Law can be used in two dimensions and defines the volumetric flow rate (Q) as a function of membrane permeability (κ), cross-sectional area normal to flow(A), pressure gradient between along length of membrane, viscosity of the working fluid (μ) and length of the membrane(L). The relationship is convenient in describing flow in simple systems, however, practically LFTs do not operate in the fully saturated regime, deeming the assumptions of Darcy's law inappropriate for this application. Thus, our group has recently challenged the assumptions of Darcy's equation and proposed an alternative model, the Richards equation, which describes flow in partially saturated materials. (Equation 5) [65]

Equation 5: Richards Equation: flow in partially saturated porous media

$$\frac{\delta\theta}{\delta t} = \frac{\delta}{\delta z}\left[K(\theta)\frac{\delta H(\theta)}{\delta z}\right]$$

Richards defined flow in partially saturated flow in porous media (also originally described in hydrogeological models) by the partial differential equation where flow rate ($\frac{\delta\theta}{\delta t}$) is a function of vertical position (z), hydraulic conductivity (K) and hydraulic pressure (H)- both functions of volumetric water content (θ). [66] This model can describe the observed phenomenon where a visibly "saturated" (e.g. colored dye fills entire membrane) continues to pull fluid from a source, indicating the membrane acts as a fluid conduit in a partially saturated regime. Practical implementation of this equation requires an empirically derived relationship between saturation level (0-100%) and capillary pressure (kPa) for each material in a multi-material network.

These relationships govern fluid flow in porous media and qualitative understanding greatly enhances design of seemingly simple fluid control systems in 2DPNs.

5.3 Materials and methods

5.3.1 Flu-NP LFT-iSDA assay parameters

The flu-NP LFT-iSDA in device assay is slightly modified from the previously described dipstick assay test card. [43] Rather than dipping the test cards vertically into pre-filled wells, fluid is delivered to glass-fiber membranes in a 2DPN format. The in-device assay test cards hold between 5 and 6 devices in parallel to maximize experimental throughput.

<u>LFT fabrication</u>

The immunoassay component was made from a 3 mm x 18 mm wide CN-95 membrane. Anti-influenza A NP monoclonal antibodies (1 mg/mL, InA108, HyTest, Turku, Finland) was striped to form a test line in the nitrocellulose membrane using a reagent dispenser (Biojet HR Solenoid Dispenser, BioDot, Irvine, CA, USA). The striped card was dried for 2 hrs at 37°C, cut into 3 mm x 18 mm wide strips and stored in sealed pouches in a desiccated chamber at room temperature.

<u>Pre-mixed sample preparation</u>

Salmon sperm DNA (D9156, Sigma) was used as a blocking agent as previously described. The salmon DNA was heated at 95 °C for 10 min, then cooled to 4°C immediately prior to use. Recombinant Flu-NP and salmon sperm DNA (0.75 µg/test) was combined with biotinylated detection antibody (3IN5 InA245, HyTest, streptavidin (S4762, Sigma), and incubated for 20 minutes at room temperature. Lastly, a biotinylated ssDNA mecA template (oEH1139 sequence) was added and the solution was vortexed. The pre-mixed sample was prepared in PBS-lysis buffer consisting of 5% Triton X-100, 1% (w/v) BSA at 70 µL / test. (Table 7)

Table 7: In device assay parameters: Concentrations for a 70 µL sample in PBS buffer from [43].

Units	Rec. Flu-NP	Salmon sperm DNA	Biotinylated Detection-Ab	Streptavidin	Biotinylated ssDNA
Copies /test	10^8	-	10^8	10^8	10^8
µg /test		0.75	-	-	-
Molarity (pM)	2.37	-	2.37	2.37	2.37

Buffer compositions

The 40 µL wash consisted of 1% (w/v) BSA in PBST, with 0.8% Triton X-100 to increase stringency the volume was increased from dipstick format because of hold-over volume in membranes. The 40 µL rinse buffer consisted of 1% (w/v) BSA and 0.05% Tween 20 (P9416, Sigma) in KiPO$_4$ buffer. Stop flow buffer was deionized water (DI).

Detailed protocol for cartridge-V1 device

Immunoassay operations were as follows: 70 µL of pre-mixed sample was pipetted into "sample pad" glass membrane. After the entire volume drained from sample pad to nitrocellulose, 40 µL of PBS wash buffer, followed by 40 µL of KiPO$_4$ rinse buffer was pipetted into the sample pad. After the wash and rinse buffers drained entirely into the nitrocellulose, DI water was added to the stop flow network to saturate the wicking pad and stop flow (volume for this step varied by test). The total time for the immunoassay was 30-40 minutes (depending on ambient humidity and temperature). Next, 13 µL of iSDA master-mix was added to the side-pad directly above the test-line. The cartridge was then sealed with PCR plate lid seal and placed in the stage-mounted ITO-coated glass heater at 50°C for 60 mins. (Figure 22) The previously described inverted fluorescence microscope apparatus and workflow was employed to generate real-time fluorescence curves.

LFT-gold detection of amplicons

Amplicon detection LFTs were comprised of an amplicon test line (400 µM hybrid pDNA-T20 (pyranosyl DNA covalently linked to 20 thymidine nucleotides) capture probe) and a control line (200 µM T20-biotin) striped at 0.3 µL/cm on nitrocellulose and attached to a wicking pad. The detection LFT strip was then guillotine-cut into 2.5-mm wide strips. After the completion of LFT-iSDA, amplified products were removed from nitrocellulose and glass fiber pads via centrifugation. The recovered fluid sample (11 µL) was mixed with 7.4 µL of amplicon detection reagents, consisting of 20 nM hybrid

DNA-pDNA capture probe (ELITech Group), 10 nM biotinylated DNA detection probe (ELITech Group) and 1.25 µL of 10 OD streptavidin-coated gold nanoparticles (Innova Biosciences, Cambridge, UK); the resulting mixture was incubated at 49°C for 30 min. The incubated samples were then mixed with 0.6 M NaCl and 0.8% v/v Triton X-100 and pipetted onto amplicon detection LFTs.

5.3.2   Device fabrication and design

The following describes the basic design and generalized construction of integrated cartridge devices. Specific dimensions, configurations, and use of these materials varied between experiments, as indicated in the results corresponding to each design.

Traditional LFT materials combined with laminated thin-film adhesive-backed polymer construction were used to fabricate cartridges because of their proven compatibility with assay chemistry, ease of rapid-prototyping with CO_2 laser-cutting, and low-cost compared to injection-molding, CNC machining, or thermoforming methods. The following materials were used in LFT-iSDA device construction: CN-95 nitrocellulose membrane supporting immunoassay capture, 8950 (Ahlstrom) glass fiber as wash buffer pad, stop flow network, and side-pad, GFDX glass fiber (Millipore, Burlington, MA, USA) as a sample pad, and C083 (Ahlstrom) for wicking pads. Double-sided PDMS tape (ARclad® IS-7876, Adhesives Research) was used to join mylar sheets (0.254 mm) between lamination layers to adhere membranes in place. PCR plate lid seal (Microseal B, Bio-Rad) was used as the top seal above the side-pad, due to its low autofluorescence and tolerance to elevated temperatures. This product was previously demonstrated to be compatible with iSDA chemistry. All glass fiber membranes were pre-blocked with 1% BSA (w/v) 0.1% Tween20 solution. Cartridge designs were drawn in 2D CAD software (AutoCAD, San Rafael, CA, USA)

5.3.3   Teflon amorphous fluoropolymer (Teflon-AF) edge sealing

To seal the edges of nitrocellulose, Teflon-AF (The Chemours Company, Wilmington, DE) was used to coat the ~ outer 1 mm width of membrane, preventing flow in these regions. Teflon-AF was

diluted 1:3 in Fluorinert (3M, Maplewood, MN, USA); 3 µL of mixture was pipetted into petri dish and nitrocellulose membrane was slid though the drop at a constant rate using tweezers. This was performed on either side of the membrane. (Figure 31)
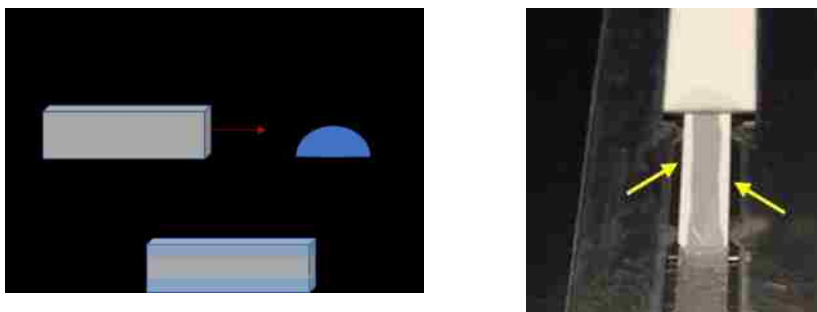

Figure 31 Teflon-AF edge sealing of nitrocellulose: Schematic shows edge sealing method. Photo shows a sealed 5 mm wide CN-95 membrane with buffer flowing through centerline. Sealed edges are white and ~1 mm wide as indicated by yellow arrows

5.4   Results

5.4.1   Assay performance in CN-95

The flu-NP LFT-iSDA assay was performed in manual format in CN-95 membrane to demonstrate (1) performance in a new material, and (2) that the protocol is robust to user variability. The assay was originally optimized in Millipore HF120, which was discontinued by the manufacturer, resulting in the material change. The assay showed ~10x worse sensitivity in CN-95 than HF120. This experiment was an important starting point to carry out prior to integration efforts.
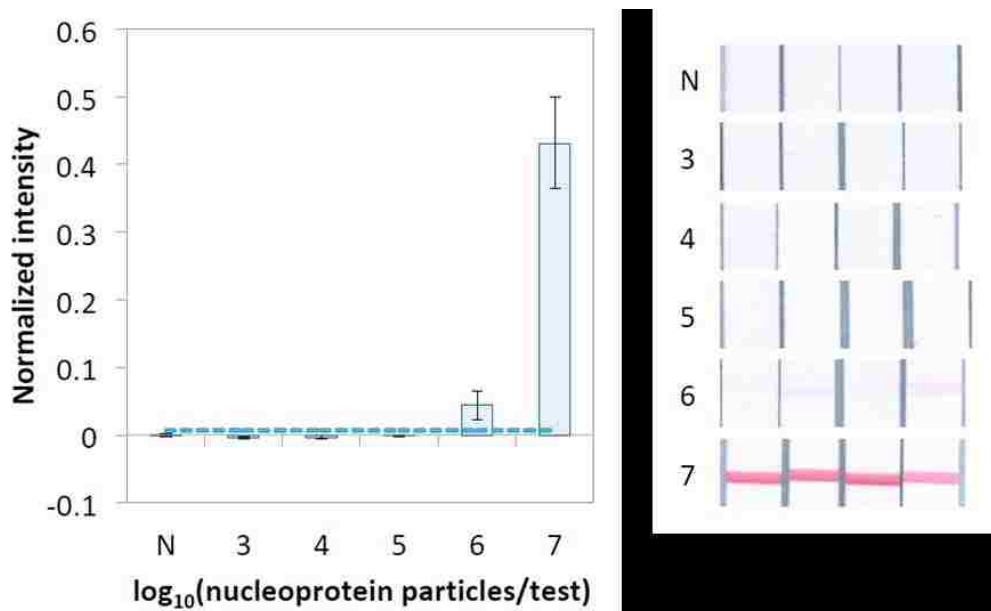
Figure 32: Manual test card flu-NP LFT-iSDA in CN-95 membrane: shows ~10x less sensitive assay than in HF120 membrane. Images show LFT-gold detection of amplicons from volume recovered from glass fiber and nitrocellulose by centrifugation. Normalized intensity measured by high-resolution flatbed scanner (Perfection V700 Photo Scanner, Epson, Nagano, Japan) and a previously-reported custom script written in MATLAB (MathWorks, Natick, MA, USA) (26). Data analysis and LFT-gold detection performed by Koji Abe. Error bars show standard deviation (n=4)

5.4.2 V1-Cartridge flow path design

The first prototype—V1 Cartridge—was made from laser-cut membranes encapsulated by laminated Mylar film spacer layers. Mylar spacer layers are combined with double-sided PDMS adhesive and aligned with two 2.5 mm dowel pins; membranes were placed manually in net-fit Mylar spacer layers to minimize alignment variability. The design featured a "key-hole" sample pad of high-capacity GFDX glass fiber. This shape was used to minimize cartridge length. (Figure 33) The sample pad overlapped the nitrocellulose immunoassay membrane by 1.5 mm and was adhered to a PDMS tape bottom plane (floor).

The stop flow membrane and side-pad were placed directly over top of the immunoassay, leveraging an automatic saturation-dependent fluid transfer valve, previously described by our group.[66]–[68] In brief, the configuration exploits a large difference in membrane capillary pressure (proportional to pore size) of membranes in direct contact, whereby liquid flow preferentially remains in the smaller pore material (more negative pressure) and does not flow into the large pore material. When a secondary fluid fills the large pore material, it saturates the membrane and flows into the primary membrane, enabling delivery of the secondary reagent to the contact area between membranes. This design is a passive valve used to deliver a secondary reagent to a test region with no moving parts, designed entirely on principles flow in partially saturated porous media, offering simplicity and a low-profile suitable for laminated construction methods.

The C083 wick was placed over top of the immunoassay membrane and the final encapsulation layer added with fill ports and vent holes to provide easy filling via pipette. The single-channel design measures 23 x 65 mm and 1.1 mm thick (Figure 33). The cartridge design was cut in arrays of 5-6 devices to facilitate construction and testing. (Appendix A: 7.5)
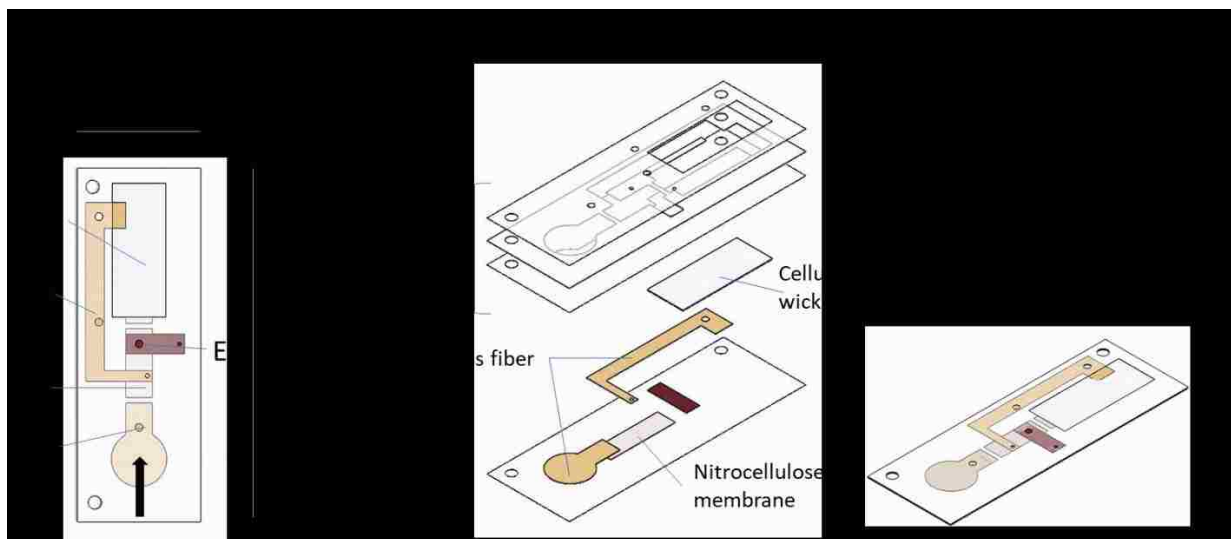

Figure 33: V1 cartridge device design Top, exploded, and isometric views of exploded and assembled device. The cartridge is made of laser-cut membranes encapsulated by Mylar film spacer layers to minimize evaporation of the liquid over the course of the incubation period. Mylar (0.0l0" thick) spacer

layers are combined with double-sided PDMS adhesive and aligned with two 2.5 mm dowel pins. Assay unit operations are as follows: (1) the pre-mixed sample is pipetted into the sample pad (GFDX, Millipore) through port (A). (2) the sample flows into the nitrocellulose (CN-95) reaction membrane (B) in (3) wash and rinse buffer solutions. The analyte and detection molecule complex are captured by an immobilized capture antibody at the test line, immediately underneath the (E) side-pad (8950). After completion of the immunoassay, (4) DI water is delivered the stop flow membrane (C) (8950) to fully saturate the nitrocellulose reaction membrane and the cellulose wick (D). By directly saturating the distal wick end, this membrane effectively stops flow in the device. (5) Freshly prepared master-mix is then added directly to membrane (E) where the iSDA signal amplification reaction proceeds from the immunocomplex captured at the test line. (6) The cartridge fill holes are then sealed with PCR-plate lid seal (Microseal B, Bio-Rad); the assembled cartridge is for 60 min at 50°C to observe signal generation. The single-channel design measures 23 x 65 mm.

To validate the V1-cartridge design, a test was performed to demonstrate unit operations with colored dyes. (Figure 34)
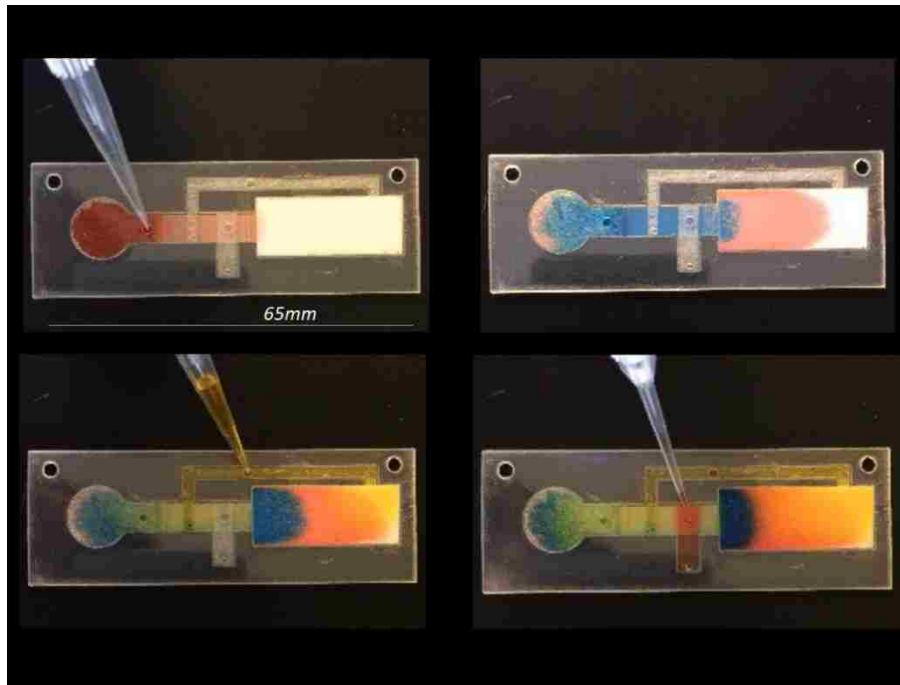
Figure 34: V1-Cartridge demonstration with colored dyes: (1) Sample was added to the keyhole shaped sample pad (70 µL, red), after the pad is completely drained, (2) wash (40 µL, blue) and rinse (40 µL, blue) buffers were added through the same fill port. After the wash/rinse drained from sample pad, (3) Stop flow DI water was added to the side fill port (120 µL) to simultaneously saturate the wicking pad and upstream nitrocellulose region, effectively stopping flow. (4) Master-mix (13 µL, red) was then added to the side-pad. Note in steps 1-3 the side-pad remains unsaturated, evidence that the saturation-dependent valve is an effective one-way fluid transfer element. The cartridge is then sealed prior to incubation. Scale bar shown in panel (1).

LFT-iSDA assay with analyte

The V1-cartridge LFT-iSDA test was run with 10^9 flu-NP input particles and real-time fluorescence detection. Figure 35 shows false positive results of NTC / 0 flu-NP test conditions. The false positive and true positive samples amplified at the same rate, with lift-off in <20 min. The no *mecA* control contained 0 flu-NP and 0 ssDNA in the detection molecule stack; it did not amplify, as expected. This test condition was used to rule-out ssDNA contamination of the iSDA reaction.
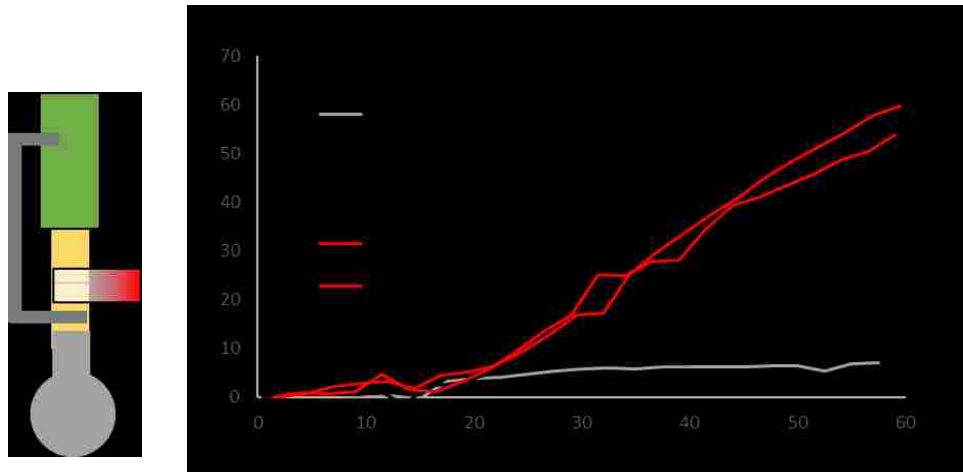
Figure 35: V1-Cartidge assay false positive results: Schematic of V1-Cartridge shown in left panel. Test line marked by "T", immunoassay shown in yellow, side-pad in red, and wick in green. Real-time curves show amplification of both positive (10^9 input copies) and negative (0 input copies) flu-NP samples. The 0 *mecA* (ssDNA) negative control did not amplify, indicating there was no DNA contamination during the protocol.

5.4.3   Unintended flow in V1 Cartridge

The false positive results from the screening test at high flu-NP concentration in the V1-cartridge design, suggested detection molecule was retained in the system after wash and rinse operations. Possible explanations of this failure modes include (1) insufficient rinsing / NSB, (2) residual detection molecule from the sample diffusing into the of wash / rinse buffers causing contamination at the test line, or (3) extra-membrane flow, whereby fluid can "short-cut" the immunoassay, potentially transporting detection molecule directly to the side-pad. Deeper analysis of these results was required.

Channeling

Analysis of the real-time fluorescence images showed MGB-probe transport from the side-pad to a downstream region of the nitrocellulose (Figure 36). The probe unquenching pattern suggests that the fluid travelled between the mylar encasement wall and nitrocellulose membrane in a capillary "channel", not through bulk flow in the membrane itself. Previous experiments showed that the probes adsorb

strongly to this substrate and do not flow through the membrane, thus ruling out the hypothesis that probe transport was driven by pressure driven bulk flow within the nitrocellulose. The strong probe adsorption inadvertently created a tracer dye which stops upon contact with nitrocellulose. While the probe transport does not itself pose a problem, it indicates that (1) master-mix may have flowed downstream, potentially amplifying washed detection molecules, or (2) existence of this channel may have allowed pre-mixed sample/detection molecule to outside the membrane directly into the side-pad, causing false positives. A minor design change widening the gap between membrane and spacer layer effectively eliminated this channeling effect and was employed in all future designs.
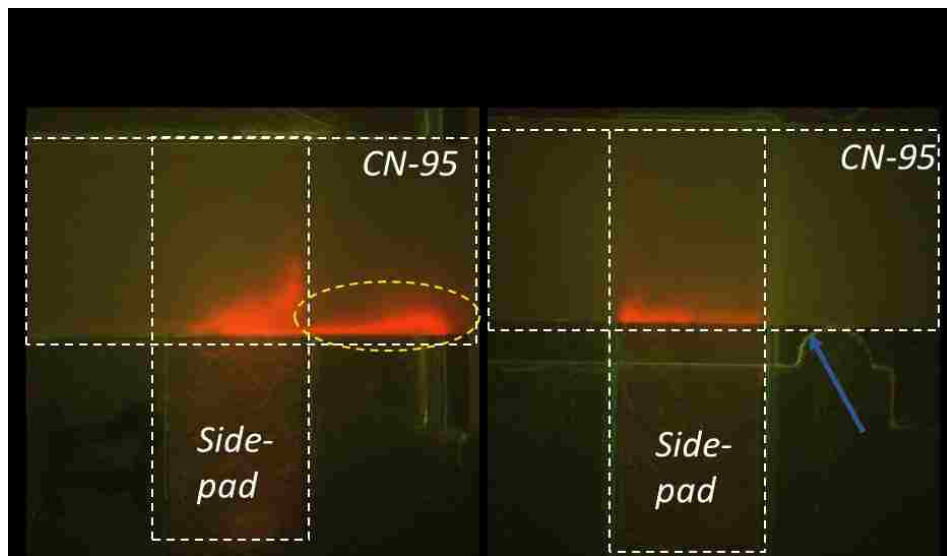

Figure 36: Channeling at the edge contact between nitrocellulose and mylar encasement: Panel (A) analysis of the real-time fluorescence image show probe transport from the side-pad into the downstream region of nitrocellulose (yellow dashed oval). The flow in nitrocellulose was from left to right. We hypothesize this transport is due to extra-membrane "channeling" flow. Panel (B) shows slight design modification (blue arrow) where gap between Mylar wall and membrane was increased by 1.0 mm , effectively eliminating channeling. Raised semicircular shape is used to align nitrocellulose to cartridge.

Dead-zones / poor rinsing

We also re-analyzed the colored-dye experiments to visualize stringency of washes and transport of the pre-mixed sample. Figure 37 shows inverted images of sample buffer and wash buffer time points in the V1-cartridge and indicate residual sample in the sample pad mixes with subsequent washes. The crescent shaped blue region in the keyhole pad was insufficiently washed, and undoubtedly diffused into wash buffers, effectively contaminating them with detection molecule. The function of the wash and rinse buffers is to release unbound detection molecule and transport them downstream. However, in this demonstration, the dead-zone at the end of the keyhole may have seeded the wash/rinse buffers with detection molecules, leading to potential NSB—deeming them ineffective washes.
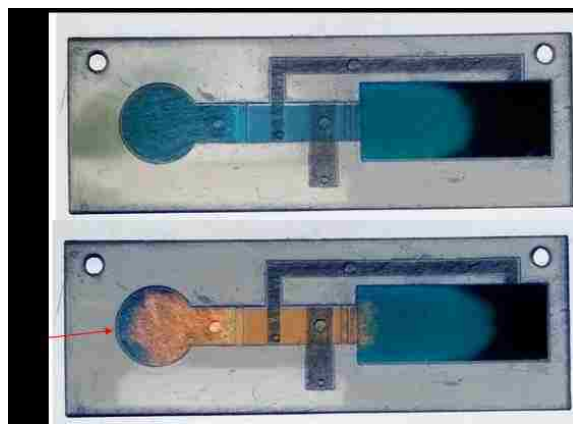

Figure 37: Insufficient rinsing in sample pad: Inverted color images from colored dye testing reveal unwashed "sample" in the round sample pad. Panel (A) shows the mock sample (blue color) flowing from the keyhole shaped sample pad through the nitrocellulose, into the wicking pad. Panel (B) Shows the device after the wash buffer (orange) was added to the same sample pad membrane and flowed through the downstream network. The red arrow indicates an unwashed sample region (still blue), where residual detection molecules could contaminate the wash buffer, increasing the likelihood of false positives from NSB.

5.4.4   Failure analysis of V1-cartridge and modifications

These simple observations from coarse resolution indicators of fluid flow in V1-cartidge motivated a failure analysis to isolate the source of the false positive results. The system was

deconstructed, univariately when possible, in a series of modifications to test several hypotheses. These iterations are not meant to be stand-alone integrated devices but are intended to isolate the failure mechanism in the V1-design. Hence, subsequent designs are more user-step intensive than V1. Due to the time-consuming fabrication and LFT-iSDA protocol (~8 hrs / test card), screening tests contained 5 or 6 test conditions and always included a 0 ssDNA (mecA) control to assess process/device DNA contamination. Given the statistically weak, low replicate nature of these tests, the criteria for successful cartridge performance is 0% false positive rate (i.e. no false positives). Positive test concentrations were reduced to 10^8 copies of flu-NP to reduce potential hook effect.

Lift off side pad (V2)

The side-pad configuration using the saturation-dependent fluid transfer valve in the V1 design was chosen for its simplicity yet is not a "perfect" one-way valve. If the differences in partial pressure between the membranes (this could be modelled computationally using water retention curves of the two materials) at the material interface is not great enough, there can be, in this case, a nonzero flow from nitrocellulose to side-pad. To the naked eye, there may be no perceived fluid transport (as verified by colored dye tests) from the nitrocellulose to the side-pad, but only 0.01 µL transport could cause false positive results. The pre-mixed sample contains ~10^6 copies of ssDNA /1 µL, and any degree of "leakage" of the saturation-dependent valve could seed the side-pad with amplifiable *mecA* template. To test this hypothesis, the cartridge was modified to have the side-pad and stop flow membranes added only after completion of the immunoassay, enforcing spatial separation of detection molecule (the "contaminant") and the side-pad until master-mix addition. Results of the V2-cartridge showed similar response to V1—false positives amplified at the same rate as true positives. (Figure 38)
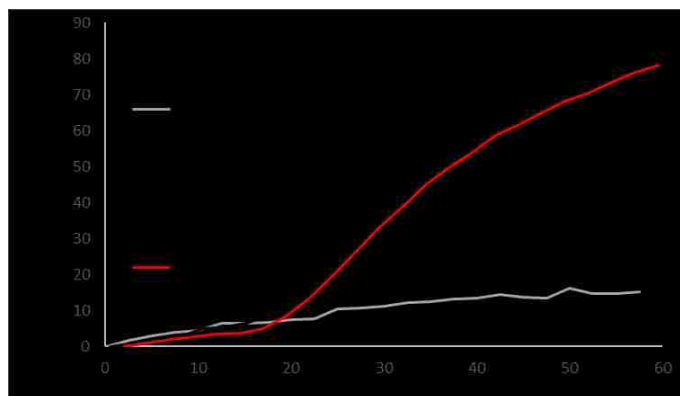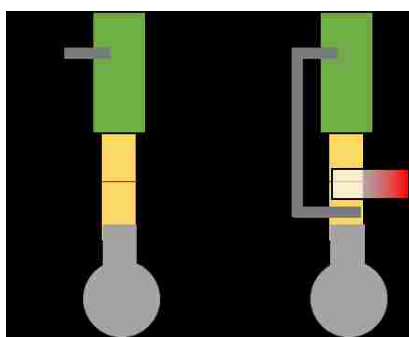
Figure 38: V2-cartridge / spatially separate side-pad: The side-pad and stopped flow membrane was separated from the system until completion of the immunoassay to prevent suspected contamination by the detection molecule. Test line marked by "T", immunoassay shown in yellow, side-pad in red, and wick in green. Real-time curves from red-channel of fluorescence image show amplification of both positive (10^8 input copies) and negative (0 input copies) flu-NP samples. The 0 *mecA* (ssDNA) negative control did not amplify, indicating there was no external DNA contamination during the protocol. Schematic of V2-Cartridge shown in left panel.

Separate sample / wash pads (V3)

After side-pad separation proved to be insufficient in preventing false positives, we addressed the insufficient rinse /dead zone observed in the sample pad. To eliminate these unwashed areas potentially contributing to contamination of the wash buffer by detection molecule (Figure 37), the V3-cartridge used a separate wash pad. Rather than use sequential delivery of reagents to the same glass fiber pad, the sample pad was removed after the pre-mixed sample drained completely. Next, a separate glass fiber wash pad was added with the same overlap and contact area, then filled sequentially with wash and rinse buffers. The V3-cartridge also eliminated the stop flow membrane, instead using manual removal of the wicking pad to stop flow in the nitrocellulose. The separate side-pad feature was retained to reduce complexity and isolate the separate wash pad hypothesis. These results (Figure 39) show the false positive rate persists: 0 NP samples amplify with similar intensity as 10^8 flu-NP samples.
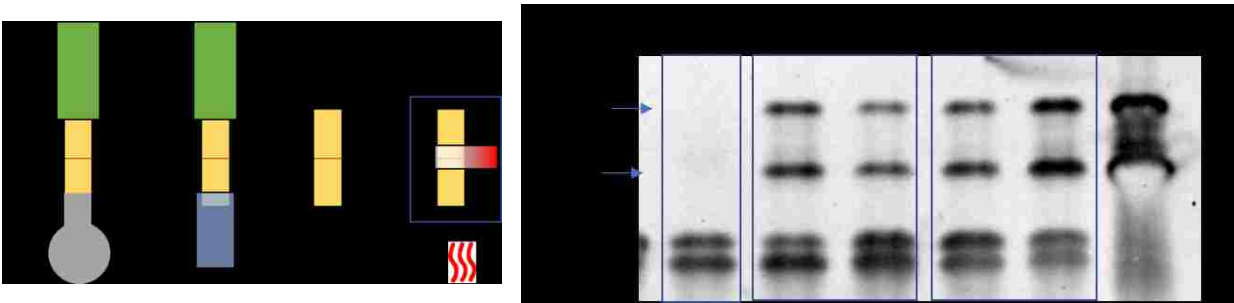
Figure 39: V3-cartridge / separate sample and wash pads: The sample pad was removed from the system after delivery of fluid (1), and a wash pad was added over the same location (2).The wick was then removed (3), side-pad added, and system sealed for incubation (4). Test line marked by "T", immunoassay shown in yellow, sample pad (1) in grey, wash pad in blue (2) side-pad in red (4), and wick in green. Gel detection (right panel) shows amplification of both positive (10^8 input copies) and negative (0 input copies) flu-NP samples of similar intensity. The 0 *mecA* (ssDNA) negative control did not amplify, indicating there was no external DNA contamination during the protocol. Schematic of V3-cartridge shown in left panel.

Sealed edge effects of nitrocellulose (V4)

Guillotine cutting, a common LFT fabrication process, may damage the nitrocellulose membrane causing flow irregularity. Macroscopic damage from this process such as stray fibers or nicked edges, has been shown to contribute to flow variability and channeling in LFT porous media [69]. Microscopic damage such as crushed pores, dust contamination, or dead-zone from irregular edges, may yield non-uniform velocity profiles and unintended fluid flow which is imperceptible to the naked-eye in colored-dye experiments. Guided by these observations, we hypothesized that the guillotine blade imparted a crushed edge region, distorting and collapsing pores, in CN-95 membranes, causing low flowrates along these edges. Slower flowrates due to increased tortuosity and pore friction increase interaction time for NSB between detection molecule and nitrocellulose—potentially the source of false positives. Fluorescence images of flu-NP LFTs with Quantum dot labelled detection antibodies showing streaking

along cut edges, support this theory. (Appendix A:7.6) Teflon-AF, an iSDA compatible polymer, was

used to seal the nitrocellulose along cut edges to eliminate these edge effects. Figure 40 shows evidence

of crushed edges in nitrocellulose examined microscopically. The V4-cartridge design also reduced the

membrane overlap between nitrocellulose and wash pad from 1.5 mm to 0.0 mm. In an LFT, the overlap

region between fluidically connected glass fiber and nitrocellulose membranes receives less rinsing than

downstream nitrocellulose because the fluid leaves the glass from the leading edge, a flow path with less

resistance than a path transversely down into the nitrocellulose. In theory, geometrically perfect, non-

overlapping membranes would not pass fluid, but practically, fluid in the glass fiber membrane "swells"

beyond the membrane edge, and readily flows into nitrocellulose from a 0.0 mm overlap.
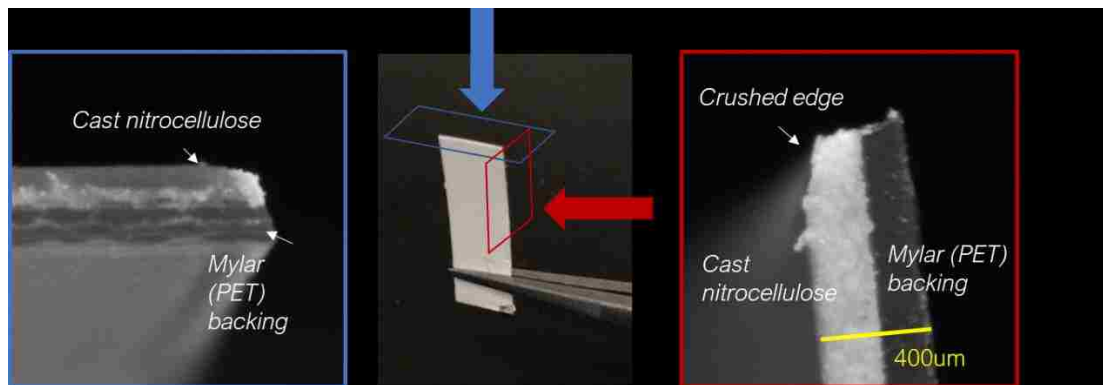

Figure 40: Microscope images of crushed edges resulting from guillotine cutting: Center photo shows

top (blue) and side (red) detail views of nitrocellulose (no magnification). Zoomed views show a thinner

profile at the site of guillotine razor cutting. The scale bar shows overall thickness (400 µm), with roughly

50% cast nitrocellulose, 50% Mylar backing.

The Teflon-AF sealed nitrocellulose and minimal overlap wash pad test showed one false positive

test, one true negative test, and two positive (10^8) LFT-iSDA tests by fluorescence detection. (Figure 41)

The false positive result amplified at the same rate as the true positives, indicating the failure event is
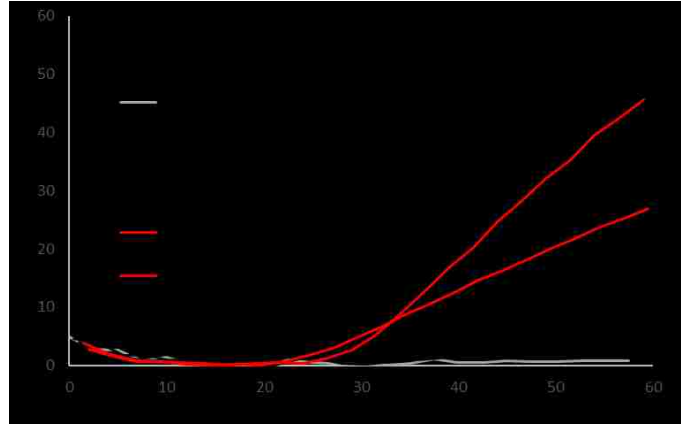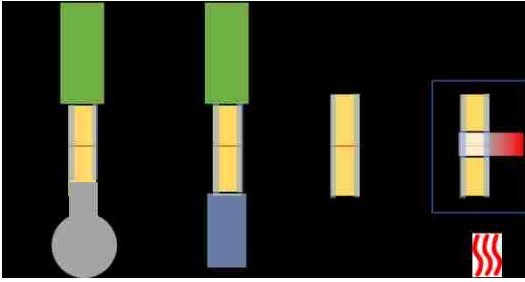
strongly amplified.

Figure 41: V4-cartridge / Teflon-AF sealed edges and minimal overlap: Nitrocellulose membranes were sealed with Teflon-AF. The sample pad was removed from the system after delivery of fluid (1), and a zero overlap wash pad was added over the same location (2). The wick was then removed (3), side-pad added, and system sealed for incubation (4). Real-time fluorescence detection in red-channel of fluorescence image (right panel) shows amplification of two positive (10^8 input copies) and one false-positive samples. One true negative (0 input copies) flu-NP samples and 0 *mecA* (ssDNA) negative control did not amplify, as expected. Schematic of V3-Cartridge shown in left panel. Test line marked by "T", immunoassay shown in yellow with grey edges representing Teflon-AF sealing, sample pad (1) in grey, wash pad in blue (2) side-pad in red (4), and wick in green.

Spatially distinct sample and wash pad regions (V5)

Lastly, given the hydrophobic nature of PDMS adhesive and previously reported adsorption of ssDNA to hydrophobic surfaces, we hypothesized that residual detection molecule from the sample pad may be adsorbing to the PDMS tape and contaminating the wash/rinse buffers in later steps. [51] Even though the sample pad is removed, the PDMS adhesive contact region may retain fluid or detection molecule (adsorbed by ssDNA).

The sample pad was rotated 90⁰ from the long axis of the cartridge to ensure a spatially distinct PDMS contact zone from the wash pad. The real-time detection results of this test are ambiguous,

80

showing only one strong amplification (10^8 input NP copies), and three weak signals (2 positives, 1 negative). (Figure 42)
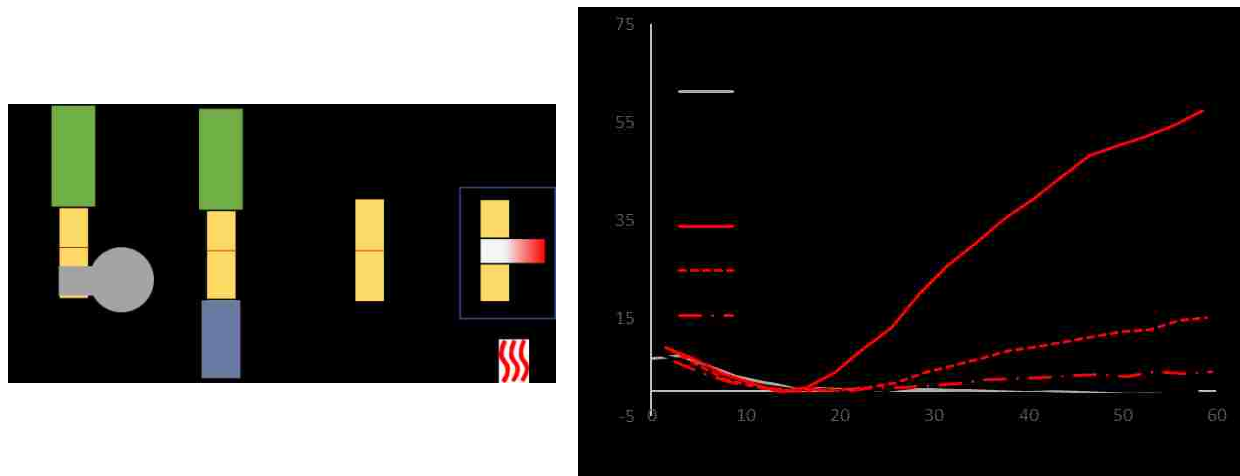

Figure 42: V5-cartridge / spatially distinct sample and wash pads: The sample pad was removed from the system after delivery of fluid (1), and a wash pad was added to a different location (2). The wick was then removed (3), side-pad added, and system sealed for incubation (4). Test line marked by "T", immunoassay shown in yellow, sample pad (1) in grey, wash pad in blue (2) side-pad in red (4), and wick in green. Real-time detection in red-channel of fluorescence image (right panel) shows one strong amplification and two weak amplifications of positive (10^8 input copies NP) samples. One negative (0 input copies) flu-NP showed weak false positive amplification, while one showed no amplification. The 0 *mecA* (ssDNA) negative control did not amplify, indicating there was no external DNA contamination during the protocol. Schematic of V5-Cartridge shown in left panel.

Amplified fluid from the side-pad was recovered by centrifugation, and analyzed by PAGE, showing 1 / 2 false positives, and 3 / 3 true positives (Figure 43). Discordance between fluorescence and gel detection may indicate that side-pads had compromised fluorescence performance due to humidity-induced MGB-probe degradation. The long-term storage of side-pads was not studied.
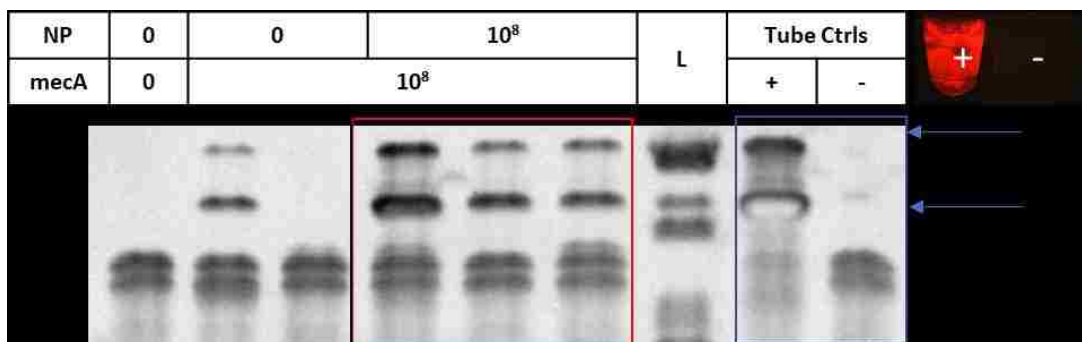
NP	0	0	10^8			L	Tube Ctrls			
mecA	0	10^8					+	-		

Figure 43: V5-cartridge / spatially distinct sample and wash pads PAGE: Fluid from the real-time experiment was centrifuged out of glass-fiber pads and analyze by PAGE. Target amplicon banding appears in 1 / 2 NP negative samples and 3 /3 NP positive samples. Tube controls indicate functional master-mix and no contamination in NTC by both detection methods. The strongest positive sample band intensity (left band) corresponds to the highest fluorescence signal response.

5.5   Discussion

5.5.1   Cartridge failure analysis

Viewed in aggregate, the results from the failure analysis of V1-cartidge are inconclusive. The integration process began by demonstrating that the manual LFT-iSDA protocol was repeatable and compatible with CN-95, yet less sensitive than in HF120—we imagine this performance could be regained through re-optimization. (Figure 32) This experiment was also an important control for the integrated cartridge as it demonstrated that the assay does not yield false positive results in a 96wp format.

The V1-cartridge, designed to perform assay unit operations in a simple format with no moving parts or complex user steps, showed false positive results (Figure 35), prompting a failure analysis through several design iterations. Although colored dye experiments demonstrated V1-cartridge ability to perform unit operations at a cursory level, (Figure 34) deeper inspection revealed a dead-zone in the distal end of the sample pad (Figure 37). Channeling along the air gap between Mylar spacer and nitrocellulose membranes was also shown to transport probes and possibly master-mix outside of the intended fluid

region. (Figure 36) Design changes responding to these data were important fundamentals to control fluid flow to the intended spatial regions but were not the dominant source of failure in the V1-cartridge. The hypothesis that the saturation dependent flow valve was "leaking" (allowing fluid to flow from the nitrocellulose to the glass fiber) and causing detection molecule to contaminate the side-pad was tested by spatial separation and shown to not be the dominant source of V1-cartridge failure. (Figure 38) This finding revealed that the saturation dependent valve may be suitable for this assay; future cartridge designs could benefit from the simplicity it affords.

Removal of the sample pad and addition of a separate wash pad to prevent contamination of the wash buffer by residual detection molecule in the dead zone proved to not be the source of the false positive cartridge failure. (Figure 39) Isolation of the crushed pore region induced by guillotine cutting by edge sealing with Teflon-AF combined with minimal overlap wash pad also failed to resolve the false positive failures. (Figure 41) Lastly, spatially distinct and separate pads, achieved by rotating the sample pad 90⁰, did not eliminate false positives. (Figure 43) V4- and V5-cartridge designs provide favorable preliminary data, achieving 1 out of 2 true negatives, but higher replicate experiments are needed to validate the potential of outcomes.

In short, failure analysis of the V1-cartridge did not definitively isolate the source of false positive LFT-iSDA results. Exponential signal amplification of an indirect binding event (i.e. LFT-iSDA) in an integrated device made of multiple materials with varying degrees of adsorptivity for the detection molecule, proved to be a challenging engineering effort.

Future work must continue to reduce the system to understand the critical design differences between dipstick manual test card and integrated cartridge device. Colored dyes, effective tools to coarsely study flow in 2DPNs, were insufficiently sensitive to illuminate the root fluid flow problem in cartridge format. A qPCR assay isolating fluids from different membranes and polymer substrates would be an effective tool to study NSB and flow anomalies in the cartridge format. Quantitative "accounting" of detection molecules through the system could be an illuminating and sensitive method to identify

cartridge failure. The key differences in the implementation of manual dipstick vs. device are presented in

Table 8. This framework may be useful to direct and analyze future work. In parallel, continued

optimization of LFT-iSDA in manual format will yield the intrinsic false positive rate of the assay, which

may have contributed to the some of the preceding results.

Table 8: Design differences between dipstick and device: Design factors hypothesized to cause false

device failure are in red. Green factors show differences unlikely to cause device failure.

	Design factor	*Dipstick*	*Device*
1	**Sample, wash, rinse**	70, 20, 40 µL	70, 40, 40 µL
2	**Membrane dimensions**	-	Same as dipstick
3	**Blocking**	0.75 µg Salmon DNA	0.75 µg Salmon DNA
4	**Master-mix**	10 µL	13 µL
5	**iSDA pad**	Full overlap	Side-pad
6	**Flow Orientation**	Vertical	Lateral
7	**Reagent delivery**	Well	Glass fiber pads
8	**Membrane contact**	Manually added	Saturation dependent valve
9	**Stop flow**	Remove wick	Fully saturate system / remove wick
10	**Detection modality**	DNA-LFT, PAGE	Fluorescence probe
11	**Incubation method / time**	Clamshell heater/30 min	ITO-glass / aluminum heater/60 min
12	**Backing material**	None (suspended in air)	PDMS tape on 10 mil-C

5.5.2   Proposed integrated design

A proposed fold-card style design to support assay unit operations with spatial separation of

membranes was demonstrated with colored dyes. (Figure 44) Assuming the root problem of false positive

results is resolved, this semi-automated format requires initial loading of buffers followed by three simple

timed user-steps before inserting the cartridge into a low-cost instrument. This design retains the 2DPN

layout of the V1-cartridge and meets the POC diagnostics design criteria outlined in 2.1. The anticipated

manufacturing method of this device would use plastic injection molded cartridge halves with hinged

elements to bring membranes in contact. Lastly, the proposed format highlights improved usability of a

semi-automated device at the expense of increased device complexity and associated cost. Optimizing this trade-off will be disease and application dependent.
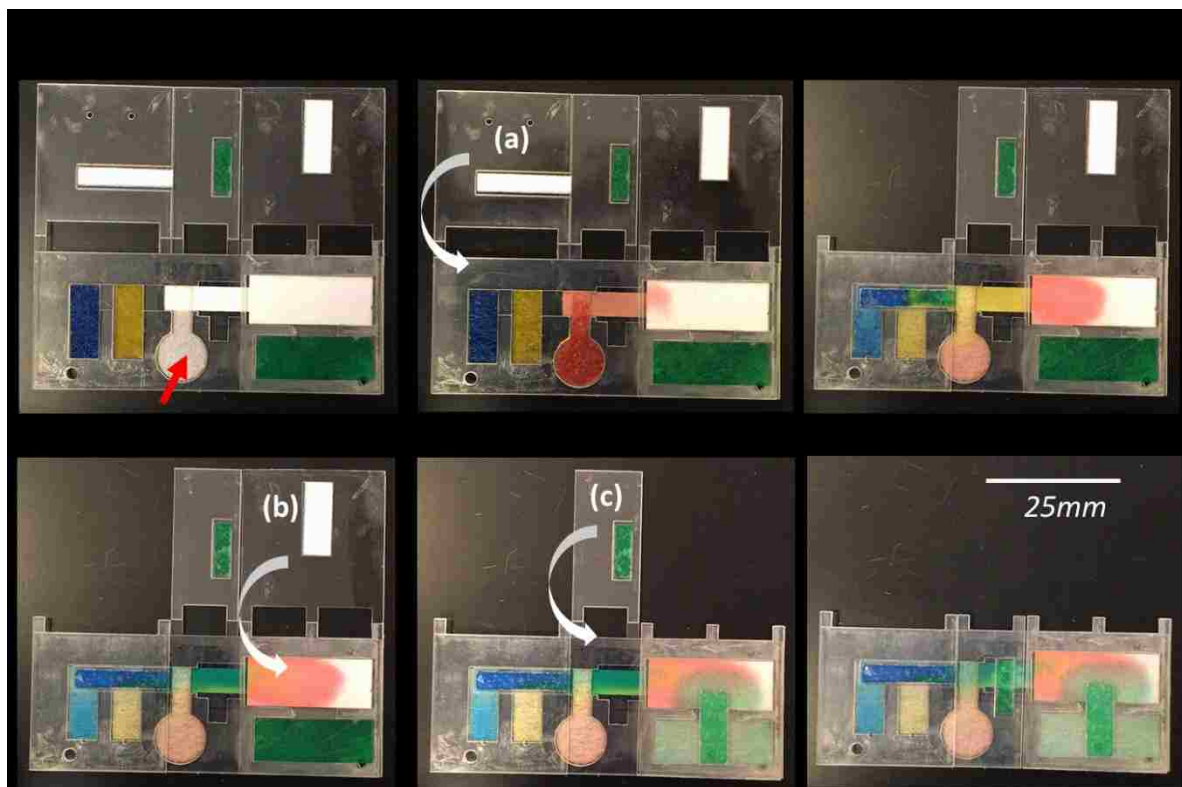

Figure 44: Proposed fold-card semi-automation: Time-lapse images show fold-card style device operation with colored dyes. (1) Sample(red) is added to the keyhole pad indicated by red arrow and flows through system (2). Fold segment (a) is then folded onto the wash (yellow) and rinse (blue) buffer pads (3), where a membrane bridge provides sequentially delivery of regents to the nitrocellulose. At the completion of rinse, fold segment (b) is folded (4), bridging stop flow buffer (green) to the wicking pad— saturating the wick, effectively stopping flow. Finally, fold segment (c) containing master-mix (5) is folded; the card is immediately placed in the low-cost instrument for incubation and detection (6). Scale

bar shown in panel 6. This visual demonstration still requires optimized sequential delivery and prevention of buffer evaporation; it is a proof-of-concept design.

5.6   Conclusions

Fluid flow path designs, as validated by colored dye experiments, showed promise in automating unit operations of LFT-iSDA. However, upon testing the integrated cartridge with the assay, we discovered that unintended fluid flow caused false positive results. Failure analysis through design modification ruled out many first principle hypotheses, but the dominant contribution was not isolated. Preliminary data suggests spatial separation of multiple pads may be required to prevent contamination of the detection molecule—leading to NSB, in successive reagent delivery. This work demonstrated that 2DPN architecture is well suited to support this process; optimization is still required to reproduce manual assay results.

6   CONCLUSIONS AND FUTURE WORK

6.1   Final conclusions

LFT-iSDA is a highly sensitive method providing up to 10,000x sensitivity improvement over gold-nanoparticle detection while retaining the simplicity of an LFT. This universal signal amplification technique offers the potential to bring NAAT-like sensitivities to protein detection at the POC. Toward this goal, demonstration of this platform technology with different analytes, detection of the signal using real-time fluorescence, and integration of the assay into a cartridge, are essential development pathways.

In the context of developing an EBOV-sGP LFT-iSDA assay, ssDNA was shown to be the dominant source of NSB of the detection molecule. This interaction leads to false positives which can be overcome by titrating the detection molecule to very low concentrations. This strategy, demonstrated with the flu-NP assay but not the EBOV-sGP assay, may be dependent on high affinity binding interactions. To utilize the large SBR and real-time response of MGB fluorogenic probes, a side-pad configuration was shown to be a viable design. MGB-probes unquench upon contact with nitrocellulose, so were lyophilized in the glass fiber side-pad orthogonal to the LFT. Real-time signals were measurable within 20 minutes by fluorescence microscope detection. A 2DPN architecture was integrated into a cartridge to extend LFT-iSDA from the lab-based format. Designs successfully integrated assay unit operations into a device, but unintended fluid flow—whose origin has not yet been identified—caused false positive results.

LFT-iSDA—a process harnessing exponential amplification of a capture event in porous media— requires both precise control of fluid flow and careful optimization of assay parameters to manage low background levels while maintaining sufficient signal to initiate iSDA. While conventional LFTs and simpler signal enhancement assays lend themselves to automation using porous media networks, the precision demanded by the near-zero tolerance for background NSB makes integration a challenging engineering effort. With the low cost of porous membranes comes limited control of morphology, surfactant chemistries, and flow homogeneity. These relatively imprecise materials paired with precise flow requirements from a multi-step assay give rise to this challenge.

The development presented in this thesis characterized and addressed many challenges in integrating the LFT-iSDA assay. The 2DPN architecture in cartridge format combined with a low-cost fluorescence detection instrument holds great promise to take highly sensitive protein detection closer to the POC.

6.2   Future work

Currently, LFT-iSDA suffers from high background due to NSB of the antibody-oligo conjugate near the test line. The ssDNA template has no proximity dependency prior to initiating iSDA—the reaction can start from detection molecules anywhere in the nitrocellulose, not specific to the test line. Future work to develop novel immuno-NAAT methods, such as circular proximity ligation assay or our group's two template variant of LFT-iSDA, into paper-based assays would assuage the wash stringency required in the current system. [70] Proximity enforced NAAT initiation could increase assay specificity, decrease time-to-result, and simplify cartridge design. Additionally, replicating this work in complex sample matrices (e.g. nasal matrix, whole blood, urine) is critical to validating LFT-iSDA's potential and robustness to sample heterogeneity. Clean, buffer systems established proof-of-concept, but clinically relevant matrices may reduce NSB and iSDA efficiency.

Salmon sperm DNA is genetically diverse, varies lot-to-lot, and likely contains endogenous nicking sites which recruit nicking enzyme activity, thus reducing iSDA efficiency. Nitrocellulose membrane blocking strategies directed at reducing ssDNA adsorption while not interfering with assay chemistry could offer performance gains. Synthetic blocking sequences, as well as synthetically designed iSDA targets could reduce the primer-dimer initiated background reaction of iSDA and accommodate a fluorogenic probe with improved and tunable SBR and hybridization kinetics.

Future work to directly conjugate the detection antibody to oligo could improve the capture efficiency and enable a lower concentration of detection molecule as the fraction of functional units is ~1, compared to the biotin/streptavidin mediated linkages which have a distribution of species existing in dynamic equilibrium.

Nitrocellulose was originally selected as the immunoassay capture media for LFT-iSDA as it is the universal material for LFTs. Alternative capture media such as glass fiber with microbead immobilization of capture antibodies, or open channel immunoassays, may offer higher flowrates, better iSDA compatibility (e.g. MGB-probes remain quenched), process higher volume washes, and provide tunable surface chemistries and morphologies (e.g. surface area-to-volume ratios, hydrophobicity). Future work to broadly screen materials offering more parameter adjustability or low degrees of NSB would be highly desirable.

Finally, continued efforts to reduce user-steps toward full automation and a single user-step are critical to interface the cartridge with a low-cost instrument.

ACKNOWLEDGEMENTS

7   APPENDIX A: Supporting Data

7.1   iSDA mecA target DNA sequences

Working Name		Modifications	Sequence
LFT-iSDA template (mecA)	oEH1139	5Biosg-iSp18 (5')	AAGATGGCAAAGATATTCAACTAACT ATT**GATGCTAAAGTTCAAAAG**AGTA TTTATAACAACATGAAAAATGATTAT GGCTCAGGTACTGCTATCCACCCTCA AACAGGTGAATTATTAGCAC
Minor-groove binder probe (mecA)	MGB-AP593	MGB-AP593(5'), EDQ (3')	CTTTTGAACTTTAGCATC
	MGB-FAM	MGB-FAM(5'), EDQ (3')	CTTTTGAACTTTAGCATC
Forward primer	mecA_E1	-	CCATTATACTACCTGTCT<u>CCTCAGC</u>GG CAAAGATATTCAACTAAC
Reverse primer	mecA_E2	-	TAGAATAGTCACTTACTT<u>CCTCAGC</u>GC CATAATCATTTTTCATGTT
Forward bumper	mecA_B1	-	GATAATAGCAATACAATCGCACA
Reverse bumper	mecA_B2	-	GTGCTAATAATTCACCTGTTTGA
Minor-groove binder probe (IC2)	MGB-probe	MGB-FAM(5'), EDQ (3')	GATCTTGTACCAATGC
IAC template			GATAATAGCAATACAATCGCACATGG CAAAGATATTCAACTAACGACCAGTT ACTTTACGGACCACGTACCGCATTGG TACAAGATCTCCAACATGAAAAATGA TTATGGCTTCAAACAGGTGAATTATTA GCAC
Molecular Beacon	MB-FAM	FAM(5'), BHQ1(3')	*CCAGC*CTTTTGAACTTTAGCATC*GCTG G*

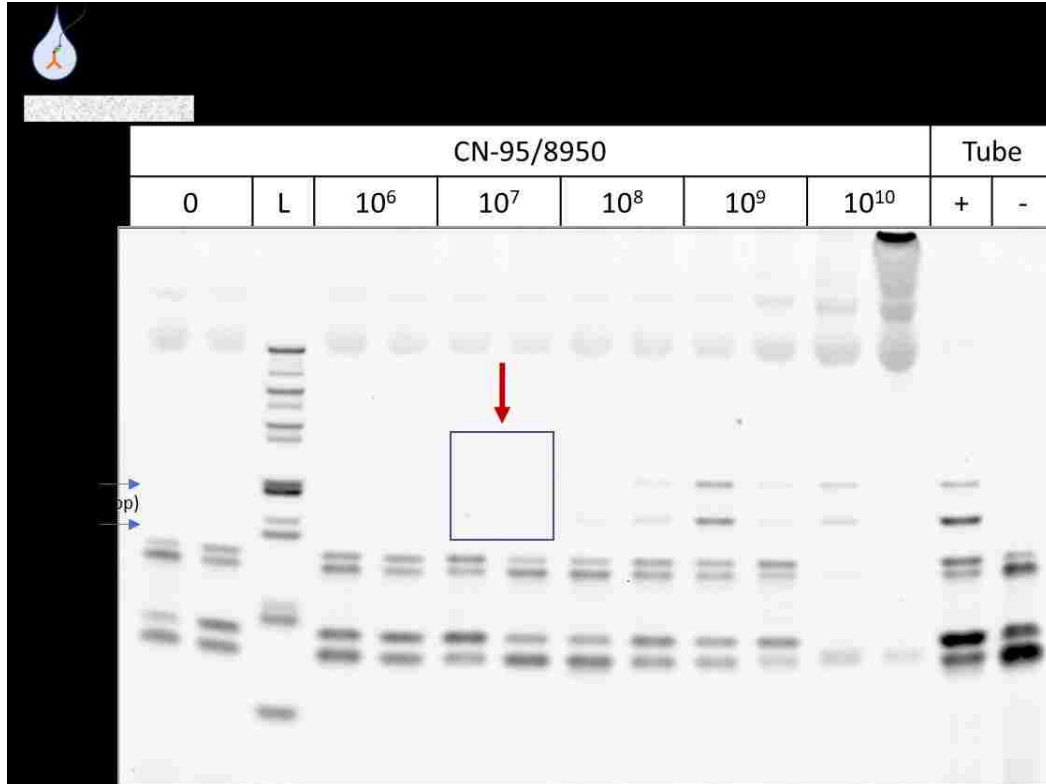## 7.2 sGP Detection molecule titration in membranes without test line

**Figure 45: Detection molecule titration to 10^7 input copies/ test on membranes without test line**: Titration of detection molecule in false positive screening test. Target amplicon length is indicated by blue arrows. Tube controls and ladder are shown at right. Red box indicates the highest concentration where true negative result was obtained. Replicates were performed at each concentration. For 10^9

cps/test, 1 /2 replicates did not amplify, as indicated by absence of iSDA background reaction. Tube controls indicate functional master-mix.

7.3   PAGE Detection of pre-blocked membrane false positive screening tests
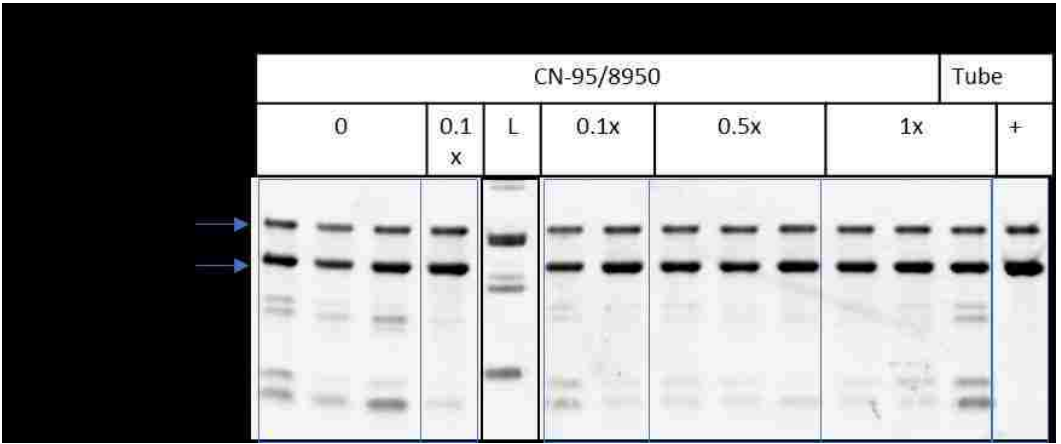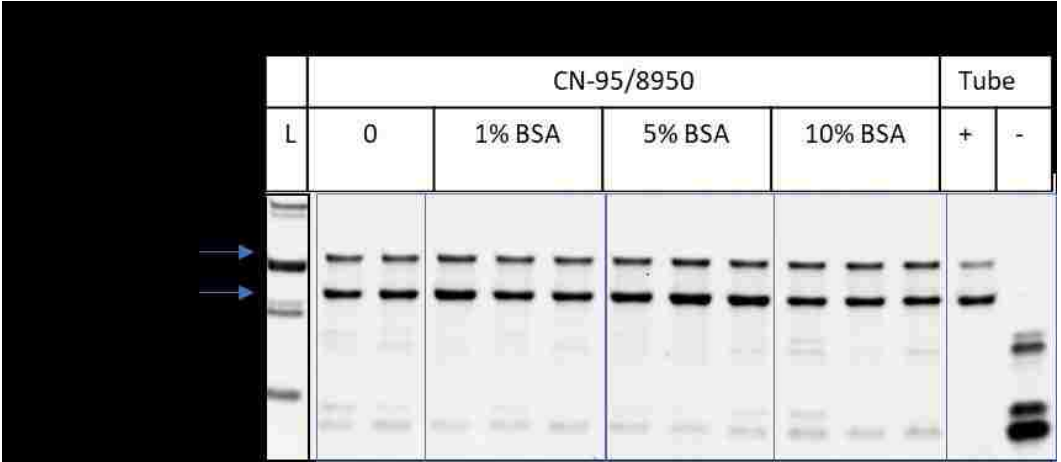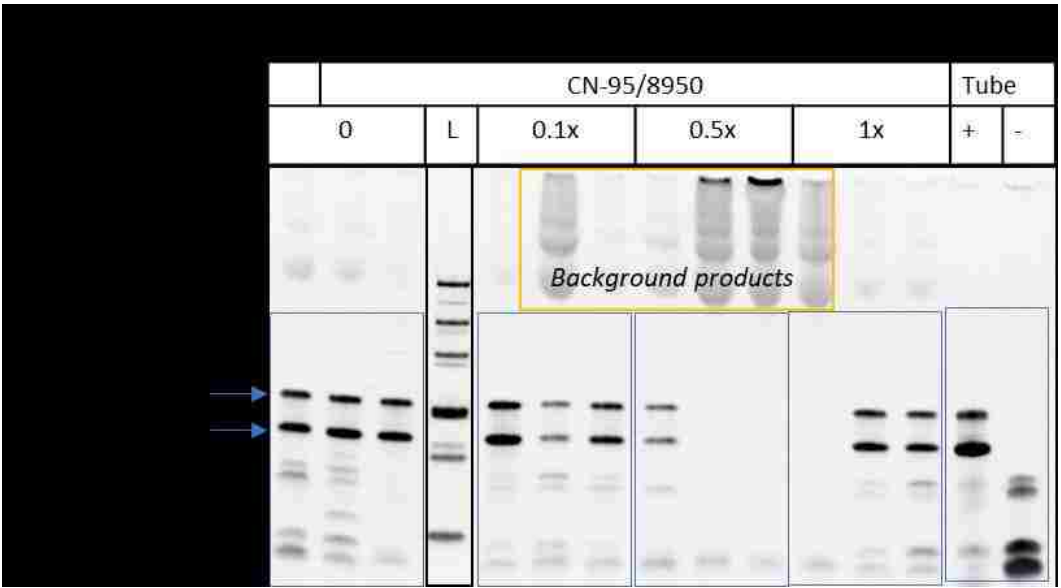
Figure 46 Various pre-blocking reagents PAGE results: DNA ladder is outlined in black box, test condition bands outlined in blue for all panels. Tube controls shown in right-most lanes. Blue arrows indicate target amplicon length from sequence specific amplification

7.4   Membrane overlap unquenching for IC2 and mecA target probes
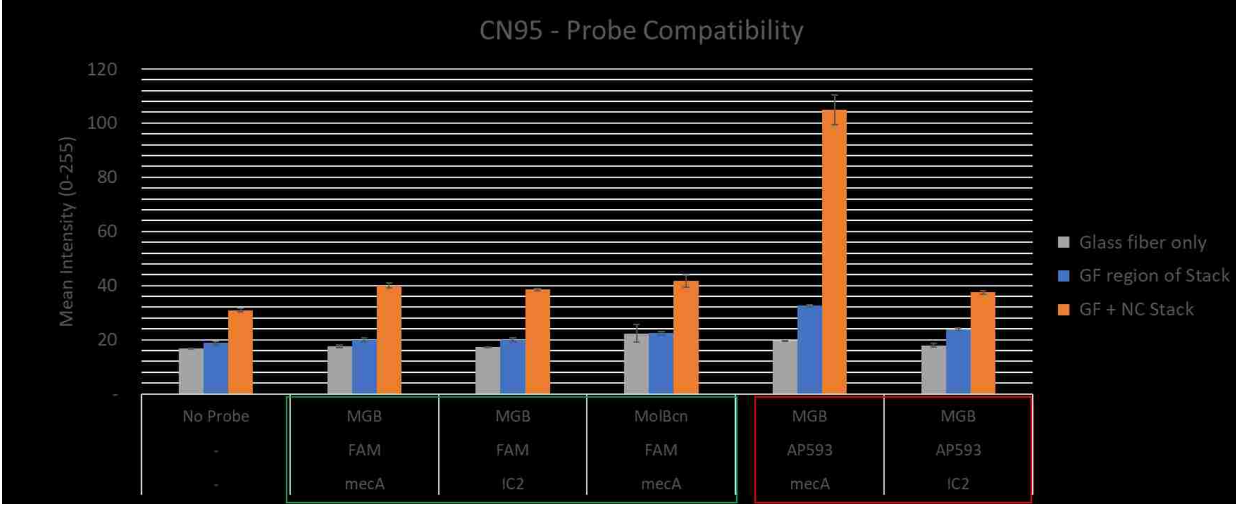
Figure 47: Probe unquenching dependency on fluorophore and target sequence: MGB-FAM, MGB-AP593, and MolBcn-FAM probes were screened in the membrane overlap tests. The mean intensity (y-

axis) indicates the magnitude of unquenching for a given probe. MGB-AP593 *mecA* shows the strongest

unquenching in both overlap and glass fiber only region of stack. The grey bars controls show glass fiber

with no-probes. The MGB-AP593 *IC2* unquenches to a lesser degree than the *mecA* version. This figure

only shows iSDA(-) reactions, so SBR cannot be estimated to fully evaluate probe compatibility with the system.

7.5   Array construction of LFT-iSDA integrated devices

Figure 48: Construction protocol for 6x array of LFT-iSDA integrated cartridge devices: this format was used to increase test throughput and fabrication time.
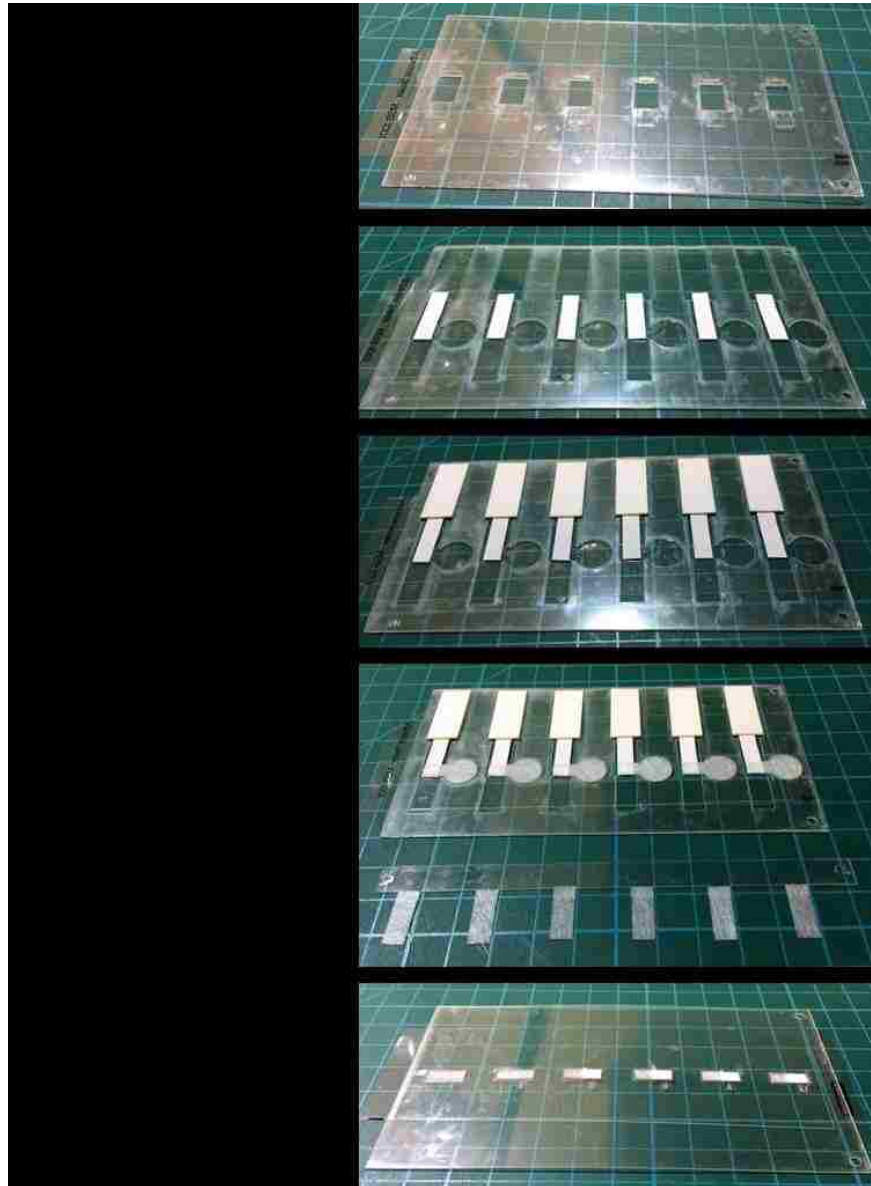
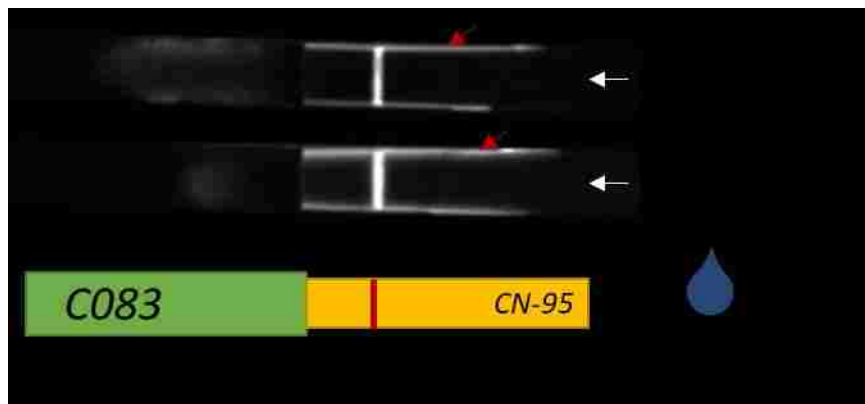## 7.6 Quantum dot LFT showing streaking along guillotine cut edges

Figure 49: Streaking along guillotine cut edges: Fluorescence image shows two LFT control lines in CN-95 from a Quantum dot-605 labelled detection antibody. The flow in strips is shown by white arrows. The white steaks along guillotine cut edges supports the hypothesis that slower flowrates in the crushed pore region contribute to increased NSB of detection molecules. Red arrows indicate streaking. Brief methods are as follows: influenza A nucleoprotein (capture: monoclonal mouse anti-influenza HyTest InA108 antibodies; control: polyclonal Jackson ImmunoResearch goat anti-mouse IgG; detection stack: biotinylated monoclonal mouse anti-influenza HyTest InA245 antibodies bound to streptavidinylated Qdot-605 from ThermoFisher; analyte: recombinant influenza nucleoprotein from IRR (FR-480)). The membranes are: Sartorius CN-95 nitrocellulose, Millipore C083 cellulose for the wicking pad, and 4 mil-thick AC Mylar backing to hold it all together. The images were acquired of dried lateral flow strips (sequential delivery of sample+detection antibody, running buffer wash, Qdot-605, and running buffer+5% Triton-x-100 wash) on the Bio-Rad gel imager with the UV tray at 0.03 second exposure. Experiment performed by Kamal Shah.

8 APPENDIX B: References

[1]   P. Yager, G. J. Domingo, and J. Gerdes, "Point-of-Care Diagnostics for Global Health," *Annu. Rev. Biomed. Eng.*, vol. 10, no. 1, pp. 107–144, 2008.

[2]   P. K. Drain *et al.*, "Diagnostic point-of-care tests in resource-limited settings," *Lancet Infect. Dis.*, vol. 14, no. 3, pp. 239–249, 2014.

[3]   IHME, "GBD Compare Data Visualization," *Inst. Heal. Metrics Eval. , 2015*, p. 2016, 2016.

[4]   P. LaBarre *et al.*, "A simple, inexpensive device for nucleic acid amplification without electricity-toward instrument-free molecular diagnostics in low-resource settings," *PLoS One*, vol. 6, no. 5, 2011.

[5]   T. R. Kozel and A. R. Burnham-marusich, "Point-of-Care Testing for Infectious Diseases: Past, Present, and Future Thomas," *J. Clin. Microbiol.*, vol. 55, no. 8, pp. 2313–2320, 2017.

[6]   Rand Health, "Estimating the Global Health Impact of Improved Diagnostic Tools for the Developing World," 2007.

[7]   D. M. Smith, "Using a Pooling Strategy," vol. 81, no. 5, pp. 754–757, 2010.

[8]   P. K. Drain and N. J. Garrett, "The arrival of a true point-of-care molecular assay-ready for global implementation?," *Lancet Glob. Heal.*, vol. 3, no. 11, pp. e663–e664, 2015.

[9]   G. Abel, "Current status and future prospects of point-of-care testing around the globe," *Expert Rev. Mol. Diagn.*, vol. 15, no. 7, pp. 853–855, 2015.

[10]   F. S. Nolte, L. Gauld, and S. B. Barrett, "Direct comparison of Alere i and cobas Liat influenza A and B tests for rapid detection of influenza virus infection," *J. Clin. Microbiol.*, vol. 54, no. 11, pp. 2763–2766, 2016.

[11]   K. M. Koczula and A. Gallotta, "Lateral flow assays," *Essays Biochem.*, vol. 60, no. 1, pp. 111–120, 2016.

[12]   R. S. Dhillon, J. D. Kelly, D. Srikrishna, and R. F. Garry, "Overlooking the importance of immunoassays," *Lancet Infect. Dis.*, vol. 16, no. 10, pp. 1109–1110, 2016.

[13]   R. E. Levin, "PCR detection of aflatoxin producing fungi and its limitations," *Int. J. Food Microbiol.*, vol. 156, no. 1, pp. 1–6, 2012.

[14]   X. Zhang *et al.*, "Development of a new broad-specific monoclonal antibody with uniform affinity for aflatoxins and magnetic beads-based enzymatic immunoassay," *Food Control*, vol. 79, pp. 309–316, 2017.

[15]   T. Kobayashi *et al.*, "Temporal and spatial patterns of serologic responses to Plasmodium falciparum antigens in a region of declining malaria transmission in southern Zambia," *Malar. J.*, vol. 11, pp. 1–9, 2012.

[16]   L. Cragin *et al.*, "Cost-effectiveness of a Fourth-Generation Combination Immunoassay for Human Immunodeficiency Virus (HIV) Antibody and p24 Antigen for the Detection of HIV Infections in the United States," *HIV Clin. Trials*, vol. 13, no. 1, pp. 11–22, 2012.

[17]   Centers for Disease Control and Prevention, "Rapid influenza diagnostic tests," p. 30329, 2017.

[18]   B. R. Lutz, P. Trinh, C. Ball, E. Fu, and P. Yager, "Two-dimensional paper networks:

Programmable fluidic disconnects for multi-step processes in shaped paper," *Lab Chip*, vol. 11, no. 24, pp. 4274–4278, 2011.

[19]   G. Wu and M. H. Zaman, "Low-cost tools for diagnosing and monitoring HIV infection in low-resource settings," *Bull. World Health Organ.*, vol. 90, no. 12, pp. 914–920, 2012.

[20]   M. Urdea *et al.*, "Requirements for high impact diagnostics in the developing world.," *Nature*, vol. 444 Suppl, pp. 73–79, 2006.

[21]   L. Bissonnette and M. G. Bergeron, "Portable devices and mobile instruments for infectious diseases point-of-care testing," *Expert Rev. Mol. Diagn.*, vol. 17, no. 5, pp. 471–494, 2017.

[22]   S. Walusimbi *et al.*, "Cost-effectiveness analysis of microscopic observation drug susceptibility test versus Xpert MTB/Rif test for diagnosis of pulmonary tuberculosis in HIV patients in Uganda," *BMC Health Serv. Res.*, vol. 16, no. 1, pp. 1–10, 2016.

[23]   Z. Ndlovu *et al.*, "Multidisease testing for HIV and TB using the GeneXpert platform: A feasibility study in rural Zimbabwe," *PLoS One*, vol. 13, no. 3, pp. 1–13, 2018.

[24]   L. K. Lafleur *et al.*, "A rapid, instrument-free, sample-to-result nucleic acid amplification test," *Lab Chip*, vol. 16, no. 19, pp. 3777–3787, 2016.

[25]   EMD Millipore, "Rapid Lateral Flow Tets Strips Considerations for Product Development," p. 36, 2013.

[26]   V. G. Panferov, I. V. Safenkova, N. A. Byzova, Y. A. Varitsev, A. V. Zherdev, and B. B. Dzantiev, "Silver-enhanced lateral flow immunoassay for highly-sensitive detection of potato leafroll virus," *Food Agric. Immunol.*, vol. 0, no. 0, pp. 1–13, 2017.

[27]   G. Shen, H. Xu, A. S. Gurung, Y. Yang, and G. Liu, "Lateral flow immunoassay with the signal enhanced by gold nanoparticle aggregates based on polyamidoamine dendrimer.," *Anal. Sci.*, vol. 29, no. 8, pp. 799–804, 2013.

[28]   E. Fu, "A two-dimensional paper network format that enables simple multi-step assays for use in low-resource settings in the context of malaria antigen detection," vol. 6, no. 10, pp. 247–253, 2009.

[29]   K. G. Shah, V. Singh, P. C. Kauffman, K. Abe, and P. Yager, "Mobile phone ratiometric imaging enables highly sensitive fluorescence lateral flow immunoassays without external optical filters," *Anal. Chem.*, 2018.

[30]   V. K. Rajendran, P. Bakthavathsalam, and B. M. Jaffar Ali, "Smartphone based bacterial detection using biofunctionalized fluorescent nanoparticles," *Microchim. Acta*, vol. 181, no. 15–16, pp. 1815–1821, 2014.

[31]   B. D. Grant, C. A. Smith, K. Karvonen, and R. Richards-, "Biotin-Streptavidin for the Detection of Malaria," vol. 88, no. 5, pp. 2553–2557, 2017.

[32]   S. Ramachandran, E. Fu, B. Lutz, and P. Yager, "Long-term dry storage of an enzyme-based reagent system for ELISA in point-of-care devices," *Analyst*, vol. 139, no. 6, pp. 1456–1462, 2014.

[33]   S. Huang *et al.*, "Disposable Autonomous Device for Swab-to-Result Diagnosis of Influenza," *Anal. Chem.*, vol. 89, no. 11, pp. 5776–5783, 2017.

[34]   T. Sano, C. L. Smith, and C. R. Cantor, "Immuno-PCR : Very Sensitive Antigen Detection by Means of Specific Antibody- DNA Conjugates Author (s): Takeshi Sano , Cassandra L . Smith

and Charles R . Cantor Published by : American Association for the Advancement of Science Stable URL : http://www.," *Science (80-.).*, vol. 258, no. 5079, pp. 120–122, 1992.

[35]   L. Chang, J. Li, and L. Wang, "Immuno-PCR: An ultrasensitive immunoassay for biomolecular detection," *Anal. Chim. Acta*, vol. 910, pp. 12–24, 2016.

[36]   P. Liu, X. Fang, H. Cao, M. Gu, J. Kong, and A. Deng, "Nano-biotinylated liposome-based immunoassay for the ultrasensitive detection of protein biomarker in urine," *Talanta*, vol. 179, no. August 2017, pp. 472–477, 2018.

[37]   D. Y. Ryazantsev, D. V. Voronina, and S. K. Zavriev, "Immuno-PCR: achievements and perspectives," *Biochem.*, vol. 81, no. 13, pp. 1754–1770, 2016.

[38]   M. S. Cordray and R. R. Richards-Kortum, "A paper and plastic device for the combined isothermal amplification and lateral flow detection of Plasmodium DNA," *Malar. J.*, vol. 14, no. 1, p. 1 DUMMY, 2015.

[39]   B. A. Rohrman and R. R. Richards-Kortum, "A paper and plastic device for performing recombinase polymerase amplification of HIV DNA," *Lab Chip*, vol. 12, no. 17, pp. 3082–3088, 2012.

[40]   J. T. Connelly, J. P. Rolland, and G. M. Whitesides, "'Paper Machine' for Molecular Diagnostics," *Anal. Chem.*, vol. 87, no. 15, pp. 7595–7601, 2015.

[41]   B. Schweitzer *et al.*, "Immunoassays with rolling circle DNA amplification: A versatile platform for ultrasensitive antigen detection," *Proc. Natl. Acad. Sci.*, vol. 97, no. 18, pp. 10113–10119, 2000.

[42]   H. Cao *et al.*, "Magnetic-Immuno-Loop-Mediated Isothermal Amplification Based on DNA Encapsulating Liposome for the Ultrasensitive Detection of P-glycoprotein," *Sci. Rep.*, vol. 7, no. 1, pp. 1–7, 2017.

[43]   K. Abe *et al.*, "Increased sensitivity for lateral flow tests through signal amplification by isothermal (in Review)," *PLOS*.

[44]   B. J. Toley *et al.*, "Isothermal strand displacement amplification (iSDA): A rapid and sensitive method of nucleic acid amplification for point-of-care diagnosis," *Analyst*, vol. 140, no. 22, pp. 7540–7549, 2015.

[45]   L. Anfossi, F. Di Nardo, C. Giovannoli, C. Passini, and C. Baggiani, "Increased sensitivity of lateral flow immunoassay for ochratoxin A through silver enhancement," *Anal. Bioanal. Chem.*, vol. 405, no. 30, pp. 9859–9867, 2013.

[46]   N. Guo, K. Cheung, H. T. Wong, and D. Ho, "CMOS time-resolved, contact, and multispectral fluorescence imaging for DNA molecular diagnostics," *Sensors (Switzerland)*, vol. 14, no. 11, pp. 20602–20619, 2014.

[47]   Quanterix, "Scientific Principle of Simoa ™ (Single Molecule Array) Technology," *Co. Whitepaper*, no. 1.0, pp. 1–2, 2013.

[48]   D. H. Wilson *et al.*, "The Simoa HD-1 Analyzer: A Novel Fully Automated Digital Immunoassay Analyzer with Single-Molecule Sensitivity and Multiplexing," *J. Lab. Autom.*, vol. 21, no. 4, pp. 533–547, 2016.

[49]   G. E. Fridley, C. A. Holstein, S. B. Oza, and P. Yager, "The evolution of nitrocellulose as a material for bioassays," *MRS Bull.*, vol. 38, no. 4, pp. 326–330, 2013.

[50] C. A. Holstein *et al.*, "Immobilizing affinity proteins to nitrocellulose: A toolbox for paper-based assay developers," *Anal. Bioanal. Chem.*, vol. 408, no. 5, pp. 1335–1346, 2016.

[51] R. Dias and B. Lindaman, Eds., *DNA Interactions with Polymers and Surfactants*. John Wiley & Sons, 2008.

[52] E. A. Lukhtanov, S. G. Lokhov, V. V. Gorn, M. A. Podyminogin, and W. Mahoney, "Novel DNA probes with low background and high hybridization-triggered fluorescence," *Nucleic Acids Res.*, vol. 35, no. 5, 2007.

[53] A. Tsourkas, M. A. Behlke, S. D. Rose, and G. Bao, "Hybridization kinetics and thermodynamics of molecular beacons," *Nucleic Acids Res.*, vol. 31, no. 4, pp. 1319–1330, 2003.

[54] W. Liu *et al.*, "Establishment of an accurate and fast detection method using molecular beacons in loop-mediated isothermal amplification assay," *Sci. Rep.*, vol. 7, no. December 2016, 2017.

[55] I. P. Oscorbin, E. A. Belousova, A. I. Zakabunin, U. A. Boyarskikh, and M. L. Filipenko, "Comparison of fluorescent intercalating dyes for quantitative loop-mediated isothermal amplification (qLAMP)," *Biotechniques*, vol. 61, no. 1, pp. 20–25, 2016.

[56] J. E. Kong *et al.*, "Highly Stable and Sensitive Nucleic Acid Amplification and Cell-Phone-Based Readout," *ACS Nano*, vol. 11, no. 3, pp. 2934–2943, 2017.

[57] S. Aldrich, "Primer and Probe Design," *Tech. Whitepaper*, pp. 6–11.

[58] K. G. Shah and P. Yager, "Wavelengths and Lifetimes of Paper Autofluorescence: A Simple Substrate Screening Process to Enhance the Sensitivity of Fluorescence-Based Assays in Paper," *Anal. Chem.*, vol. 89, no. 22, pp. 12023–12029, 2017.

[59] M. M. Azar and L. Landry, "crossm Detection of Influenza A and B Viruses and Respiratory," vol. 1988, pp. 1–13, 2018.

[60] P. Wang and L. J. Kricka, "Current and Emerging Trends in Point-of-Care Technology and Strategies for Clinical Validation and Implementation," *Clin. Chem.*, vol. 64, no. 10, 2018.

[61] B. J. Toley, B. McKenzie, T. Liang, J. R. Buser, P. Yager, and E. Fu, "Tunable-Delay Shunts for Paper Micro fl uidic Devices," *Anal. Chem.*, vol. 85, no. 23, pp. 11545–52, 2013.

[62] B. J. Toley *et al.*, "A versatile valving toolkit for automating fluidic operations in paper microfluidic devices," *Lab Chip*, vol. 15, no. 6, pp. 1432–14444, 2015.

[63] E. Fu, P. Kauffman, B. Lutz, and P. Yager, "Chemical signal amplification in two-dimensional paper networks," *Sensors Actuators, B Chem.*, vol. 149, no. 1, pp. 325–328, 2010.

[64] E. Fu *et al.*, "Enhanced sensitivity of lateral flow tests using a two-dimensional paper network format," *Anal. Chem.*, vol. 83, no. 20, pp. 7941–7946, 2011.

[65] J. R. Buser, J. E. Atwood, and P. Yager, "Nothing is saturated: correcting the assumptions made while predicting flow in paper microfluidics," *microTAS*, pp. 2–3, 2016.

[66] J. Buser, P. Yager, and B. Lutz, "Heat , Fluid , and Sample Control in Point-of-Care Diagnostics Joshua Ronald Buser A dissertation submitted in partial fulfillment of the requirements for the degree of Doctor of Philosophy University of Washington Reading Committee : Program Authorized t," *Dissertation*, 2016.

[67] S. A. Byrnes, J. R. Buser, E. Kline, J. D. Bishop, M. D. Wheeler, and P. Yager, "An integrated sample preparation system for large volume processing at the point of care," *20th Int. Conf.*

Miniaturized Syst. Chem. Life Sci. MicroTAS 2016, pp. 687–688, 2016.

[68] C. E. Anderson *et al.*, "A rapid, swab to result device for the detection of the influenza hemagglutinin (Manuscript in review)," *Lab Chip*, 2018.

[69] M. A. Mansfield, "Troubleshooting Problems with Lateral Flow Assays Complexity of a Lateral Flow Test," *EMD Millipore*, 2015.

[70] R. Jalili, J. Horecka, J. R. Swartz, R. W. Davis, and H. H. J. Persson, "Streamlined circular proximity ligation assay provides high stringency and compatibility with low-affinity antibodies," *Proc. Natl. Acad. Sci.*, p. 201718283, 2018.